CHANNEL DEFORMATION, TURBULENCE STRUCTURE AROUND SPUR DIKE, AND REDUCTION OF LOCAL SCOUR AT BRIDGE ABUTMENTS USING SPUR DIKES UNDER ICE-COVERED CONDITIONS - AN EXPERIMENTAL STUDY

by

Rahim Jafari

B.Sc., Islamic Azad University of Mashhad, Iran 2010
M.Sc., Kerman Graduate University of Advance Technology, Iran, 2013

DISSERTATION SUBMITTED IN PARTIAL FULFILLMENT OF THE REQUIREMENTS FOR THE DEGREE OF DOCTOR OF PHILOSOPHY IN NATURAL RESOURCES AND ENVIRONMENTAL STUDIES

UNIVERSITY OF NORTHERN BRITISH COLUMBIA

July 2024

Abstract

Local scour around bridge abutments and piers presents a significant challenge in hydraulic engineering, threatening the structural integrity of bridges. Scour refers to removing sediment around bridge foundations due to high-velocity flow and turbulence from water passing around these structures. This process can undermine the stability of bridges by exposing and weakening their foundations, potentially leading to failures and catastrophic collapses. Several factors contribute to scour, including water flow characteristics, surface conditions, hydraulic structure features, and riverbed geomorphology.

Effective mitigation of scour is essential to ensure bridge safety and longevity. Traditional methods, such as riprap, concrete aprons, and various hydraulic structures, aim to alter flow patterns and reduce erosive forces. However, these methods can be constrained by environmental conditions and site-specific characteristics. This research explores using spur dikes, hydraulic structures extending from the riverbank to redirect the flow, to mitigate local scour at bridge abutments, especially under ice cover conditions. The study utilizes a large-scale outdoor hydraulic flume at the Quesnel River Research Center in British Columbia, Canada. The flume measures 38.5 meters in length, 2 meters in width, and 1.3 meters in depth, with a longitudinal bed slope of 0.2% to replicate natural flow conditions with non-uniform flow characterized by longitudinal variations in water depth. Two sandboxes are filled with natural sediments of different median grain sizes (0.48 mm, 0.60 mm, and 0.90 mm) to replicate riverbed conditions.

Spur dikes made from marine plywood were positioned upstream of the abutment (25 cm and 50 cm) and at different alignment angles (45º, 60º, 90º) in the flume. Abutments constructed from galvanized plates were installed in the sandboxes. Styrofoam panels simulated smooth and rough ice cover conditions, with smooth panels representing natural sheet ice and rough panels

mimicking ice jams through attached Styrofoam cubes. Flow rate and water depth were measured using a SonTek-IQ Plus, an advanced instrument with six sensors for comprehensive flow field coverage and high-accuracy data collection. Acoustic Doppler Velocimetry (ADV) captured detailed 3D velocity components and turbulence intensities, measuring the velocity of scattering particles in the flow to provide insights into complex flow dynamics around the spur dikes and abutments.

This experimental study aims to enhance understanding of scour dynamics by investigating the interactions between different spur dike configurations, flow conditions, and ice cover types. It provides detailed insights into how these factors influence local scour and sediment transport processes. Additionally, the study seeks a comprehensive understanding of the flow field and 3D velocity distribution around spur dikes under various conditions, analyzing the effects of different alignment angles and ice cover on flow patterns and turbulence structure, which are critical for predicting and mitigating scour. Another goal is to develop effective scour mitigation strategies, identifying optimal configurations that provide maximum protection under various hydraulic and environmental conditions. Overall, the combined studies aim to advance the field of hydraulic engineering by offering practical solutions for mitigating scour-related risks, thereby ensuring the stability and safety of bridge abutments in diverse hydraulic environments.

Table of Contents

List of Figures

List of Tables

ACKNOWLEDGEMENT

I would like to express my deepest gratitude to my supervisor, Dr. Jueyi Sui, for his invaluable guidance, support, and encouragement throughout my PhD journey. His expertise, patience, and unwavering trust in my capabilities have played a fundamental role in shaping the outcome of this thesis. His mentorship and constructive feedback not only enhanced the quality of my research but also enriched my academic growth. I consider myself incredibly fortunate to have had him as my supervisor.

I am also immensely grateful to all my committee members, Dr. Faran Ali, Dr. Liang Chen, and Dr. Wenbo Zheng, for their indispensable input, which significantly influenced the direction of my research. Their astute observations played a crucial role in shaping this thesis.

I extend my heartfelt appreciation to Dr. Ellen Petticrew and Dr. Phil Owens, whose support made this research possible. Furthermore, the provision of resources and facilities at the Quesnel River Research Center (QRRC) has profoundly enriched the calibre and depth of my research endeavours. Additionally, I am thankful for the kindness and support of John Orlowsky, Doug Thompson, Vincent Aubichon and Todd French, whose passing was a great loss. A special thanks to two of my dear friends, Parima Sattari and Mahboubeh Barahimi, who provided continuous motivation and encouragement throughout my research.

Finally, I would like to express my deepest gratitude to my family for their love, patience, and encouragement. To my beloved wife, Saede, for her unconditional love, constant support, and understanding, and for being my rock throughout this challenging yet rewarding journey. To my parents for their steadfast belief in me and for instilling in me the values of perseverance and hard work.

This dissertation is dedicated to my family, whose sacrifices and support have been the foundation of all my achievements.

1 CHAPTER ONE: Introduction and Literature Review

Bridges are essential structures facilitating road connectivity, significantly easing transportation and reducing traffic congestion. They play a crucial role in both economic activities and the daily lives of commuters. Given their extensive use, ensuring the safety of bridges is paramount. A bridge collapse represents one of the most hazardous forms of structural failure. Several factors can contribute to such a collapse, including natural disasters such as earthquakes and floods, fires, construction and design defects, manufacturing flaws, inadequate maintenance, and hydraulic issues like local scour around bridge abutments or piers (Chang, 1973; Kattell & Eriksson, 1998; Richardson & Davis, 1995).

According to Kattell and Eriksson (1998), the most common cause of bridge failures on the highways in the USA is local scour. Scour is an engineering term referring to a specific form of erosion around bridge piers and abutments in riverbeds. It involves the removal of soil around the abutments and piers of a bridge or the granular bed material in natural watercourses. Scour is a dynamic and complex process that can be categorized into three types: general scour, contraction scour, and local scour (Brandimarte et al., 2012).

General scour refers to the removal of sediment from the main channel bed by river flow, resulting in the lowering of the river bed and the gradual removal of large amounts of sediment (Warren, 2011). This process can occur as either degradation, the general reduction of river bed material by river flow and can accelerate during floods, or aggradation, defined as the deposition of sediment eroded from the river bed or watershed upstream of the channel (Richardson et al., 1993). Contraction scour involves the removal of sediment from the bottom and sides of the river due to increased velocity caused by a reduction in the cross-sectional area of streamflow. According to the continuity equation, a decrease in flow areas results in increased average velocity and bed shear stress in the contraction section. These contractions can be caused by natural phenomena such as earthquakes and landslides or by human-made structures like bridges (Umbrell et al., 1998). Local scour is caused by an increased flow velocity in the vicinity of hydraulic structures, such as bridge piers, abutments, and other obstacles that block the flow (Chang, 1992).

In the USA, 503 bridge failures between 1989 and 2000 were reviewed by Wardhana and Hadipriono (2003). This study concluded that these failures were mainly related to scour and flood. Between 1969 and 1991, there were more than 1000 bridge failures, 60% of which were due to local scour (Briaud et al., 1999). Further, in 1994, more than 500 bridges in Georgia were damaged by scouring (Richardson & Davis, 2001). These bridge failures incur substantial financial costs. For instance, the US Federal Highway Administration reported that major local floods between 1964 and 1972 caused approximately $100 million in damages per event to bridges over rivers (Brice et al., 1978). New Zealand's road administration also reported that scour caused by rivers results in NZ$36 million per year (Macky, 1990). In another study, the US Transportation Research Board in 1997 declared that there were over 488 thousand bridges over streams and rivers in the USA, and scour-related bridge failures cost roughly $30 million annually (Lagasse et al., 1997).

Another critical concern associated with bridge failures is the potential loss of human life. While the financial costs are substantial, the loss of human life is even more significant. For example, the Schoharie Creek Bridge collapse in New York on April 5th, 1987, resulted from scouring and tragically led to the loss of ten lives (LeBeau et al., 2007). In 1995, the failure of a bridge over the Arroyo Pasajero River in California resulted in the loss of seven lives. A 3-meter-deep scour hole caused this tragic incident (Arneson, 2013).

Riverbeds undergo erosion to a specific depth, known as scour depth, and numerous studies have been conducted to understand scour patterns and their maximum depth (Chang, 1992).

However, most of these studies have used uniform sediment, which does not accurately represent natural river conditions. These studies primarily focused on open channel conditions, often neglecting rivers with unique characteristics, such as those in cold northern regions. In such regions, river surfaces can remain frozen for extended periods, impacting scour processes. Canada is an example of a region where river surfaces freeze for about six months each year. The Fraser River, the longest river in British Columbia, exemplifies this phenomenon. With an annual discharge of 3,550 cubic meters per second, the Fraser River's entire surface in the northern regions freezes during winter (Figure 1.1).

Ice cover can introduce additional hydraulic boundaries on river flow, leading to significant changes in velocity, flow rate, sediment transport, and scour patterns. Under ice-covered conditions, the maximum flow velocity shifts closer to the riverbed, increasing bed shear stress around bridge abutments and piers (Namaee & Sui, 2019a, 2019b; Sui et al., 2010; Wang et al., 2008; Wu, Hirshfield, Sui, et al., 2014; Peng Wu et al., 2015).

Figure 1. 1:CN Rail Bridge over Fraser River, Prince George, BC, Canada.

Bridge failure remains a critical area of research, with local scour around bridge abutments or piers identified as one of the primary causes of collapses. According to a study by the US Federal Highway Administration in 1973, 75% of 383 bridge failures involved abutment damage, while 25% involved pier damage (Chang, 1973). Additionally, a study found six out of ten bridge failures in New Zealand during Cyclone Bola were due to abutment scour (Kandasamy & Melville, 1998). Accurately predicting scour depth is essential for the safe design of bridge foundations. Since abutments are more vulnerable to scour than piers, further research on scour patterns around abutments is necessary. Developing strategies to reduce or prevent local scour at abutments is crucial for enhancing bridge safety and longevity.

One effective method for reducing scour is using spur dikes to protect abutments and piers. Spur dikes are structures that extend from the riverbank and project a certain distance into the river flow (Kuhnle et al., 1999). These dikes serve various purposes, including riverbank protection and flood control, and have been suggested as a countermeasure for reducing local scour (Nazari et al., 2017). Despite the widespread application of spur dikes, there is still a lack of published data addressing their effectiveness as a scour reduction method. To date, no research has been reported on using spur dikes to protect bridge abutments from local scour under ice-covered conditions. Therefore, it is crucial to study the influence of spur dikes on local scour around bridge abutments in ice-covered rivers to fill this knowledge gap and enhance bridge safety in such environments.

This experimental research investigates the application of spur dikes to reduce scour under various flow surface conditions, including open flow, smooth ice cover, and rough ice cover. The study will also consider different flume bed materials and flow properties. Additionally, the research will examine the scour morphology and flow field around the spur dike inside and outside the scour hole.

1.1 Scour

1.1.1 The Role of Vortex Dynamics in the Scour Process

Based on previous research, local scour at bridge abutments and piers is one of the leading causes of bridge failures (Wardhana & Hadipriono, 2003). Local scour is a complex hydrodynamic process in which an object, such as piers or abutments, interferes with the river's flow, accelerating the water flow and generating a system of vortices around the obstacle. In fluid dynamics, a vortex system refers to fluid particles' organized motion around a central axis, creating circular or spiral patterns. This system is crucial in understanding various fluid flow phenomena, especially around objects immersed in a fluid stream (Dey & Raikar, 2007). This vortex system, coupled with high turbulence in the water flow, is primarily responsible for removing sediments at the base of any object obstructing the streamflow. These vortices are categorized into three main types: Primary Vortex, Horseshoe Vortex, and Wake Vortex (Ishigaki et al., 2000).

The primary vortex is the fluid's initial swirling motion created by an object's disturbance in the fluid flow. It forms directly downstream of the object and is characterized by its relatively stable and large-scale circulation. This vortex plays a fundamental role in determining the overall flow pattern around the object (Bearman, 1978). The horseshoe vortex is a specific type of vortex system that forms around the base of an object, such as a bridge pier or a ship's bow, when it obstructs the fluid flow. This vortex wraps around the front and sides of the object, resembling the shape of a horseshoe. It consists of two counter-rotating vortices originating from the object's sides and extending downstream. The horseshoe vortex is significant in scour formation and sediment transport around structures (Melville & Sutherland, 1988). The wake vortex is formed in the wake region downstream of an object as the fluid flow separates and creates a turbulent trail. This vortex system is characterized by alternating vortices shed from either side of the object, forming a vortex street. The wake vortices are crucial in understanding drag forces and turbulent mixing in the flow. Suspended sediments are subsequently transported downstream by wake vortices (Figure 1.2) (Baker et al., 1974).

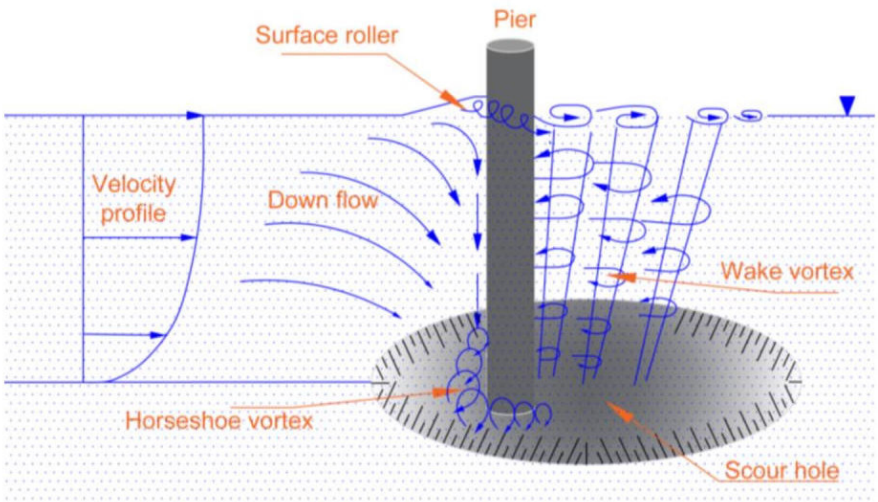

Figure 1. 2:Development of a vortex system around a bridge pier (Ranjbar-Zahedani et al., 2019)

The primary vortex, horseshoe vortex, and wake vortex are interconnected and influence each other in various ways. The primary vortex generated by the object's presence influences the formation of the horseshoe vortex around its base. The interaction between these vortices can intensify the swirling motion and increase the turbulence in the flow (Melville & Sutherland, 1988). Energy is transferred between these vortices, where the primary vortex feeds energy into the horseshoe vortex, enhancing its strength. This energy transfer contributes to the stability and intensity of the vortex system (Baker et al., 1974). The horseshoe vortex affects the flow patterns around the object's base, influencing the wake vortex's characteristics. The wake vortex inherits the disturbances created by the horseshoe vortex, leading to complex flow structures downstream (Cheng et al., 2011; Melville & Sutherland, 1988). The combined action of the primary, horseshoe, and wake vortices is critical in sediment transport and scour around structures. The horseshoe vortex, in particular, is responsible for initiating scour by lifting sediment from the base, while the wake vortex can transport sediment further downstream (Das et al., 2013).

1.1.2 Local Scour Evolution and Mechanism

As water flows around the structure, it accelerates and increases in turbulence. The initial stages of scour are characterized by the rapid sediment removal around the structure's base. This initial phase is often the most intense, with high sediment transport rates due to the strong horseshoe vortices and downward flow (Melville & Coleman, 2000). As the scour progresses, the depth of the scour hole increases. The process continues as long as the shear stress exerted by the flowing water exceeds the critical shear stress required to move the sediment particles. The dimensions of the scour hole, including its depth and width, depend on several factors, such as the flow velocity, sediment size and type, and the size and shape of the obstruction. As the scour hole develops, the bed shear stresses are reduced (Benedict, 2016). The shape of the scour hole typically progresses from a narrow and shallow form to a broader, deeper, and more stable configuration. This broadening occurs as the flow continuously removes sediment from the sides of the hole and deposits it further downstream. The process creates a more uniform and gradual slope along the edges of the scour hole, reducing the intensity of the local flow and the associated shear stress (Melville & Sutherland, 1988).

Eventually, under steady flow conditions, the development of scour will reach a point where the shear stresses are no longer sufficient to remove significant amounts of bed material. This condition is defined as the equilibrium state. This state refers to the condition where the rate of sediment removal by water flow, such as in a river or around a structure, is equal to the rate at which sediment is deposited or remains stable (Richardson & Davis, 1995). This balance indicates that the depth and shape of the scour hole do not change significantly over time, signifying a stable system. At this point, the depth and extent of the scour hole stabilize, meaning that the erosion and deposition processes are in a dynamic balance. Equilibrium scour depth represents the maximum scour for the existing river flow. This equilibrium depth is influenced by the flow characteristics, sediment properties, and structure dimensions (Breusers & Raudkivi, 2020).

Several factors influence the evolution of a scour hole. Higher flow velocities increase the shear stress on the sediment, accelerating the erosion process and leading to deeper scour holes (Chiew, 1984). The sediment particles' size, shape, and cohesiveness affect how easily they are eroded. Coarser and more cohesive sediments are more erosion-resistant, resulting in shallower scour holes (Breusers & Raudkivi, 2020). Larger and more streamlined structures alter the flow patterns differently, influencing the intensity and distribution of erosive forces around the structure (Melville & Coleman, 2000). The duration of exposure to flowing water impacts the extent of scour. More extended exposure periods typically result in deeper and more extensive scour holes until equilibrium is reached. Understanding the evolution of scour holes is crucial for designing and maintaining hydraulic structures. Engineers must account for the potential maximum depth of scour when designing foundations to ensure structural stability (Richardson & Davis, 2001).

1.1.3 Previous Research on Scour

Studies on various types of scouring have garnered significant attention, with numerous scholars contributing extensively to this field. Research on local scour at piers, abutments, piles, pile caps, and pile groups has been particularly intriguing to researchers from diverse disciplines (Froehlich, 1989; Garde et al., 1961; Laursen & Toch, 1956; Liu et al., 1961; Melville, 1992; Raudkivi, 1986). Bridge scour is related to many aspects, such as the river bed material, channel form, flow type, velocity profile, and the size and shape of bridge piers or abutments (Deng et al., 2009). Coleman et al. (2003) suggested that the relationship between scour depth and various factors of the river system can be represented within dimensionless frameworks. This approach has facilitated the development of models demonstrating how local scour depth varies with parameters such as flow profile, sediment grain size distribution (D_{50}), and flow depth. Melville and Coleman (2000) indicate that a typical way to predict the total erosion depth for any bridge is to consider the combination of general, contraction, and local scour. A complete review of local scour formulae is provided by Dey and Barbhuiya (2005). However, the development of these formulas has been a complex process due to the discrepancies between natural river conditions and laboratory settings and the limitations in data collection (Ataie Ashtiani et al., 2006; Lu et al., 2008).

Several scholars studied the obstruction ratio, defined as the ratio between the abutment length and the width of the river Melville and Coleman (2000). Breusers (1991) reported that this factor does not significantly affect the local scour depth if it is calculated to be less than 40%. Accordingly, the obstruction ratio is neglected in many types of research on scouring topics (Coleman et al., 2003; Kothyari & Ranga Raju, 2001; Melville, 1997). In the case of channel contraction, Melville and Coleman (2000) stated that if a contraction is significant due to the blockage ratio of an obstacle, the resulting scour depth would be greater than that caused by the same abutment in a wider channel. This phenomenon, known as contraction scour, occurs due to the increase in average velocity over the cross-section rather than the vortices developing at the obstacle.

Time is another crucial factor in the study of scour. Investigating the transient characteristics of the scour process is necessary to determine the time scales for the initial scour development and the duration required to reach a specific scour depth and equilibrium state. To draw comprehensive conclusions on the role of time in the scour process, experimental research should be conducted across a range of flow conditions, riverbed sediment types, and abutment sizes and geometries. (Chiew, 1992). Ballio et al. (2004) utilized a time scale of scour progression phases to demonstrate that this scale decreases as flow velocity increases. Once a scour hole is formed, the scouring mechanism is governed by a vortex system known as the principal vortex. This vortex is initiated by the pressure gradient that develops ahead of the structure (Kwan, 1988). This vortex has been recognized as the main scouring factor at bridge piers and abutments (Kwan & Melville, 1994). Despite extensive research to enhance the understanding of scour-related issues, the scour of piers and abutments remains a complex and challenging subject in the field.

1.1.4 Scour Mitigation Measures

Bridges are among the most crucial components of transportation infrastructure, and their failure can have profound social and economic impacts. Numerous bridges fail each year worldwide due to local scour at their piers and abutments. (Johnson & Ayyub, 1996; Lagasse et al., 1995). The application of rocks and stones for scour protection has a long history in hydraulic engineering. Breusers et al. (1977) suggested using boulders with high critical entrainment velocity around the piers to protect them from floods and local scours. Traditional engineering methods of solving local scour problems, such as placing rocks or flexible mattresses around the pier foundations, were ineffective (Chiew, 1992). Therefore, several methods have been made to control scouring around bridge sites, for example, using an array of small piles in front of the pier (Chabert & Engeldinger, 1956), applying a collar around the pier (Ettema, 1980; Tanaka & Yano, 1967; Thomas, 1967), a delta-wing-like fin in front of the pier (Gupta & Gangadharaiah, 1992), a slot through the pier (Chiew, 1992), a limited number of pier-groups (Vittal et al., 1994), submerged vanes (Odgaard & Wang, 1987), and various other efforts such as caissons and footings below the pier shaft, using riprap, streamlined piers, mats and bags, gabions, and reno mattresses (Kumar et al., 1999).

All these efforts and methods for preventing or reducing local scour can be classified into three categories. The first method is geometrical, investigating length, width, nosing shape, alignment of structure, etc. The second one is the physical features of an obstacle, such as permeability, porosity, density, etc. The third and most effective method is to use protective means and structures to prevent or minimize scour (Singh et al., 2022). This last technique can be divided into direct methods (bed armouring countermeasures) and indirect methods (river flow altering).

1.1.4.1 Direct Method of Controlling Scour

The direct method of scour reduction involves controlling scour by enhancing the stream bed's resistance to erosion. This can be achieved by installing protective layers of coarse materials or solid structures around bridge piers and abutments to improve the bed material's ability to withstand erosive forces (Kumar et al., 1999; Parola, 1993; Wörman, 1989; Yoon et al., 1995). Various scholars have investigated these methods, using an armouring structure to reduce local scour (Chiew & Lim, 2000; Dey & Raikar, 2007; Lauchlan & Melville, 2001). Experimental research was conducted to reduce scour by using submerged vanes (Odgaard & Wang, 1987) and fins in the form of delta wings in front of the pier (Gupta & Gangadharaiah, 1992). One of the common methods to reduce local scour at bridge piers and abutments is to place riprap as an armour layer around them (Chiew, 1995; Chiew & Lim, 2000; Parola, 1993; Richardson & Davis, 2001; Unger & Hager, 2006). Many researchers focused on the design of riprap size around circular piers. They investigated how the volume and sizing of riprap for rectangular piers affected their aspect ratios (Chiew & Lim, 2000; Lagasse, 2007; Lauchlan & Melville, 2001). However, riprap can enhance piezometric gradients at the riverbed, increasing sediments' erosion potential (Koloseus, 1984).

Another countermeasure for local scour is to install a collar around the pier. The collar shields the sediment particles and protects the riverbed from direct impact (Zarrati et al., 2006). Research on circular piers has demonstrated collars' effectiveness in reducing scour depth. The efficiency of a collar is reported to depend on its size and vertical placement on abutments and piers (Alabi, 2006; Kumar et al., 1999). Wider collars installed at the lower position of piers are more effective for scour reduction (Zarrati et al., 2004). An experimental study on collars at vertical face wing wall abutments shows that collars can protect the bridge abutments considerably by eliminating secondary vortex systems (horseshoe vortex) that generally could cause local scour (Li et al., 2006). However, another study on this topic revealed that scour first occurs downstream of the collar, then slowly advances upstream and erodes the collar, accelerating local scour. Therefore, collars mostly postpone scour rather than reduce it long-term (Zarrati et al., 2004). To solve this problem, Zarrati et al. (2006) used a combination of collars and riprap, considerably reducing the size of scour holes. However, it is difficult and relatively expensive to install collars on piers with large spacing (Zarrati et al., 2006).

1.1.4.2 Indirect Method of Controlling Scour

In this method, the flow pattern around bridge sites is changed to reduce shear stresses and decrease the power of the eroding vortex system around piers and abutments. These efforts can be cost-effective compared to direct methods, mainly when the required amount of stones and other materials are unavailable near the bridge site (Zarrati et al., 2004). Indirect reduction of scouring is possible by modifying the flow pattern around piers. For example, using slots in piers reduces the downflow strength and decreases the large pressure field around the piers, preventing the formation of the horseshoe vortex. However, if a slot is jammed by debris, the effectiveness is reduced, making hydraulic flow conditions around piers more challenging to control (Chiew, 1992; Kumar et al., 1999; Vittal et al., 1994).

Another common indirect countermeasure for local scour is bed sills. A bed sill, also known as a submerged sill, is a hydraulic structure placed on the riverbed downstream of a pier to reduce local scour. Its primary function is to stabilize the bed material and dissipate the energy of the flowing water, thereby minimizing the erosive forces that contribute to scour (Pagliara et al., 2010). A bed sill alters the flow pattern downstream of the pier. Raising the bed level induces a backwater effect, which reduces the flow velocity near the bed. The reduced velocity decreases the shear stress exerted on the sediment, thereby limiting the sediment's potential to be eroded. This change in flow dynamics helps to mitigate the depth and extent of the scour hole around the pier. The sill creates a wake vortex zone at piers, which decreases velocity and reduces local scour (Figure 1.3). The bed sill acts as an energy dissipator by breaking the flow's energy. The turbulence and kinetic energy of the water are partially absorbed by the structure of the sill, which reduces the energy available for sediment entrainment and transport. This energy reduction is crucial in preventing the initiation and progression of local scour (Pagliara et al., 2010).

The bed sill provides a protective layer that resists erosion by stabilizing the sediment near the pier. The presence of the sill reduces the likelihood of sediment particles being lifted and transported by the flow. This stabilization effect is especially significant in maintaining the integrity of the riverbed around the pier (Tafarojnoruz et al., 2010). The effectiveness of a bed sill in reducing local scour depends on its placement and dimensions. The sill should be placed at an appropriate distance downstream of the pier, where it can effectively influence the flow pattern. Its height and width must ensure adequate flow redistribution and energy dissipation without causing excessive backwater effects or flow obstruction (Sanadgol et al., 2021). While bed sills effectively reduce local scour, their environmental impact must also be considered. The design should ensure minimal disruption to aquatic habitats and maintain natural sediment transport processes. Environmental assessments and mitigation measures may be necessary to address potential adverse effects (Sohrabi et al., 2019). Several laboratory experiments were conducted on bed sills to control scour at bridges. They showed that a bed sill installation a short distance downstream of the bridge site causes a reduction of scour depth, area, and volume. The shorter the distance between the two structures is, the greater the efficiency of decreasing the scour hole. However, sometimes bed sills take effect after the scour is initiated around bridge piers, reducing the effectiveness of the countermeasure vortex system they create (Grimaldi et al., 2009).

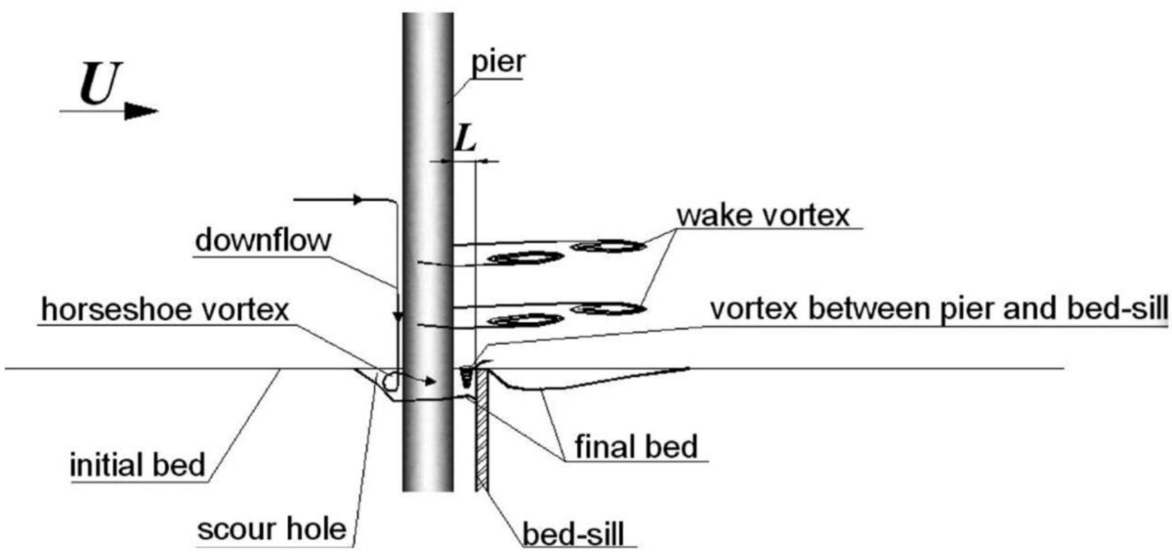

Figure 1. 3:A vortex system around the pier with a bed sill as a scour mitigation measure (Grimaldi et al., 2009)

Applying caissons and footings below the pier shaft is another standard indirect method of preventing local scour. Caissons and footings provide stable foundations for bridge piers and help mitigate scour by altering flow patterns and reducing erosive forces. The caisson averts the upstream flow and vortex system from directly impacting sediment particles around piers and abutments (Chiew, 1992). Depending on the construction method and site conditions, they can be open, pneumatic, or floating. Open Caissons are box-like structures that sunk into place by excavating soil from within. They stabilize the pier base, reducing scour (Wei et al., 2022). Pneumatic caissons are used in deeper water, which keeps water out with compressed air, allowing precise foundation placement, which helps resist scour (Kodaki et al., 1997). Floating Caissons are constructed on land and floated to the site, creating a solid barrier against erosive forces (Chakrabarti et al., 2006). Spread Footings extend laterally from the pier base and distribute loads over a larger area, reducing localized erosion (Kumar & Chatterjee, 2023). Pile-Supported Footings transfer loads to deeper, stable layers, while the footing protects against scour by stabilizing the soil around the piles (Tu et al., 2022).

While caissons and footings are commonly used to provide stable foundations for bridge piers, they can also present specific problems when used to reduce scour. Installing caissons and footings significantly increases the complexity of bridge construction. The process requires specialized equipment and skilled labour, which can complicate the construction schedule and increase the risk of construction delays. This added complexity, particularly in deep water or difficult soil conditions (Breusers & Raudkivi, 2020). Caissons and footings can significantly alter the flow patterns around the pier. The presence of large submerged structures can create complex flow dynamics, including increased turbulence and vortex formation. These altered flow patterns can exacerbate local scour instead of mitigating it (Chiew, 1984). If not correctly designed and installed, caissons and footings can be undermined by scour. Scouring can erode the material around and beneath these structures, potentially compromising their stability (Breusers & Raudkivi, 2020). Another effective indirect method for preventing or controlling various types of scour is the application of spur dikes. A comprehensive literature review on this topic is presented below.

1.2 Spur Dike

Spur dikes, or groynes, are extended structures in which one end is at the riverbank, and the other is projected toward the river flow. The application of spur dikes is one of the most efficient means of stabilizing the river flow (Kuhnle et al., 1999). Regardless of the different types of spur dikes, they redirect flow from the river bank and affect the flow regime, flow velocity, sediment transportation, and the scour process (Giglou et al., 2018). They have been widely used for many purposes, such as river bank protection, flood control, landscape improvement, ecosystem restoration, and scour process control. Different aspects of spur dikes, including their design, types, materials, and environmental impact, play crucial roles in their effectiveness (Sadat, 2015).

1.2.1 Design and Orientation

The design and orientation of spur dikes are crucial factors that determine their effectiveness in reducing scour and protecting riverbanks or bridge piers. These factors include the angle of orientation relative to the flow, the length and height of the dikes, and the spacing between multiple dikes (Kehe, 1984). Spur dikes are typically oriented at an angle to the flow direction. Common orientations include perpendicular (90º) and upstream-angled (between 30º and 60º). The angle of orientation affects how the structure redirects the flow and impacts sediment deposition patterns. Upstream-angled dikes are more effective at diverting flow away from the protected area (Kuhnle et al., 2002). The length of a spur dike is a critical design parameter. Longer spur dikes extend further into the river or stream, affecting a significant portion of the flow. However, they can also cause more significant changes in the overall flow pattern and may increase the risk of unwanted sediment deposition or erosion in other areas (Esmaeli et al., 2022). The height of a spur dike should be designed to influence the flow effectively without causing overtopping during high-flow events. Typically, the height is kept below the water surface during normal flow conditions to minimize disruption to navigation and reduce visual impact (Esmaeli et al., 2022).

When multiple spur dikes are used, close spacing can provide continuous protection along a riverbank or around a bridge pier. However, it may lead to excessive sediment deposition between the dikes, reducing the flow capacity of the channel. Optimal spacing ensures that each dike effectively influences the flow without causing adverse effects such as excessive turbulence or sediment build-up. The spacing should be determined based on hydraulic modelling and site-specific conditions to balance protection and flow efficiency (Sadat, 2015). Numerous field studies and practical applications have demonstrated the effectiveness of well-designed spur dikes in reducing local scour. For example, using spur dikes in the Missouri River has shown significant reductions in bank erosion and improved stability of bridge piers. Hydraulic models are often used to optimize the design and orientation of spur dikes. These models help predict flow patterns, sediment transport, and potential scour around the structures, ensuring that the dikes are designed to maximize their protective benefits while minimizing negative impacts (Rajaratnam & Nwachukwu, 1983)

Spur dikes can be constructed from various materials, including bamboo or timber piles, tree trunks, rock, soil, gravel, sandbags, riprap, concrete elements, and steel. Stone and riprap are commonly used due to their availability and effectiveness in dissipating flow energy. These materials are also flexible, adapting to minor shifts in the riverbed without losing effectiveness. Concrete spur dikes are durable and provide strong resistance against high-velocity flows. They are often used in locations with severe hydraulic conditions. Timber is used for permeable spur dikes, providing a cost-effective and environmentally friendly option. Timber structures are more easily constructed and effective in less aggressive hydraulic environments (Karami et al., 2011).

1.2.2 Spur Dike Types

Spur dikes can be categorized into two main types based on their construction and interaction with water: permeable and impermeable spur dikes. Each type has distinct features, advantages, and applications. A spur dike is considered permeable if it allows river flow to pass, whereas it is impermeable if it blocks and redirects the flow. In rivers with impermeable spur dikes, the energy gradient steepens, and water velocity increases due to the reduction in river width. To recover its original cross-sectional area, the river may erode the riverbed, reducing velocity and returning to its original state. The extent of this process is determined by the shape and size of the spur dike and the strength of the bed material (Pandey et al., 2018).

Permeable spur dikes are constructed with materials that allow water to pass through them, reducing the impact on flow patterns and minimizing turbulence. They are often made of timber piles, steel, or rock-filled gabions, creating water flow openings. Permeable spur dikes usually slow down sediment transportation by reducing the velocity on their upstream side. Allowing water to flow through the structure reduces the turbulence and vortex formation downstream, which helps mitigate local scour around the dike and the protected area. They can also reduce scour by redirecting or creating a laminar flow. The partial obstruction of flow causes sediment to deposit in the low-velocity zones around and behind the dike, helping to stabilize the riverbed and banks (Gu et al., 2011). On the other hand, impermeable spur dikes can benefit flood control. By deflecting turbulent flow in certain parts of the river, they help prevent riverbank erosion. These structures can reduce flow energy during floods, redirecting and controlling the rapid flows to mitigate flood impact (Klingeman et al., 1984).

Based on the flow conditions and water levels in rivers, spur dikes can either be submerged or non-submerged. Impermeable spur dikes are typically designed to be non-submerged because overflow over solid obstacles creates a vertical jet behind the dike. This vertical jet forms a layer along the longitudinal axis of the dike, which moves toward the downstream bank and can cause significant erosion (Yossef & Klaassen, 2002). Based on the orientation angle of spur dikes relative to the river flow, they can be classified into three categories: attracting, deflecting, and repelling (Figure 1.4). Attracting spur dikes point downstream, directing the river flow toward the center of the channel and protecting the area on their downstream side. Repelling spur dikes are oriented upstream, diverting the river flow from the banks. By deflecting rapid and turbulent currents away from the riverbank, they offer adequate protection against upstream bank erosion. However, these structures are prone to significant scour, particularly around their tips (Sadat, 2015). Deflecting spur dikes are well-known for altering the direction of river flow without repelling it. These dikes locally protect banks against erosion by contracting the river width and increasing water velocity. Deflecting dikes facilitate sediment transportation management by enhancing the velocity in the middle of the river. In other words, they generate turbulent flow, promote greater sediment transport in the river's center, and deepen the river channel (Sadat, 2015).

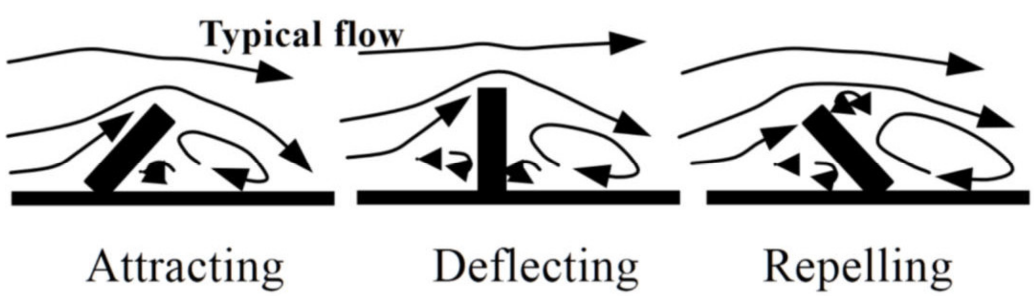

Figure 1. 4:Types of spur dikes in terms of the orientation angle (Zhang & Nakagawa, 2008)

According to their appearance in a plan, they can have many different shapes such as straight, mole-head, T shape, L shape, J shape, hockey shape, inverted hockey shape, etc (Figure 1.5). These shapes with different lengths can have vast applications in the river. For example, L-head spur dikes, where the outer tip is towards downstream flow, have less scour around their tips than straight ones. However, they can generate more sediment deposition inside the spur dike area. The L-head dikes can function better in widespread streams. Using them as the first and last spur dike is usually recommended when there are several dikes as a series (Mansoori, 2014).

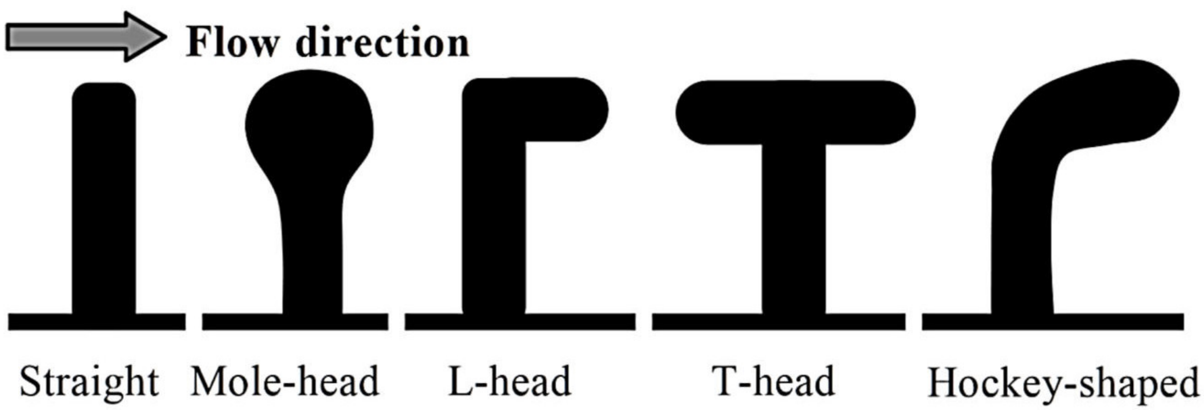

Figure 1. 5:Different shapes of spur dikes (Zhang & Nakagawa, 2008)

The design of spur dikes is influenced by numerous critical parameters, including river width and depth, mean velocity, channel sinuosity, bed material type and size, sediment transport rate, bank cohesiveness, spur dike length and shape, orientation angle relative to the flow, and construction materials. Given the unique conditions of each engineering project, the design of a spur dike often relies heavily on practical experience and informed decision-making (E. Richardson et al., 1975).

1.2.3 Previous Researches Overview

Numerous studies have investigated the behaviour of water flow when encountering obstacles. Mushtaq (1953) performed one of the earliest studies on spur dikes, which examined scour around a spur dike using sand as the bed material. His research yielded significant findings on various parameters influencing the maximum scour depth. Derrick et al. (1989) studied spur dikes, pile dikes, and similar constructions widely used in large river development projects. Some researchers focus on the flow and the sediment transportation pattern downstream of a dike and measure the velocity profile behind a permeable spur dike (Tominaga et al., 2000). Furthermore, Ishigaki et al. (2000) investigated the vortex system around the spur dike and examined how it affects the local scour. They found that the development of the vortex takes place aside from the dike. Therefore, the deepest hole is created at some distance from the obstacle.

Sukhodolov et al. (2002) applied flow velocity measurement on the Elbe River, one of the major rivers in Central Europe, to find the number and the location of vortexes inside the spur dike field. Muto et al. (2002) conducted two experimental studies about the effects of opening ratio and water depth on velocity distribution profiles. Their first experiment was a large-scale particle image velocimetry in the Yodo River in Japan, and the second experiment was conducted in a laboratory using downscaled spur dike. Based on the field study experiment, they illustrated that the flow was highly unsteady inside the scour hole area. However, the collected data in the laboratory did not show the same unsteady characteristics. The authors concluded that because of the complex bathymetry of the natural river and lower Reynolds numbers, the results are different in field and laboratory studies. Furthermore, with experimental and computational techniques improvement, several researches have been performed on the flow field, velocity profile, and sediment transport for different obstacles in a river (Namely, spur dikes, bridge piers, and abutments) (Barbhuiya & Dey, 2004; Nasrollahi et al., 2008; Zhang & Nakagawa, 2008; Zhang et al., 2005).

The permeability of spur dikes has been extensively investigated as a technique for managing sediment deposition transportation as well as the countermeasures methods against scour (Alauddin et al., 2011; Baba et al., 2010; Koken & Constantinescu, 2011; Rajaratnam & Nwachukwu, 1983; Richardson et al., 1975; Shields Jr et al., 1995; Teraguchi et al., 2010). Michioku et al. (2004) researched permeable spur dikes made of stone gabion to reduce local scour. The results illustrate the steady bed material formed near the spur dike tip. Zhang et al. (2005) studied bed morphology, sediment distribution, and flow fields in a channel featuring a series of impermeable spur dikes on both sides. Their findings indicated that the flow field and scour are most significantly impacted around the upstream pairs of spur dikes. Teraguchi et al. (2008) studied flow field, scour, and sediment patterns around permeable and impermeable spur dikes using experimental and simulation methods. They described that the local scour hole on the upstream side of impermeable spur dikes is more significant and deeper than permeable ones. Mizutani et al. (2011) examined the effects of spur dike height and the grain size distribution of riverbed material on the morphology around an impermeable spur dike. They found that increasing the median particle size of the bed material reduces the maximum scour depth. Further research on the permeability of spur dikes, specifically on the morphodynamics around stone-lined spur dikes in the Akashi River, revealed that the maximum scour depth for permeable spur dikes is reduced by 40% compared to impermeable ones (Kanda et al., 2019).

Few studies have employed spur dikes as a countermeasure for local scour around bridge sites. Karaki (1959) conducted an experimental study to protect bridge abutments by setting a spur dike perpendicular to the abutment at the highway embankment. His findings indicated that bridges with smaller openings require longer dikes to protect abutments from scour effectively. He also noted that the efficiency of spur dikes depends on the geometry of the roadway embankments and the size of the bridge opening. Herbich (1966) demonstrated that curved spur dikes reduce scour around abutments. His results showed that using a dike to redirect flow reduces local scour and promotes sediment deposition around the abutment, whereas, without dikes, scour would occur. Li et al. (2005) investigated various configurations of spur dikes using two different materials, solid thin walls and rock walls, to protect wing wall abutments. The findings indicated that a single solid spur dike with the same or shorter protrusion length as the abutment, when placed upstream, is insufficient for protection. Additionally, rock wall dikes proved more effective than solid spur dikes in safeguarding the abutment.

The researchers concluded that the most effective configuration for preventing local scour at abutments involves using three rock wall spur dikes: one placed upstream of the abutment and the others positioned at the upstream and downstream corners. Zhang and Nakagawa (2008) employed a protective spur dike upstream of a set of parallel spur dikes, significantly reducing scour depth around the main spur dike. They also noted that the farthest upstream spur dike should be constructed more robustly, as it would be subjected to the most destructive flow influences. Karami et al. (2011) demonstrated that critical parameters for a protective spur dike include its length and distance from the obstacle, such as an abutment or another spur dike. Basser et al. (2014) proposed a numerical approach to predict the optimal parameters of a protective spur dike. Their findings indicated that the support vector regression (SVR) model provides better accuracy than the ANFIS and ANN approaches. Additionally, the radial basis function of the SVR model outperformed the polynomial-based SVR approach, making it the recommended model for predicting the parameters of protective spur dikes.

1.3 Riverbed Material and Sediment Transportation

1.3.1 Riverbed Material

Sediment transportation, bed material, and grain size distribution of riverbeds are other essential and effective scour-related criteria. Understanding riverbed material and sediment transportation is crucial in predicting and mitigating scour phenomena, particularly around hydraulic structures such as bridge piers and abutments. Sediment is defined as solid particles created by the disintegration process of organic and inorganic materials (Bortone, 2006). These particles can be transported by water, wind, glaciers, and other natural causes and can be found in diverse shapes and sizes. The type and characteristics of riverbed material play a significant role in the scour process. Riverbeds typically comprise sediments ranging from fine silt and clay to larger sand, gravel, cobbles, and boulders. The composition and cohesion of these materials determine their susceptibility to erosion(Montgomery et al., 2000).

Fine Sediments (Silt and Clay) are small and cohesive, making them more resistant to initial erosion, but they can be transported over long distances once entrained. Fine sediments can form a protective layer that can resist scouring until the shear stress exceeds a certain threshold. Coarse Sediments (Sand, Gravel, and Cobble) are non-cohesive and more easily eroded and transported by flowing water. The critical shear stress for these particles' erosion is lower than cohesive sediments. Larger particles like gravel and cobbles are more resistant to movement but can cause significant scour when mobilized (Breusers & Raudkivi, 2020). Riverbeds often have stratified layers of different sediment types. The top layers might be finer sediments, while deeper layers consist of coarser materials. This stratification affects how scour develops, as finer materials are eroded first, exposing coarser, more resistant layers underneath (Melville & Coleman, 2000).

1.3.2 Sediment Transportation

Study sediment transportation includes terms such as entrainment, deposition, critical shear stress, suspended load transport, bed shear stress, settling velocity, incipient motion, and sediment transportation rate. Entrainment is when turbulent flow removes the sediment from the top of the riverbed and carries it into suspension. It happens when the bed shear stress exceeds a threshold value (critical shear stress). After the entrained phase, the sediment is carried by the water flow within a particular height overhead of the riverbed, known as the suspended load transport. Deposition occurs when suspended sediments are settled in the riverbed due to gravity, buoyancy, and friction (Bortone, 2006).

Bed shear stress provides an index of fluid force per unit area on the stream bed, which has been related to sediment transport in several theoretical and empirical researches. Bed shear stress and shear velocity are essential parameters in river investigation to estimate the transport rate, scour, and deposition (Wilcock et al., 1996). The moment where the shear forces overcome protective forces (inertia, friction), known as the moment of incipient motion, is the start of sediment movement (Kanellopoulos, 1998). The threshold is the two forces equivalent to the directive forces, balancing the resisting forces (Wiberg & Smith, 1987). Generally, it can be categorized into bed load, suspended load, and dissolved load, each interacting differently with hydraulic structures (Yang et al., 2003).

Bed load consists of particles that roll, slide, or bounce along the riverbed. This type of transport is dominant for larger, heavier particles such as gravel and cobbles. The movement of bed load is a primary mechanism of local scour around bridge piers and abutments, where high flow velocities can mobilize these particles and create scour holes (Chiew, 1984). The suspended load consists of finer particles like silt and clay in the water column. These particles are transported over longer distances and can contribute to sedimentation downstream. Suspended load plays a crucial role in the overall sediment budget of a river system and can influence the extent of scour by altering sediment availability (Lewis, 1998). The dissolved load includes minerals and organic matter dissolved in the water. While it does not directly contribute to scour, changes in dissolved load can affect water chemistry and the deposition of sediments, indirectly influencing scour processes (Liu, 1998).

1.3.3 Literature Review

Shields (1936) was one of the pioneering scholars who identified the relationship between hydraulic parameters and sediment characteristics in explaining the conditions for incipient motion of bed material and established that sediment is about to be mobilized by water flow. This condition introduces the Critical Shields Value (τ_c) and the Shear Reynolds Number (R_e). The relationship between these two parameters is depicted in the Shields diagram (Figure 1.6).

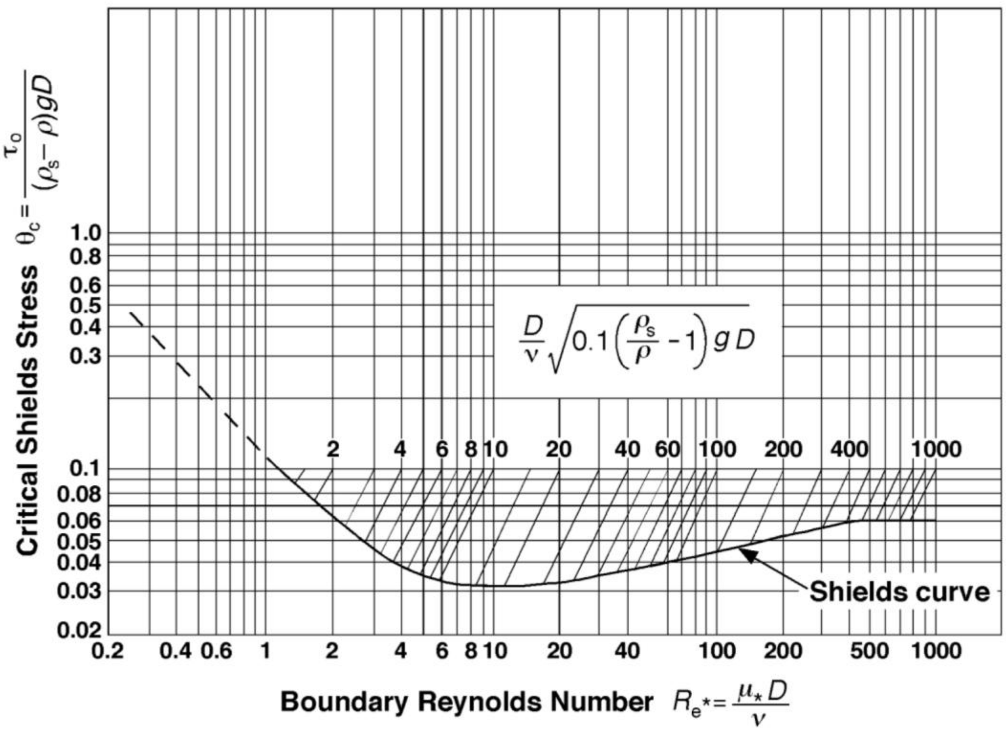

Figure 1. 6:The Shield's Diagram (Schwimmer, 2006)

Shear stress and shear velocity in the riverbed are essential parameters in river research to calculate sediment transportation, deposition, and different types of scouring (Wilcock, 1996). Accurate estimation and calculation of these variables are complex processes, especially in the compound flow of natural rivers. Therefore, many scholars have focused on this topic, such as Prandtl tubes (Ahmed & Rajaratnam, 1998) and shear plates (Rankin & Hires, 2000). Dietrich and Whiting (1989) conducted an experimental study to measure shear stress directly. Afterward, many others also investigated this topic (Cardoso et al., 1991; Haizhou & Graf, 1993; Tsujimoto et al., 1990).

It is noted that one of the main reasons for bridge failure is local scour around its piers and abutments (Dey & Barbhuiya, 2005; Melville et al., 2002; Namaee & Sui, 2019b; Wu, Peng, et al., 2014). Local scour can be categorized into clearwater and live-bed scour groups (Chabert &

Engeldinger, 1956). Clearwater scour occurs when the upstream flow approaching the bridge piers or abutments carries no sediment. In contrast, live-bed scour happens when the flow contains a significant sediment load transported into the scour holes, while vortices within the scour remove sediments from the hole. Distinguishing between these two types of scour is essential because the temporal development of scour holes and the relationship between maximum scour depth and flow velocity depend on whether clearwater or live-bed scour occurs (Raudkivi & Ettema, 1983).

Chabert and Engeldinger (1956) illuminated that the clear water maximum scour depth is 10% greater than live-bed sour (Figure 1.7). Researchers observed that the equilibrium condition in clearwater scours is reached more slowly than the live bed scour (Kiraga & Popek, 2016). Moreover, after the complete development of the scour hole under clearwater conditions, the flow can no longer remove sediment from inside the hole. The armour layer (a layer of bigger particle size that protects the smaller ones beneath them from getting eroded) protects the river bed material from more erosion (Chee, 1982; Melville, 1984; Richardson & Davis, 2001). In investigating live-bed scour, scholars mainly focused on estimating and predicting maximum scour depth rather than the temporal development of the scouring equilibrium conditions (Chiew & Melville, 1987; Lim & Cheng, 1998; Melville, 1997).

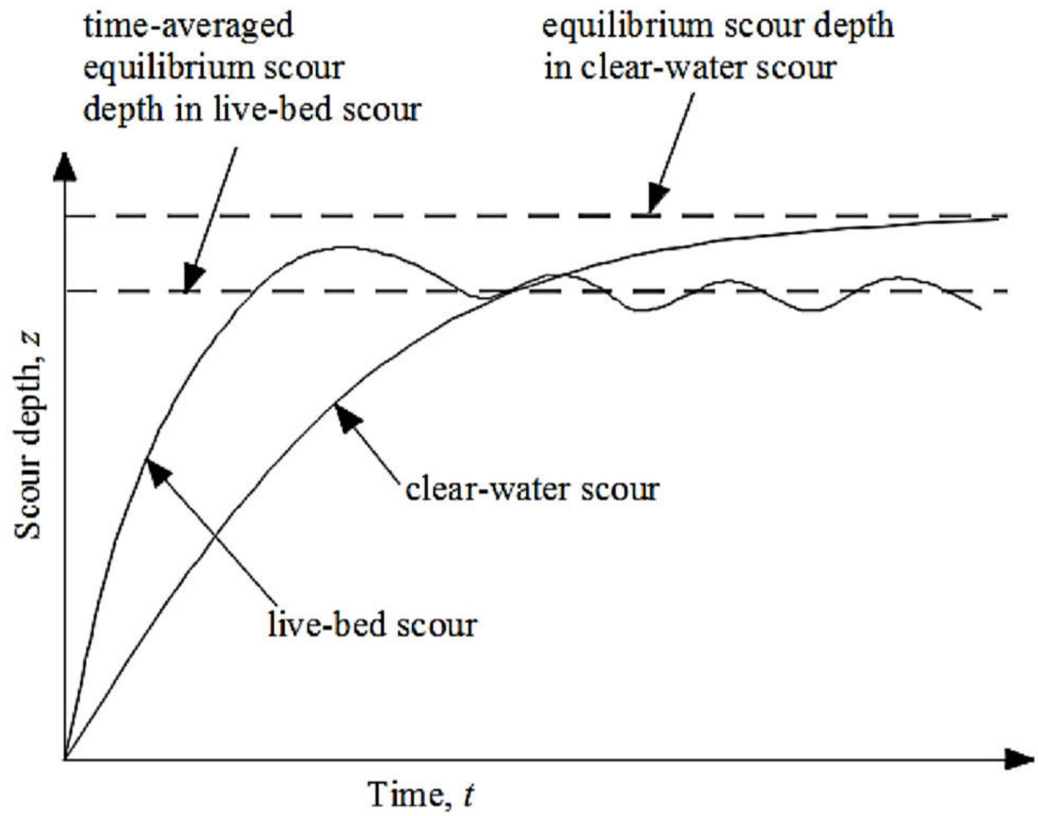

Figure 1. 7:Comparison of time development for clearwater and live-bed scour (Kiraga & Popek, 2016)

More research on live-bed scour specifies that the mean equilibrium value of scour holes is related to different types of river bedforms (Melville & Coleman, 2000; Sheppard & Miller Jr, 2006). There have been several studies on the incipient motion of uniform sediment (Aguirre-Pe et al., 2003; Beheshti & Ataie-Ashtiani, 2008; Buffington & Montgomery, 1997; Shvidchenko & Pender, 2000; Vollmer & Kleinhans, 2007). The movement of nonuniform sediment is more complex because it is affected by variables other than the approaching flow, such as grain shape, the median grain size of bed material, interactions between grains, and the formation of the river bed (Wu, Peng, et al., 2014). Accordingly, there are limited studies on nonuniform sediment transportation and incipient motion.

Haitao et al. (2008) investigated the incipient velocity of nonuniform sediment on a riverbed. The findings indicate that the incipient velocity of fine and coarse particles varies based on the type of bed material. For fine particles in nonuniform sediment, the incipient velocity is higher than in uniform sediment. Conversely, the incipient velocity for coarse particles is higher in uniform sediment than in nonuniform sediment. Additionally, they developed a formula for determining the incipient velocity of nonuniform sediment in rivers. Hirshfield (2015) demonstrated that sediment nonuniformity could significantly affect local scour, as an armour layer forms within the scour hole for nonuniform sediments. This armouring reduces the scour depth compared to that in uniform sediments.

1.4 Ice Cover

1.4.1 Ice Cover and Its Impact on Flow Dynamics

Ice formation on river surfaces and the associated challenges are complex topics. Many rivers freeze during winter, especially in northern regions, with ice cover persisting for several months. Ice cover on rivers and streams significantly affects hydraulic conditions and scour phenomena. The presence of ice changes the flow dynamics, alters sediment transport, and influences the stability of riverbanks and hydraulic structures (Shen, 2010). Ice cover can create several issues, such as ice blocking, flooding, interrupting the generation of a hydropower station, blocking rivers, and interfering with ecosystem balance. The river hydrology will be dramatically changed compared to open channel conditions such as velocity profile, bed shear stress distribution, and sediment transportation (Sui et al., 2000).

Ice cover can form in various ways, including frazil ice, anchor ice, and surface ice. The type and extent of ice cover affect the flow characteristics in several ways. Ice cover reduces the cross-sectional flow area of a river, leading to higher flow velocities under the ice. This increase in velocity can enhance the shear stress on the riverbed, potentially increasing scour around structures such as bridge piers (Hicks, 2009). The presence of ice forces the water to flow in a more confined space beneath the ice cover. Flow redistribution can change the velocity profile and turbulence characteristics, impacting sediment transport and deposition patterns. Ice jams occur when floating ice accumulates and obstruct the flow. This obstruction can cause water levels to rise upstream and increase flow velocities downstream once the jam is released, potentially leading to significant scour events (Prowse & Beltaos, 2002).

1.4.2 Roughness Coefficient of Ice Cover

One of the critical factors in understanding the impacts of ice cover is the roughness coefficient of the ice cover, which plays a pivotal role in determining flow resistance and subsequent scour. The roughness coefficient, often represented as Manning's coefficient quantifies the resistance exerted by the ice cover on the flowing water. The roughness of ice cover depends on several factors, including the type of ice and surface texture. The two common types of ice cover are smooth and rough. Smooth cover is formed under calm conditions, and smooth ice has a lower roughness coefficient, leading to less flow resistance. However, it can still significantly alter flow dynamics due to the reduced flow area (Sui et al., 2005). Rough cover is formed under turbulent or windy conditions, and Rough ice includes features such as pressure ridges and hummocks. These features increase the roughness coefficient, leading to higher flow resistance and more complex flow patterns beneath the ice (Hicks & Beltaos, 2008).

The roughness coefficient of the ice cover increases the overall flow resistance, which can reduce flow velocities under the ice but increase water levels upstream. The increased resistance can lead to higher shear stress on the riverbed, affecting sediment transport and potentially enhancing scour around structures (Sui et al., 2006). The roughness coefficient of ice cover is typically measured through field observations and empirical correlations. Various studies have provided different values for Manning's coefficient based on ice type and conditions, emphasizing the need for site-specific assessments. The flow under ice cover conditions can be divided into two portions: the upper part, mainly influenced by the ice cover, and the lower part, which is affected by the riverbed (Sui et al., 2010). The maximum velocity location depends on the roughness coefficient of the two boundaries and shifted toward the smoother edge. Therefore, the roughness coefficient is essential in the flow velocity profile under ice cover (Ashton, 1986; Smith & Ettema, 1995; Sui et al., 2010; Sui et al., 2000).

1.4.3 Scour Phenomena Under Ice Cover

The increased flow velocities under ice cover can enhance local scour around bridge piers and abutments. The confined flow and increased shear stress can further erode the riverbed material, deepening scour holes. Ice cover can also contribute to general scour by altering the sediment transport capacity of the river (Sui et al., 2010). The changed flow dynamics can lead to uneven sediment deposition and erosion patterns, affecting the stability of the riverbed over broader areas. Ice jams can cause sudden changes in water levels and flow velocities. When a jam releases, the downstream surge can significantly increase scour, posing risks to hydraulic structures and riverbanks. Rapid changes in flow conditions during ice jam events are critical to understanding and mitigating scour risks (Prowse & Beltaos, 2002).

Ice cover and the roughness coefficient of ice cover are essential factors in understanding and managing scour phenomena in rivers and streams. The presence of ice alters flow dynamics, increases flow resistance, and impacts sediment transport, leading to changes in velocity structure and distribution. This change in velocity profile increases kinetic energy at the riverbed and causes extra bed shear stress (Sui et al., 2010; Wang et al., 2008). These alterations would affect the hydraulic structures and local scour around bridge sites and can damage them significantly. Accurate assessment and consideration of these factors are crucial for designing and protecting hydraulic structures in cold regions. Collapsing of a bridge over the White River in Ontario was one of the first bridge failures due to the scour under the ice cover (Zabilansky, 1996). Since Ice-covered rivers play significant roles in the safety of bridges and other hydraulic structures, the following section will present some of the most critical research on this topic.

1.4.4 Previous Researches Overview

Lau and Krishnappan (1985) investigated sediment transport under ice-covered flows using the k-ε model, demonstrating that this model effectively predicts average flow properties with sufficient accuracy. The results indicate that ice formation on the river surface can lead to increased depth, reduced average velocity, and significant changes in bed shear stress, significantly impacting sediment transport. Subsequently, many scholars have considered ice-covered flows to have a double-wetted perimeter, where the flow is divided at the point of maximum velocity. However, Smith and Ettema (1997) discovered that the assumption of two layers is inadequate for describing flow resistance and sediment transportation, especially in dune regimes.

Zabilansky (1996) investigated ice force at bridge settlement and compared it to open flow conditions. His research shows that although the change in velocity profile affected the scour, a considerable amount of scouring happens in the initial phase of a breakup of the ice on the surface, emphasizing the importance of the roughness coefficient. Muste et al. (2000) declare that a rough cover in a flume reduces the overall sediment transport rates but amplifies the sediment suspension loads. Ackermann et al. (2002) conducted an experimental study on local scour around bridge piers under three different flow surface conditions (open, Smooth, and rough) with uniform sand. They explained that the cover condition generally creates a larger scour depth for different flow velocities. However, the scour development pattern remains unchanged regardless of water surface conditions.

As different scholars have done more research, Hains (2004) tried to find the relation between different ice cover roughness and shear stress. He concluded that the roughness of the cover considerably affects bed shear stress, and the increase of shear stress will result in amplified bed erosion and scour depth. Furthermore, Hains and Zabilansky (2004) illustrated that a rougher cover can push the maximum velocity toward the bed, increasing shear stress on the river bed and enlarging the scour hole. They also presented that ice cover can increase scour depth at bridge piers and abutments by 10 to 35 percent. Zabilansky et al. (2006) explained that ice cover roughness can be increased under different conditions, such as dynamic evolution in steep or wave streams, which occurs in narrow rivers while ice cover still exists on the surface. In this regard, Beltaos (2007) concluded that differences in the thickness of an ice jam can lead to variations in sediment transport amount and significantly affect general and local scour around bridge piers, abutments, and other hydraulic structures.

Laboratory experiments on the incipient motion under ice cover demonstrated the role of flow velocity and critical shear Reynolds stress (Wang et al., 2008). It was concluded that increasing water depth under the ice cover requires a higher flow velocity for the incipient motion of bed material. They explained that by increasing the roughness coefficient of ice cover, the location of maximum flow moves even more toward the river bed. Also, it should be considered that the roughness of ice cover changes with the melting down of ice at the beginning of the spring (Wang et al., 2008). Sui et al. (2010) conducted experiments on the incipient motion of frazil particles under ice cover, demonstrating that smaller sediment sizes in bed material require less critical dimensionless shear stress to initiate motion. Ettema and Kempema (2012) illuminate that suspended sediment loads during breakup are nearly 10 times bigger than ice cover conditions. Moreover, they explained that the magnitude of sediment transportation and deposition is the function of water depth, ice thickness, and ice roughness.

1.5 Research Objectives

One of the most critical river structures is the bridge. Scour is a significant issue affecting the stability and longevity of bridges. The leading cause of bridge failure is local scour at bridge abutments and piers (Wardhana & Hadipriono, 2003). Local scour at bridge abutments is particularly concerning as these structures are more vulnerable than piers (Kandasamy & Melville, 1998). According to the US Federal Highway Administration (1973), 383 bridges failed over various rivers, with 72% of these failures involving damage to abutments and 25% to piers (Richardson & Davis, 2001). Consequently, further investigation into local scour around abutments is essential. Among the various countermeasures to mitigate scour, spur dikes have shown promising results. Spur dikes, by altering flow patterns and reducing flow velocities, can effectively minimize erosion around abutments. This experimental research project aims to enhance the understanding of how spur dikes influence scour phenomena and to develop optimized configurations for their implementation under diverse hydraulic conditions.

The study will address critical aspects such as the velocity profile around spur dikes, local scour at dikes and abutments, and the optimal design and configuration of spur dikes to reduce scour at the downstream abutment. By combining physical flume experiments with advanced measurement techniques, the research seeks to provide practical insights into effective scour mitigation strategies. The following objectives elaborate on the specific goals of the study and the methodologies to be employed. These objectives aim to enhance the understanding of how spur dikes influence scour phenomena around bridge abutments to develop more effective scour mitigation strategies, ensuring the stability and longevity of hydraulic structures.

1.5.1 Objective One: Analysis of Flow Fields and 3D Velocity Distribution Around Spur Dike

Understanding the Flow fields, velocity profile, and 3D velocity distributions around spur dikes is crucial for predicting how they influence flow patterns and sediment transport. Velocity profiles indicate how water speed changes at different points around the dike, directly affecting the erosion and deposition of sediments. This objective involves capturing detailed flow dynamics using advanced measurement techniques like ADV. The study will focus on identifying the vortices and turbulence patterns generated by spur dikes, which are critical in determining scour zones. By examining these flow characteristics under different flow rates and sediment conditions, the research aims to comprehensively understand flow interactions that influence scour. This information is vital for improving the design and placement of spur dikes to maximize their protective benefits. This objective will be assessed in chapter Three of this experimental research.

1.5.2 Objective Two: Investigation of the Impact of Ice Cover and Roughness Coefficient on the Scour Process

Ice cover significantly impacts hydraulic conditions and scour processes by altering flow dynamics, increasing flow resistance, and affecting sediment transport. This objective aims to study how ice cover and its roughness coefficient influence the velocity distribution and sediment movement around spur dikes and abutments. The research will employ two different models of Ice cover to analyze the effects of different surface roughness (smooth and rough) on scour depth and patterns. Understanding these impacts is essential for designing effective scour mitigation strategies in cold regions with common ice cover. This experimental research will assess this objective in chapters three, four, and five.

1.5.3 Objective Three: Investigation of Local Scour at Spur Dikes with different alignment angles and flow surface condition

Local scour refers to erosion at the base of structures due to flowing water. This objective focuses on understanding how spur dikes' different configurations (Alignment angles) affect the local scour around them. The study will use scaled physical models in flume experiments to replicate real-world conditions. Three different bed materials will be tested to observe how they influence scour depth and extent. The research aims to develop predictive models for scour depth and distribution by analyzing scour patterns under different flow rates and water levels. This information is crucial for designing effective scour protection measures. This objective will be assessed in chapter four of this experimental research.

1.5.4 Objective Four: Analysis of Effects on Sediment Removal and Deposition

To assess the effects of spur dikes on sediment removal and deposition throughout the flume. Spur dikes influence sediment transport dynamics, leading to changes in sediment removal and deposition patterns. This objective focuses on understanding how spur dikes alter these patterns across the flume. The study will model the sediment deposition dunes using the Surfer 2D & 3D data modelling and mapping to plot the deposition patterns and locations. The findings will provide insights into how spur dikes can be designed to promote beneficial sediment deposition and reduce harmful erosion, ensuring the stability and longevity of riverbanks and hydraulic structures. This experimental research will assess this objective in chapters three, four, and five.

1.5.5 Objective Five: Development of a Predictive Formula for Maximum Scour Depth at Spur Dike

To develop a predictive formula that estimates the maximum scour depth at spur dikes under different alignment angles, flow surface conditions, and flow characteristics. Accurately predicting the maximum scour depth is essential for designing effective scour protection measures. This objective involves conducting comprehensive experiments and data analysis to derive a formula incorporating various factors influencing scour depth. The study will consider different alignment angles of spur dikes, flow surface conditions (such as water depth and velocity), and sediment characteristics. Dimensional analyses will be employed to develop a robust predictive model. This formula will help engineers and researchers design spur dikes that mitigate scour risks under diverse hydraulic conditions. This experimental research will assess this objective in chapters four and five.

1.5.6 Objective Six: Optimization of Spur Dike Configuration to Protect Abutment

To determine the optimal distance and orientation angle of non-submerged impermeable spur dikes for minimizing local scour at bridge abutments under various flow conditions, water surfaces, and bed materials. The configuration of spur dikes, including their distance from the abutment and their orientation angle, significantly affects their effectiveness in reducing scour. This objective involves conducting a series of experiments to test different configurations. The research will explore a range of distances and angles to identify the setup that provides maximum protection against scour at abutment. The goal is to develop design guidelines that specify the best practices for installing spur dikes to protect abutments under various environmental conditions. This objective will be assessed in chapter five of this experimental research.

1.6 Research Innovation

This experimental research focuses on using spur dikes as a countermeasure for local scour at abutments. The study aims to determine the optimal setup for the dike, including the best distance and orientation angle, to minimize local scour at the abutment. Additionally, the research seeks to investigate methods to reduce local and contraction scour at the dike, ensuring sustained protection for the abutment. A comprehensive analysis of the flow field, 3D velocity distribution, and scour patterns around dikes with varying alignment angles has been conducted to achieve this goal. The innovations of this experimental research are as follows:

1.6.1 Empirical Formula for Scour Depth

One of the significant innovations of this study is the development of an empirical formula to estimate scour depth at the spur dike under ice-covered conditions. This formula was derived using dimensional analysis, considering parameters like flow velocity, sediment size, alignment angles, and ice cover characteristics. The empirical formula enhances predictive capabilities, allowing engineers to estimate potential scour depths more accurately in cold regions with prevalent ice cover. This predictive tool is crucial for designing and implementing effective scour mitigation strategies.

1.6.2 Comprehensive Parameter Analysis

The study uniquely combines the analysis of multiple parameters simultaneously to understand the scour process in detail. The parameters investigated include velocity profiles, which are used to understand how flow velocity changes in the presence of spur dikes and ice cover. Reynolds Shear Stress: measuring the shear stress exerted by the flowing water on the riverbed, which is a critical factor in sediment transport and scour. Turbulent Kinetic Energy (TKE): Evaluating the turbulence levels in the flow, which influence the erosion and deposition processes.

Non-uniform bed material: Modeling real-life river conditions using three different non-uniform sediments to investigate the impact of varying sediment sizes. Identifying specific scour patterns and extents around the dike and abutment using Surfer 3D modelling software.

1.6.3 Application of Non-Submerged Spur Dikes

The research demonstrated the effectiveness of non-submerged impermeable spur dikes as a countermeasure for local scour at bridge abutments. Unlike submerged dikes, which can be less effective under high-flow conditions, non-submerged dikes maintain their protective function by altering flow patterns and reducing the flow velocity near the abutment. This study showed that non-submerged dikes are particularly effective in diverse flow conditions, including those with ice cover. This finding is critical for designing more resilient and effective scour protection measures.

1.6.4 Optimal Spur Dike Design

Identifying the optimal distance and orientation angle of spur dikes relative to the abutment was another critical contribution of this research. By systematically varying these parameters, the study found configurations that minimized local scour at the abutment. This knowledge helps design spur dikes that protect abutments and do so efficiently with minimal impact on the surrounding environment. Optimal design parameters ensure that spur dikes perform their protective role without causing excessive turbulence or sediment transport issues upstream or downstream.

1.6.5 Impact of Ice Cover on Scour Processes

The study's investigation into the impact of ice cover on protective spur dikes represents a novel contribution to the field. Ice cover significantly alters flow resistance and sediment transport dynamics. The research provides insights into how ice affects scouring by comparing open channel conditions with smooth and rough ice-covered conditions. Understanding these impacts is crucial for regions with seasonal ice cover, and infrastructure must be designed to withstand such conditions. The findings aid in predicting and managing channel bed erosion in cold regions, improving the design of structures to mitigate the impacts of ice cover effectively.

1.6.6 Innovative Experimental Setup

Using a large-scale outdoor flume, which resembles a natural stream environment, is an innovative aspect of this research. The dimensions of the flume (2 meters wide, 1.3 meters deep, and 38 meters long) allowed for realistic simulation of flow conditions and provided valuable data that small-scale laboratory experiments might not capture. This realistic setup enhances the findings' validity and applicability to real-world scenarios.

1.7 Thesis Structure

Chapter One provides a comprehensive overview of the research problem, underscoring its critical importance in the fields of hydraulic engineering and bridge safety. It delineates the specific objectives of the study, followed by an exhaustive review of the existing literature on scour, spur dikes, riverbed material, sediment transport, and ice cover. The chapter concludes by identifying gaps in the current body of knowledge and introducing the novel contributions of this research, including the development of new empirical formulas, in-depth parameter analysis, and the innovative experimental setup employed in the study.

Chapter Two details the experimental site and setup, focusing on the large-scale hydraulic flume and the specific configurations of spur dikes and abutments utilized in the research. It further elaborates on the sophisticated measurement equipment employed, such as instruments for quantifying flow rate, water depth, velocity components, and turbulence intensities. The chapter concludes with a meticulous description of the data collection procedures, ensuring the repeatability and transparency of the research methods.

In bridge construction, a Fracture Critical Member (FCM) is a structural element whose failure could precipitate a catastrophic collapse or significant structural compromise of the bridge. The integrity of FCMs is paramount, as they are critical to the structure's overall stability. Consequently, these members are subject to stringent design criteria, rigorous inspection protocols, and ongoing maintenance to ensure their resilience. The primary objective of this research is to investigate the efficacy of spur dikes in mitigating scour at bridge abutments. In this context, the spur dike is identified as FCM. Given that in this research, the spur dike is designed to protect the abutment from scour and prevent potential failure. The failure of the spur dike could intensify scour at the abutment, compromising its foundation and potentially leading to structural failure. Consequently, ensuring the stability and longevity of the spur dike is of paramount importance.

Chapters Three and Four are dedicated to a comprehensive analysis of the turbulence structure and scour patterns around the spur dike to ensure its stability and durability. **Chapter Three** investigates the velocity fields and turbulence structures in relation to scour and hydraulic structures. It provides a detailed account of the experimental setup and data collection methods specific to this phase of the research. The results section presents an analysis of the streamwise, lateral, and vertical velocity components under varying conditions, along with a discussion on turbulence intensities and Reynolds shear stress, and their implications for scour dynamics. **Chapter Four** focuses on the study of channel deformation and scour morphology under different alignment angles and ice cover conditions. It provides a thorough description of the experimental methodology and materials, followed by the presentation of results concerning vortex systems, scour morphology, and maximum scour depth. The chapter summarizes the insights gained regarding channel deformation and their implications for scour mitigation.

Chapter Five examines the critical factors influencing local scour at abutment, with particular attention to the alignment of spur dikes and the roughness of ice cover. It details the experimental procedures, including site description, flume setup, and data collection methods. The results section offers a comparative analysis of maximum scour depth around abutments with and without the application of protective spur dikes, discussing how varying alignment angles and ice cover conditions impact scour patterns. The chapter concludes by highlighting key findings on the effectiveness of different scour mitigation strategies.

Chapter Six is the final chapter, and it synthesizes the key findings of the research, emphasizing their contribution to understanding scour dynamics and developing mitigation strategies. It addresses the limitations encountered during the study, such as those related to experimental design or data collection, and proposes directions for future research, identifying potential areas for further exploration based on the findings of this thesis.

2 CHAPTER TWO: Materials and Experimental Procedures

2.1 Site Description

This experimental study was conducted at the Quesnel River Research Center (QRRC) in Likely, British Columbia, Canada. The QRRC provides a unique setting for research due to its access to a large-scale outdoor hydraulic flume. This flume is specifically designed to replicate the natural dynamics of river systems, allowing for studying complex hydrodynamic and sediment transport processes under controlled conditions. Experimental studies are typically conducted in small indoor hydraulic flumes due to the high construction costs associated with large outdoor flumes. Small-scale flumes generally offer a limited range of flow depths and discharge, whereas larger flumes provide various hydraulic parameters that closely resemble actual river conditions. However, working with equipment and collecting accurate data in large-scale flumes presents significant challenges (Namaee et al., 2017). The QRRC flume, designed to replicate the natural dynamics of river systems, measures 38.2 meters in length, 2.0 meters in width, and 1.3 meters deep (Figure 2.1). The flume's longitudinal bed slope is set at 0.2%, closely mimicking the gentle gradients in natural riverbeds. This slight slope ensures a realistic flow velocity and sediment transport behaviour, which is crucial for accurately simulating riverine conditions.

An essential feature of the flume is the upstream holding tank, which has a capacity of 90 cubic meters (dimensions: 40 meters in length, 2 meters in width, and 1.3 meters in depth). This tank ensures a consistent and controlled water supply throughout the experimental runs. The tank is equipped with three valves that allow for precise control of flow rates, facilitating a range of experimental conditions. The study can simulate different discharge scenarios by adjusting these valves, from low-flow conditions to high-flow events. Additionally, a roof covers the entire flume section, protecting it from environmental factors such as precipitation, wind, and debris, thereby ensuring the consistency and reliability of the experimental conditions.

Within the flume, two sandboxes are constructed to simulate riverbed conditions. These sandboxes are placed 10.2 meters apart and provide a controlled environment for observing sediment dynamics and scour development around spur dikes and abutments. The upstream sandbox measures 5.6 meters in length, while the downstream sandbox is slightly longer at 5.8 meters. Both sandboxes are 2 meters wide and 0.3 meters deep (Figure 2.2). The sandboxes are filled with three types of natural sediments, each with different median grain sizes (D_{50}) of 0.48

mm, 0.60 mm, and 0.90 mm, with respective standard deviations of 1.97, 2.39, and 1.41. Figure 2.1 illustrates the grain size distribution of the bed materials.

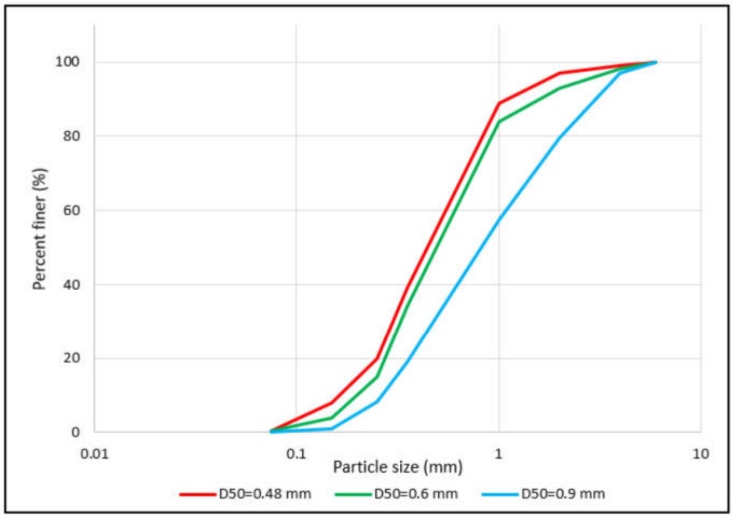

Figure 2. 1:Grain size distribution of the bed materials

Plexiglass sidewalls are installed on one side of each sandbox to enable detailed visual observation and monitoring of the scouring process. The average density of the sediments used is approximately 1.7 g/cm³, closely matching the properties of natural riverbed materials.

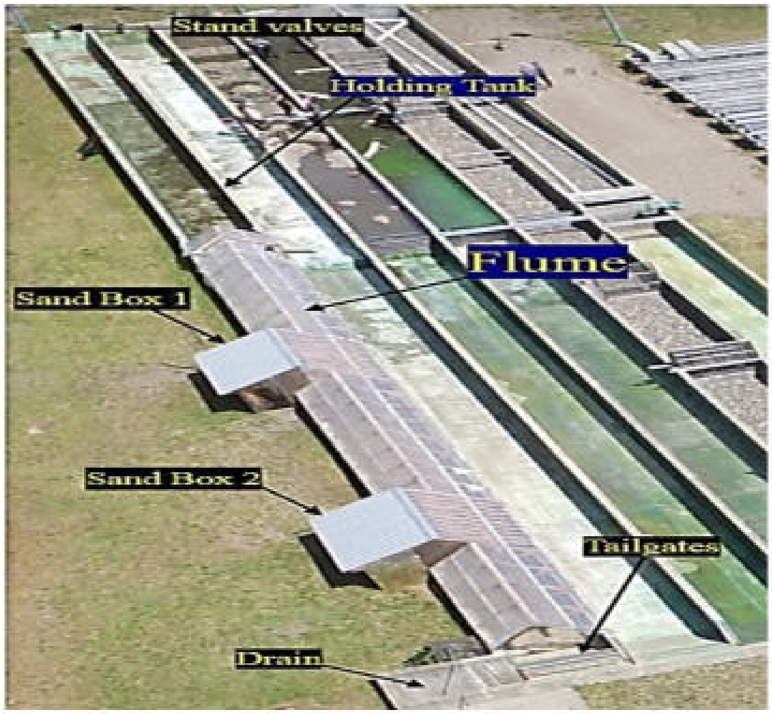

Figure 2. 2: Overview of Flume

2.2 Experimental Setup

The flume is equipped with a tailgate at the downstream end to control water depth and flow velocity. Three different tailgate heights (10 cm, 20 cm, and 30 cm) are used to create varying flow depths, directly influencing flow velocities and scour patterns around the dike and abutment. Adjusting the tailgate can generate various hydraulic conditions with different flow depths. This ability to control water depth and flow velocity is critical for simulating real-world conditions and understanding how different hydraulic parameters affect sediment transport and scour.

The experiment involves installing spur dikes and abutments in each sandbox to investigate the local scour surrounding the spur dike and the influence of the dike on scour reduction abutment. The spur dikes are constructed from marine-grade plywood, chosen for its durability and resistance to water. Each dike measures 80 cm in height, 5 cm in width, and 50 cm in length, with 30 cm of its height buried in the sand bed, leaving 50 cm exposed to the flow. This setup allows the dikes to interact directly with the flowing water, replicating real-world conditions where such structures are used to manage river flow and prevent erosion. The abutments are fabricated from galvanized plates with dimensions of 20 cm in width, 80 cm in height, and 40 cm in length. Abutmets are placed downstream of the dikes at 25 cm and 50 cm distances. The dikes are tested at three alignment angles relative to the downstream abutments: 90º, 60º, and 45º. These configurations correspond to blockage ratios of 25%, 20%, and 15%, respectively, allowing researchers to study how different orientations and positions of the spur dikes affect flow patterns and sediment transport around the abutments.

Three distinct experimental layouts were employed. The first setup aimed to investigate the flow field, 3D velocity distribution, and local scour around the spur dike. In this configuration, the dike was installed in the center of each sandbox at varying alignment angles (90º, 60º, and 45º) (Figure 2.3). The second setup focused on exploring the application of spur dikes in reducing scour at abutments. For this purpose, the dike was positioned upstream of the abutment at distances of 25 cm and 35 cm, with different alignment angles (Figure 2.4). The final setup examined abutment scour without protective measures against rapid flow and local scour. In this scenario, the abutment was installed in the middle of the sandbox without any upstream dike. All experimental layouts are depicted in Figure 2.5.

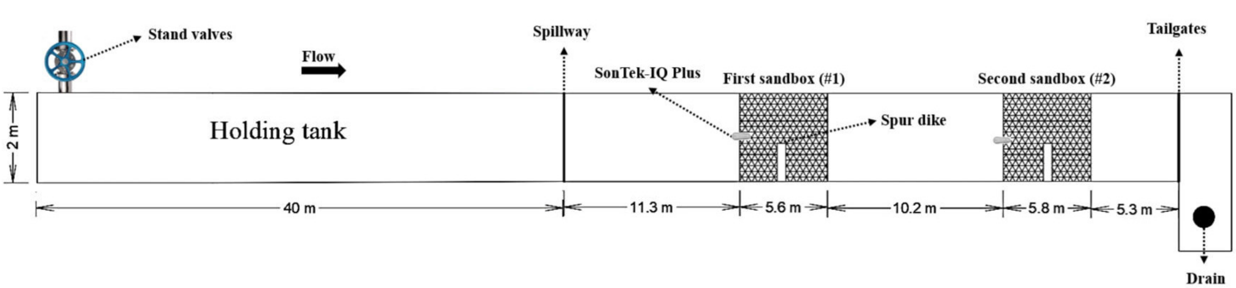

(a) Plan view

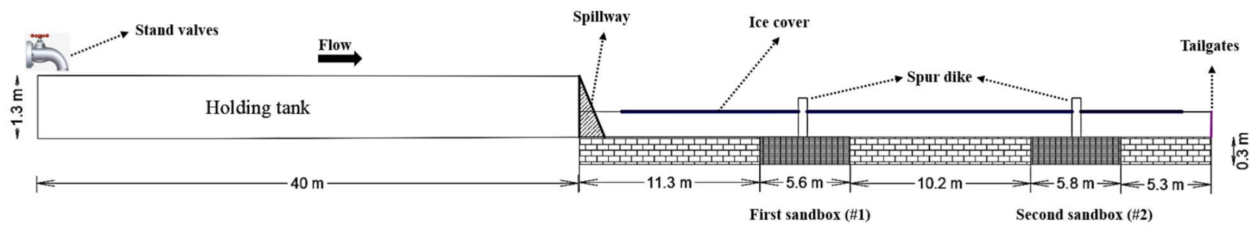

(b) Vertical view

Figure 2. 3:Experimental Flume, Dike layout: (**a**) Plan view; (**b**) Vertical view

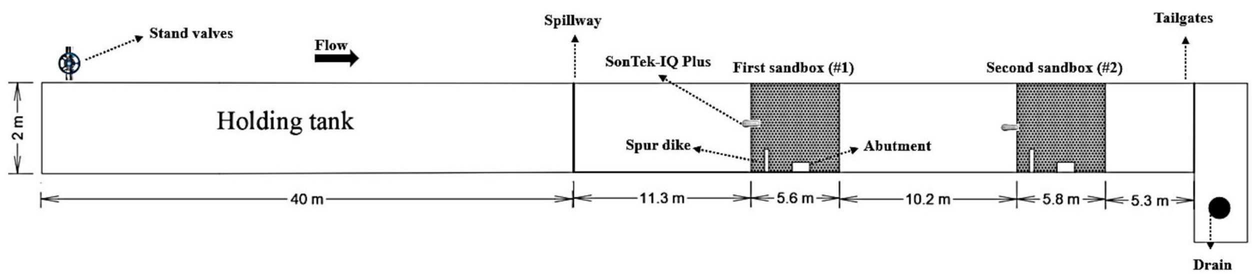

(a) Plan view

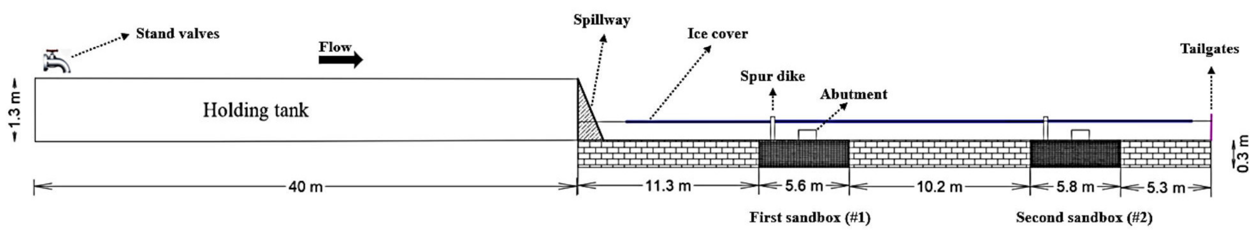

(b) Vertical view

Figure 2. 4:Experimental flume, Protective Dike layout: (a) Plan view, (b) Vertical view

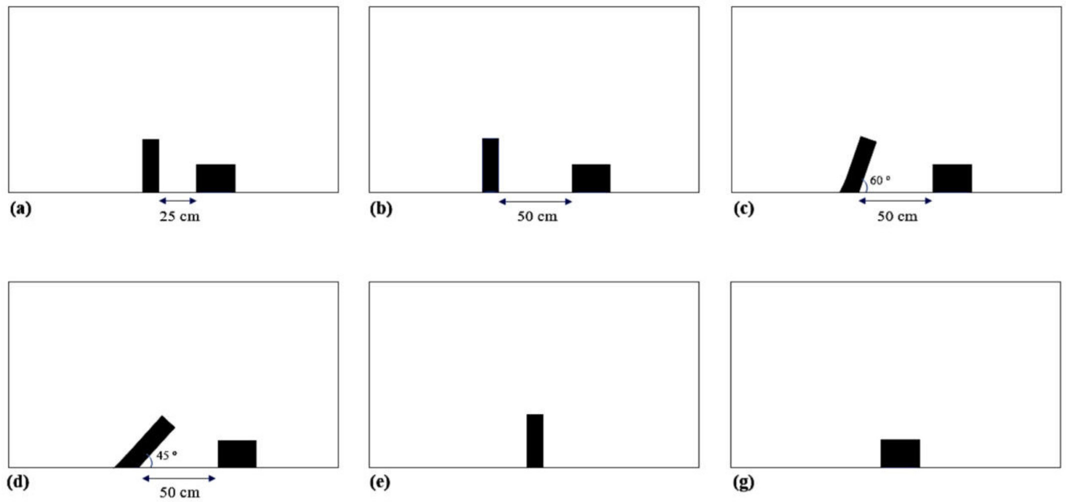

Figure 2. 5:Different setups of the experiment

Styrofoam panels are used to simulate the effects of ice cover on flow dynamics and scour processes. Two types of ice covers are tested: smooth and rough. Untreated Styrofoam panels represent the smooth ice cover, mimicking the sheet ice common in natural rivers during winter. The rough ice cover is created by attaching 2.5 cm^3 Styrofoam cubes to the underside of the panels, replicating the roughness and complexity of ice jams. Sixteen panels, each measuring 1.99 meters by 2.4 meters, are employed to cover the entire flow surface within the flume (Figure 2.6). This setup allows for a detailed examination of the impact of ice cover roughness on hydraulic conditions and sediment transport. The smooth ice cover simulates the uniform surface of natural sheet ice, while the rough ice cover replicates the irregular surface of ice jams formed by accumulated ice floes. The distinction between these two ice cover types is crucial for understanding how different surface roughnesses affect flow dynamics and scour processes. With its irregular surface, the rough ice cover introduces additional complexity to the flow patterns, providing valuable insights into how natural ice formations impact river hydraulics.

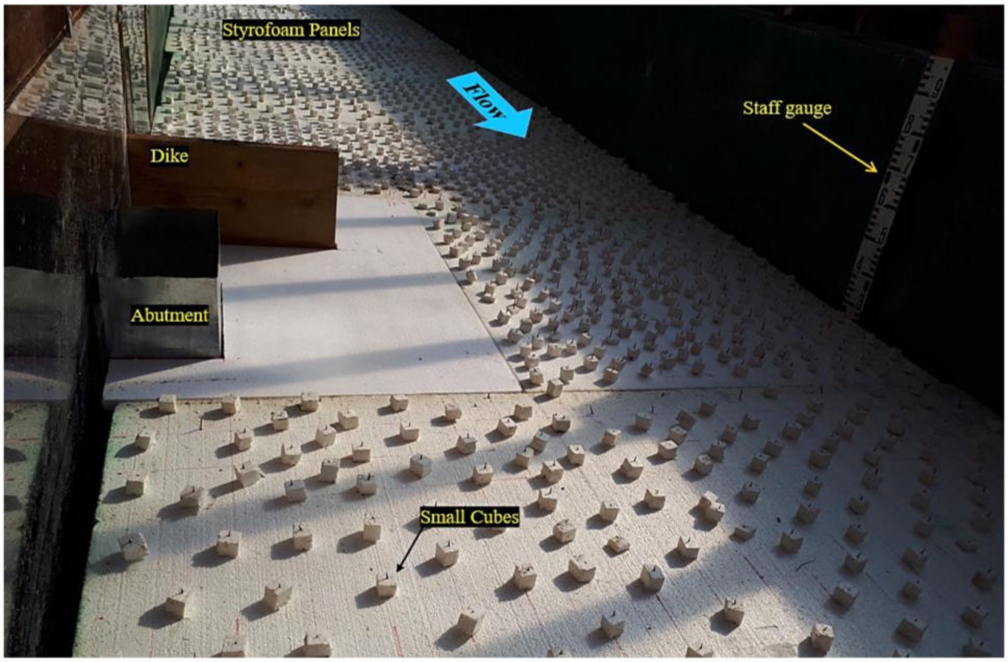

Figure 2. 6:An experimental run under smooth cover condition

2.3 Measurement Equipment

Accurate and continuous data collection is crucial for understanding the interactions between hydraulic structures, flow dynamics, and scour processes. The SonTek-IQ Plus is a key instrument used for flow monitoring in the flume. This advanced acoustic Doppler device is specifically designed for precise flow measurement in natural rivers and controlled environments such as hydraulic flumes. It features six sensors: four velocity beams and two additional beams for water level and vertical acoustic measurements. The four-velocity beams are oriented to measure flow velocities along the longitudinal and latitudinal axes, ensuring comprehensive coverage of the flow field. This multi-beam setup allows for accurately determining flow velocity profiles, which is essential for understanding spatial variations in flow speed and direction. The vertical acoustic beam and the pressure sensor measure water depth accurately, providing critical data for calculating flow discharge and depth-averaged velocities (SonTek, 2017). The data collected by the instrument are processed using SonTek software, which utilizes advanced post-processing functions to offer detailed insights into the flow and volume of data. According to the SonTek-IQ Series User's Manual, the data collected by the SonTek-IQ Plus has a measurement error margin of 1% within the specified measurement range (SonTek, 2017).

An Acoustic Doppler Velocimeter (ADV) measures the three-dimensional flow velocities around the spur dikes and abutments. The ADV is ideal for capturing detailed flow structures and turbulence characteristics, essential for understanding the dynamics within scour holes and around the spur dike. This instrument provides high-frequency velocity measurements, which is crucial for analyzing fine-scale variations in flow speed and direction (Sontek, 1997).

The ADV setup includes a probe with a transmitter and three receivers, creating a sampling volume located 10 cm beneath the probe head. This configuration allows for precise measurements of instantaneous velocity components within a cylindrical sampling volume. To ensure data reliability, the signal-to-noise ratio (SNR) and correlation (COR) are maintained above 15 and 70%, respectively. These parameters are vital for filtering out noise and ensuring the consistency of the measured velocity data (Wahl, 2000).

Data collected by the ADV are processed using WinADV software, which filters the data based on SNR and COR values to remove spikes and ensure accuracy. The sampling rate of the ADV is set at 25 Hz, with measurements taken for 120 to 150 seconds at each location to capture a representative dataset. The ADV is positioned at various points within the flume, including the bottoms of scour holes, around the spur dikes, and within the main flow paths, to provide a comprehensive view of the flow field (Martin et al., 2002; Rehmel, 2007; Wahl, 2000).

2.4 Data Collection Procedures

Before each experimental run, several preparatory steps were undertaken to ensure that the conditions within the flume were consistent and controlled. The surfaces of the sandboxes are carefully levelled to ensure uniform starting conditions for the experiments. This is crucial for preventing any initial sediment movement and scour patterns that could arise from uneven surfaces. For ice cover experiments, Styrofoam panels are gently placed on the bottom of the flume. These panels simulate natural sheet ice or ice jams, depending on whether smooth or rough panels are used. These panels are placed carefully to avoid disturbing the sediment bed and to ensure they float uniformly on the water surface once the flume is filled.

Once the preparatory steps were completed, Water was gradually fed into the flume from the upstream holding tank to prevent initial scouring around the spur dikes and abutments. This slow filling process helps maintain the stability of the sediment bed and the ice cover (if applicable) as the water level rises. The water flow was monitored continuously as it filled the flume. The flow depth is measured using staff gauges positioned at the midpoint of each sandbox and by using SonTek-IQ. After achieving the desired flow depth, the valves were adjusted to attain the target flow rate, ensuring alignment with the planned experimental conditions. Flow characteristics such as average approach velocity, Reynolds number, and vertical velocity profile were then calculated and monitored to confirm the development of fully turbulent flow. These steps were essential in maintaining a steady and consistent flow rate throughout the experiment, which is critical for accurately studying equilibrium scour processes.

Continuous monitoring during the experimental runs is essential for capturing the dynamic flow and sediment transport processes. Flow parameters, including depth and velocity, are continuously monitored using the SonTek-IQ Plus. This device provides real-time data on the flow conditions, ensuring the flow remains within the desired parameters throughout the experiment. The SonTek-IQ Plus is strategically positioned in front of each sandbox to capture the flow conditions directly affecting the experimental setups (Figure 2.7). The Acoustic Doppler Velocimeter (ADV) was used to measure the flow velocities around the spur dikes and abutments. The ADV is positioned at various locations within the flume to capture a comprehensive dataset of velocity profiles. Measurements are taken at different heights within the water column and various distances from the spur dike to provide a detailed view of the flow dynamics. Plexiglass sidewalls installed on one side of each sandbox allow for detailed visual observation and monitoring of the scouring process. These visual observations complement the quantitative data collected by the SonTek-IQ and ADV, providing a holistic view of the experimental conditions.

After each experimental run, several post-experiment procedures are carried out to preserve and analyze the scour patterns and sediment deposition. Upon completion of the experimental run, the flume was carefully drained to preserve the scour patterns. The draining process is done gradually to avoid disturbing the sediment bed and to maintain the integrity of the scour holes and deposition dunes formed during the experiment. The Styrofoam panels are carefully removed from the water surface for ice cover experiments. This step is performed cautiously to prevent any disruption of the scour patterns and sediment deposition. The geometries of the scour holes and deposition dunes are measured using precision callipers. These measurements are critical for quantifying the extent and dimensions of the scour hole and sediment deposition, providing valuable data for subsequent analysis. The data collected during the experimental run were processed using Surfer Golden Software to generate detailed 3D profiles and contour maps of the scoured regions. These visualizations help to understand the spatial distribution of scour and sediment deposition dunes, allowing for a comprehensive analysis of the experimental results.

To ensure the consistency and accuracy of the data, supplementary experimental runs are conducted with extended observation periods of 48 and 72 hours. These extended experiments confirm that equilibrium conditions are typically achieved within 24 hours, as no significant variations in scour depth are observed beyond this timeframe. The extended runs also help validate the robustness of the observed scour patterns and flow dynamics. To further validate the data, some of the experimental runs are repeated to ensure repeatability and consistency. The repeated experiments help verify that the observed scour patterns and sediment transport behaviours are consistent across different runs under the same conditions. This validation step is crucial for ensuring the experimental results' reliability and building confidence in the conclusions drawn from the data.

2.5 Bibliography

Ackermann, N., Shen, H. T., Olsson, P., & Squire, V. (2002). Local scour around circular piers under ice covers. Proceeding of the 16th IAHR International Symposium on Ice, International Association of Hydraulic Engineering Research, Dunedin, New Zealand,

Afzalimehr, H., Maddahi, M. R., Naziri, D., & Sui, J. (2019). Effects of non-submerged boulder on flow characteristics–a field investigation. *International Journal of Sediment Research*, *34*(2), 136-143.

Afzalimehr, H., & Rennie, C. (2009). Determination of bed shear stress using boundary layer parameters in a gravel-bed river. *Hydrological Sciences Journal*, *54*(1), 147-159.

Aguirre-Pe, J., Olivero, M. ı. a. L., & Moncada, A. T. (2003). Particle densimetric Froude number for estimating sediment transport. *Journal of Hydraulic Engineering*, *129*(6), 428-437.

Ahmed, F., & Rajaratnam, N. (1998). Flow around bridge piers. *Journal of Hydraulic Engineering*, *124*(3), 288-300.

al., A. e. (2002). Local scour around circular piers under ice covers. International Symposium on Ice: 02/12/2002-06/12/2002,

Alabi, P. D. (2006). *Time development of local scour at a bridge pier fitted with a collar* University of Saskatchewan].

Alauddin, M., Tashiro, T., & Tsujimoto, T. (2011). Design of groynes modified with both alignment and permeability for lowland river problems. *Journal of Japan Society of Civil Engineers, Ser. A2 (Applied Mechanics (AM))*, *67*(2), I_645-I_652.

Arneson, L. (2013). *Evaluating scour at bridges*.

Ashton, G. D. (1986). *River and lake ice engineering*. Water Resources Publication.

Ataie Ashtiani, Behzad Beheshti, & A, A. (2006). Experimental investigation of clear-water local scour at pile groups. *Journal of Hydraulic Engineering*, *132*(10), 1100-1104.

Baba, Y., Camenen, B., Peltier, P., Thollet, F., & Zhang, H. (2010). Flows and bedload dynamics around spur dyke in a compound channel.

Baker, G., Barker, S., Bofah, K., & Saffman, P. (1974). Laser anemometer measurements of trailing vortices in water. *Journal of Fluid Mechanics*, *65*(2), 325-336.

Ballio, F., Radice, A., & Franzetti, S. (2004). An experimental study of live-bed scour at bridge abutments. Proceedings 2nd International Conference on Scour and Erosion (ICSE-2). November 14.–17., 2004, Singapore,

Barbhuiya, A. K., & Dey, S. (2004). Velocity and turbulence at a wing-wall abutment. *Sadhana*, *29*(1), 35-56.

Basser, H., Karami, H., Shamshirband, S., Jahangirzadeh, A., Akib, S., & Saboohi, H. (2014). Predicting optimum parameters of a protective spur dike using soft computing methodologies–A comparative study. *Computers & Fluids*, *97*, 168-176.

Bearman, P. (1978). Flow-Induced Vibration. By ROBERT D. BLEVINS. Van Nostrand Reinhold, 1977. 363 pp.£ 13.75. *Journal of Fluid Mechanics*, *89*(1), 206-207.

Beg, M., & Beg, S. (2013). Scour reduction around bridge piers: A review. *International Journal of Engineering Inventions*, *2*(7), 7-15.

Beheshti, A., & Ataie-Ashtiani, B. (2008). Analysis of threshold and incipient conditions for sediment movement. *Coastal Engineering*, *55*(5), 423-430.

Beltaos, S. (2007). The role of waves in ice-jam flooding of the Peace-Athabasca Delta. *Hydrological Processes: An International Journal*, *21*(19), 2548-2559.

Benedict, S. T. (2016). *Clear-water abutment and contraction scour in the Coastal Plain and Piedmont Provinces of South Carolina, 1996-99*.

Bortone, P. (2006). *Sediment and dredged material treatment* (Vol. 2). Elsevier.

Brandimarte, L., Paron, P., & Di Baldassarre, G. (2012). Bridge pier scour: A review of processes, measurements and estimates. *Environmental Engineering and Management Journal*, *11*(5), 975-989.

Breusers, H. (1991). Scour around spur dikes and abutments. Scouring,

Breusers, H., Nicollet, G., & Shen, H. (1977). Local scour around cylindrical piers. *Journal of Hydraulic Research*, *15*(3), 211-252.

Breusers, H., & Raudkivi, A. (2020). *Scouring: hydraulic structures design manual series, vol. 2*. Crc Press.

Briaud, J.-L., Hurlebaus, S., Chang, K.-A., Yao, C., Sharma, H., Yu, O.-Y., Darby, C., Hunt, B. E., & Price, G. R. (2011). *Realtime monitoring of bridge scour using remote monitoring technology*.

Briaud, J.-L., Ting, F. C., Chen, H., Gudavalli, R., Perugu, S., & Wei, G. (1999). SRICOS: Prediction of scour rate in cohesive soils at bridge piers. *Journal of Geotechnical and Geoenvironmental Engineering*, *125*(4), 237-246.

Brice, J., Blodgett, J., Carpenter, P., Cook, M., Craig Jr, G., Eckhardt, D., Hines, M., Lindskov, K., Moore, D., & Parker, R. (1978). *Countermeasures for Hydraulic Problems at Bridges, Volume 1—Analysis and Assessment: Washington, DC*.

Buffington, J. M., & Montgomery, D. (1997). Channel-reach morphology in mountain drainage basin. *Geological Society of America Bulletin*, *109*(5), 596-611.

Cardoso, A., Graf, W. H., & Gust, G. (1991). Steady gradually accelerating flow in a smooth open channel. *Journal of Hydraulic Research*, *29*(4), 525-543.

Chabert, J., & Engeldinger, P. (1956). Study of scour around bridge piers. *Rep. Prepared for the Laboratoire National d'Hydraulique*.

Chakrabarti, S. K., Chakrabarti, P., & Krishna, M. S. (2006). Design, construction, and installation of a floating caisson used as a bridge pier. *Journal of waterway, port, coastal, and ocean engineering*, *132*(3), 143-156.

Chang, F. F. (1973). *A statistical summary of the cause and cost of bridge failures*.

Chang, H. H. (1992). *Fluvial processes in river engineering*.

Chee, R. K. W. (1982). Live-bed scour at bridge piers. *Publication of: Auckland University, New Zealand*(290).

Cheng, M.-H., Hsu, J. R.-C., & Chen, C.-Y. (2011). Laboratory experiments on waveform inversion of an internal solitary wave over a slope-shelf. *Environmental Fluid Mechanics*, *11*, 353-384.

Chiew, Y.-M. (1992). Scour protection at bridge piers. *Journal of Hydraulic Engineering*, *118*(9), 1260-1269.
Chiew, Y.-M. (1995). Mechanics of riprap failure at bridge piers. *Journal of Hydraulic Engineering*, *121*(9), 635-643.
Chiew, Y.-M., & Lim, F.-H. (2000). Failure behavior of riprap layer at bridge piers under live-bed conditions. *Journal of Hydraulic Engineering*, *126*(1), 43-55.
Chiew, Y.-M., & Melville, B. W. (1987). Local scour around bridge piers. *Journal of Hydraulic Research*, *25*(1), 15-26.
Chiew, Y. M. (1984). *Local scour at bridge piers* ResearchSpace@ Auckland].
Coleman, S. E., Lauchlan, C. S., & Melville, B. W. (2003). Clear-water scour development at bridge abutments. *Journal of Hydraulic Research*, *41*(5), 521-531.
Dargahi, B. (1990). Controlling mechanism of local scouring. *Journal of Hydraulic Engineering*, *116*(10), 1197-1214.
Das, S., Midya, R., Das, R., & Mazumdar, A. (2013). A study of wake vortex in the scour region around a circular pier. *International Journal of Fluid Mechanics Research*, *40*(1).
Deng, J., Xu, W., Liu, S., & WANG, W. (2009). Influence of water jet aeration on pressure in scour pool and plunge pool. *Advances in Water Science*, *20*(3), 373-378.
Deng, L., & Cai, C. (2010). Bridge scour: Prediction, modeling, monitoring, and countermeasures. *Practice periodical on structural design and construction*, *15*(2), 125-134.
Derrick, D. L., Gernand, H. W., & Crutchfield, J. P. (1989). *Inventory of river training structures in shallow-draft waterways*.
Dey, S., & Barbhuiya, A. K. (2005). Time variation of scour at abutments. *Journal of Hydraulic Engineering*, *131*(1), 11-23.
Dey, S., & Barbhuiya, A. K. (2006). Velocity and turbulence in a scour hole at a vertical-wall abutment. *Flow Measurement and Instrumentation*, *17*(1), 13-21.
Dey, S., & Raikar, R. V. (2007). Characteristics of horseshoe vortex in developing scour holes at piers. *Journal of Hydraulic Engineering*, *133*(4), 399-413.
Dietrich, W. E., & Whiting, P. (1989). Boundary shear stress and sediment transport in river meanders of sand and gravel. *River meandering*, *12*, 1-50.
Duan, J. G., He, L., Fu, X., & Wang, Q. (2009). Mean flow and turbulence around experimental spur dike. *Advances in Water Resources*, *32*(12), 1717-1725.
Duan, J. G., & Nanda, S. (2006). Two-dimensional depth-averaged model simulation of suspended sediment concentration distribution in a groyne field. *Journal of Hydrology*, *327*(3-4), 426-437.
Esmaeli, P., Boudaghpour, S., Rostami, M., & Mirzaee, M. (2022). Experimental investigation of permeability and length of a series of spur dikes effects on the control of bank erosion in the meandering channel. *Ain Shams Engineering Journal*, *13*(4), 101701.
Ettema, R. (1980). *Scour at bridge piers*.
Ettema, R., & Kempema, E. W. (2012). River-Ice Effects on Gravel-Bed Channels. *Gravel-Bed Rivers: Processes, Tools, Environments*, 523-540.
Ettema, R., Melville, B. W., & Barkdoll, B. (1998). Scale effect in pier-scour experiments. *Journal of Hydraulic Engineering*, *124*(6), 639-642.
Fang, D., Sui, J., Thring, R. W., & Zhang, H. (2006). Impacts of dimension and slope of submerged spur dikes on local scour processes- an experimental study. *International Journal of Sediment Research*, *21*(2), 89-100.
Fotherby, L. M., & Randle, T. J. (2007). SedVeg-Gen3 Platte River model: a sediment transport and riparian vegetation model. World Environmental and Water Resources Congress 2007: Restoring Our Natural Habitat,
Froehlich, D. C. (1989). Local scour at bridge abutments. Proceedings of the 1989 national conference on hydraulic engineering,
Garde, R., Subramanya, K., & Nambudripad, K. (1961). Study of scour around spur-dikes. *Journal of the Hydraulics Division*, *87*(6), 23-37.

Ghaderi, A., & Abbasi, S. (2019). CFD simulation of local scouring around airfoil-shaped bridge piers with and without collar. *Sadhana*, *44*(10), 1-12.

Giglou, A. N., Mccorquodale, J. A., & Solari, L. (2018). Numerical study on the effect of the spur dikes on sedimentation pattern. *Ain Shams Engineering Journal*, *9*(4), 2057-2066.

Grimaldi, C., Gaudio, R., Calomino, F., & Cardoso, A. H. (2009). Control of scour at bridge piers by a downstream bed sill. *Journal of Hydraulic Engineering*, *135*(1), 13-21.

Gu, Z.-p., Akahori, R., & Ikeda, S. (2011). Study on the transport of suspended sediment in an open channel flow with permeable spur dikes. *International Journal of Sediment Research*, *26*(1), 96-111.

Gupta, A., & Gangadharaiah, T. (1992). Local scour reduction by a delta wing-like passive device. Proceeding of 8th Congress of Asia & Pacific Reg. Div,

Hains, D., & Zabilansky, L. (2004). *Laboratory test of scour under ice: Data and preliminary results*.

Hains, D. B. (2004). An experimental study of ice effects on scour at bridge piers.

Haitao, X., Jinyou, L., & Xiaobin, L. (2008). Non-uniform sediment incipient velocity. *International Journal of Sediment Research*, *23*(1), 69-75.

Haizhou, T., & Graf, W. H. (1993). Friction in unsteady open-channel flow over gravel beds. *Journal of Hydraulic Research*, *31*(1), 99-110.

Haltigin, T. W., Biron, P. M., & Lapointe, M. F. (2007). Predicting equilibrium scour-hole geometry near angled stream deflectors using a three-dimensional numerical flow model. *Journal of Hydraulic Engineering*, *133*(8), 983-988.

Heibaum, M., & Trentmann, J. (2010). Partial grouted riprap for enhanced scour resistance. In *Scour and Erosion* (pp. 1-10).

Herbich, J. (1966). Spur Dikes Prevent Scour at Bridge Abutments, Lehigh University Institute of Research, Fritz Engineering Laboratory Report 280.20, Paper 136. *Bethlehem, Pennsylvania, December*.

Hicks, F. (2009). An overview of river ice problems: CRIPE07 guest editorial. In: Elsevier.

Hicks, F., & Beltaos, S. (2008). River ice. In *Cold Region Atmospheric and Hydrologic Studies. The Mackenzie GEWEX Experience: Volume 2: Hydrologic Processes* (pp. 281-305). Springer.

Hirshfield, F. (2015). The impact of ice conditions on local scour around bridge piers. *University of Northern British Columbia*.

Huai, W., Zeng, Y., Xu, Z., & Yang, Z. (2009). Three-layer model for vertical velocity distribution in open channel flow with submerged rigid vegetation. *Advances in Water Resources*, *32*(4), 487-492.

Ishigaki, T., & Baba, Y. (2004). Local scour induced by 3D flow around attracting and deflecting groins. Proceedings 2nd International Conference on Scour and Erosion (ICSE-2). November 14.–17., 2004, Singapore,

Ishigaki, T., Baba, Y., & Muto, Y. (2000). Vortex motion around a plate with footing in open channel flow and its effect on local scouring. *Advances in Hydro Science and-Engineering*, *4*, 169-176.

Jafari, R., & Sui, J. (2021). Velocity Field and Turbulence Structure around Spur Dikes with Different Angles of Orientation under Ice Covered Flow Conditions. *Water*, *13*(13), 1844.

Jennifer, D., Li, H., Guangqian, W., & Xudong, F. (2011). Turbulent burst around experimental spur dike. *International Journal of Sediment Research*, *26*(4), 471-523.

Johnson, P. A., & Ayyub, B. M. (1996). Modeling uncertainty in prediction of pier scour. *Journal of Hydraulic Engineering*, *122*(2), 66-72.

Kadota, A., & Suzuki, K. (2010). Local scour and development of sand wave around T-type and L-type groynes. In *Scour and Erosion* (pp. 707-714).

Kanda, K., Samoto, Y., & Li, Z. (2019). Study on morphodynamics around stone-lined spur dikes in the Akashi river. In *River, Coastal and Estuarine Morphodynamics: RCEM 2007, Two Volume Set* (pp. 1176-1182). CRC Press.

Kandasamy, J., & Melville, B. (1998). Maximum local scour depth at bridge piers and abutments. *Journal of Hydraulic Research*, *36*(2), 183-198.

Kanellopoulos, P. M. (1998). *Incipient motion under shallow flow conditions* Virginia Tech].

Karaki, S. (1959). Laboratory study of spur dikes for highway bridge protection. *CER; 59-54*.

Karami, H., Ardeshir, A., Behzadian, K., & Ghodsian, M. (2011). Protective spur dike for scour mitigation of existing spur dikes. *Journal of Hydraulic Research*, *49*(6), 809-813.
Kattell, J., & Eriksson, M. (1998). Bridge Scour Evaluation: Screening. *Analysis, & Countermeasures*, *9877*.
Kehe, S. M. (1984). *Streambank Protection by Use of Spur Dikes*. Oregon State University.
Kiraga, M., & Popek, Z. (2016). Using a modified Lane's relation in local bed scouring studies in the laboratory channel. *Water*, *8*(1), 16.
Klingeman, P. C., Kehe, S. M., & Owusu, Y. A. (1984). Streambank erosion protection and channel scour manipulation using rockfill dikes and gabions.
Kodaki, K., Nakano, M., & Maeda, S. (1997). Development of the automatic system for pneumatic caisson. *Automation in Construction*, *6*(3), 241-255.
Koken, M., & Constantinescu, G. (2011). Flow and turbulence structure around a spur dike in a channel with a large scour hole. *Water Resources Research*, *47*(12).
Koloseus, H. J. (1984). Scour due to riprap and improper filters. *Journal of Hydraulic Engineering*, *110*(10), 1315-1324.
Kothyari, U., & Ranga Raju, K. (2001). Scour around spur dikes and bridge abutments. *Journal of Hydraulic Research*, *39*(4), 367-374.
Kuhnle, R. A., Alonso, C. V., & Shields, F. D. (1999). Geometry of scour holes associated with 90 spur dikes. *Journal of Hydraulic Engineering*, *125*(9), 972-978.
Kuhnle, R. A., Alonso, C. V., & Shields Jr, F. D. (2002). Local scour associated with angled spur dikes. *Journal of Hydraulic Engineering*, *128*(12), 1087-1093.
Kuhnle, R. A., Jia, Y., & Alonso, C. V. (2008). Measured and simulated flow near a submerged spur dike. *Journal of Hydraulic Engineering*, *134*(7), 916-924.
Kumar, M., & Chatterjee, K. (2023). Load-Sharing Behavior of Caisson Foundations in Layered Soil under Seismic Conditions. *International Journal of Geomechanics*, *23*(6), 04023055.
Kumar, V., Raju, K. G. R., & Vittal, N. (1999). Reduction of local scour around bridge piers using slots and collars. *Journal of Hydraulic Engineering*, *125*(12), 1302-1305.
Kwan, & Melville, B. (1994). Local scour and flow measurements at bridge abutmentslJ JJ Hydrau1. *Res. IAHR*, *32*.
Kwan, T. F. (1988). A study of abutment scour.
Lagasse, P. F. (2007). *Countermeasures to protect bridge piers from scour* (Vol. 593). Transportation Research Board.
Lagasse, P. F., Richardson, E. V., Schall, J., & Price, G. (1997). *Instrumentation for measuring scour at bridge piers and abutments*.
Lagasse, P. F., Thompson, P. L., & Sabol, S. A. (1995). Guarding against scour. *Civil Engineering*, *65*(6), 56.
Lau, Y. L., & Krishnappan, B. G. (1985). Sediment transport under ice cover. *Journal of Hydraulic Engineering*, *111*(6), 934-950.
Lauchlan, C. S., & Melville, B. W. (2001). Riprap protection at bridge piers. *Journal of Hydraulic Engineering*, *127*(5), 412-418.
Laursen, E. M., & Toch, A. (1956). *Scour around bridge piers and abutments* (Vol. 4). Iowa Highway Research Board Ames, IA.
LeBeau, K. H., Wadia, F., & Sara, J. (2007). Fault tree analysis of Schoharie Creek Bridge collapse. *Journal of performance of constructed facilities*, *21*(4), 320-326.
Lewis, J. (1998). Evaluating the impacts of logging activities on erosion and suspended sediment transport in the Caspar Creek watersheds. *USDA forest service general technical report PSW-GTR-168*, 55-69.
Li, H., Barkdoll, B. D., Kuhnle, R., & Alonso, C. (2006). Parallel walls as an abutment scour countermeasure. *Journal of Hydraulic Engineering*, *132*(5), 510-520.
Li, H., Kuhnle, R., & Barkdoll, B. D. (2005). Spur dikes as an abutment scour countermeasure. In *Impacts of Global Climate Change* (pp. 1-12).

Li, S. S. (2012). Estimates of the Manning's coefficient for ice-covered rivers. Proceedings of the Institution of Civil Engineers-Water Management,

Lim, S.-Y., & Cheng, N.-S. (1998). Prediction of live-bed scour at bridge abutments. *Journal of Hydraulic Engineering*, *124*(6), 635-638.

Liu, H.-K., Chang, F. M., & Skinner, M. M. (1961). Effect of bridge constriction on scour and backwater. *CER; 60-22*.

Liu, Z. (1998). Sediment transport.

Lu, J.-Y., Hong, J.-H., Su, C.-C., Wang, C.-Y., & Lai, J.-S. (2008). Field measurements and simulation of bridge scour depth variations during floods. *Journal of Hydraulic Engineering*, *134*(6), 810-821.

Macky, G. (1990). Survey of roading expenditure due to scour. *CR 90_09, Department of Scientific and Industrial Research, Hydrology Centre, Christchurch, New Zealand*.

Mansoori, A. R. (2014). *Study on Flow and Sediment Transport around Series of Spur Dikes with Different Head Shape* [Dissertation, Kyoto University]. https://doi.org/10.14989/doctor.k18560

Manual, S.-I. S. U. s. (2017). SonTek-IQ Series Intelligent Flow Featuring Smart Pulse HD User’s Manual [User’s Manual]. *Xylem brand*, *SmartPulse HD*

User’s Manual(Firmware Version 3.0), 135. https://doi.org/SonTek-IQ□Series

Intelligent Flow (Xylem Inc)

Markovic, M. (2012). Multi criteria analysis of hydraulic structures for river training works. *Water Resources Management*, *26*(13), 3893-3906.

Martin, V., Fisher, T., Millar, R., & Quick, M. (2002). ADV data analysis for turbulent flows: Low correlation problem. Hydraulic Measurements and Experimental Methods 2002,

Mays, L. W. (1999). *Hydraulic design handbook*. McGraw-Hill Education.

McLelland, S. J., & Nicholas, A. P. (2000). A new method for evaluating errors in high-frequency ADV measurements. *Hydrological processes*, *14*(2), 351-366.

Melville, B. (1992). Local scour at bridge abutments. *Journal of Hydraulic Engineering*, *118*(4), 615-631.

Melville, B., & Sutherland, A. (1988). Design method for local scour at bridge piers. *Journal of Hydraulic Engineering*, *114*(10), 1210-1226.

Melville, B. W. (1984). Live-bed scour at bridge piers. *Journal of Hydraulic Engineering*, *110*(9), 1234-1247.

Melville, B. W. (1997). Pier and abutment scour: integrated approach. *Journal of Hydraulic Engineering*, *123*(2), 125-136.

Melville, B. W., Coleman, S., & Hoe, D. (2002). Countermeasures for Scour at Spill-Trough Bridge Abutments. First International Conference on Scour of Foundations. November 17-20, 2002, College Station, USA,

Melville, B. W., & Coleman, S. E. (2000). *Bridge scour*. Water Resources Publication.

Michioku, K., ISHIGAKI, T., MAENO, S., NANJYO, M., & IKEMATSU, T. (2004). Experiment and analysis on flow field around and inside a permeable groin. *PROCEEDINGS OF HYDRAULIC ENGINEERING*, *48*, 799-804.

Mizutani, H., Nakagawa, H., Kawaike, K., Baba, Y., & Zhang, H. (2011). STUDY ON LOCAL SCOUR AND VARIATION OF BED COMPOSITION AROUND NON-SUBMERGED SPUR DYKE. *Journal of Japan Society of Civil Engineers, Ser. B1 (Hydraulic Engineering)*, *67*.

Montgomery, D. R., Zabowski, D., Ugolini, F. C., Hallberg, R. O., & Spaltenstein, H. (2000). Soils, watershed processes, and marine sediments. In *International Geophysics* (Vol. 72, pp. 159-iv). Elsevier.

Mushtaq, A. (1953). *SIMILARITY OF CONDITIONS OF FLOW OF WATER IN MODELS AND THEIR PHOTOTYPES AND ITS APPLICATION TO PROBLEMS OF WEIR DESIGN AND RIVER CONTROL* University of the Punjab].

Muste, M., Braileanu, F., & Ettema, R. (2000). Flow and sediment transport measurements in a simulated ice-covered channel. *Water Resources Research*, *36*(9), 2711-2720.

Muto, Y., Baba, Y., & Aya, S. (2002). Velocity measurements in open channel flow with rectangular embayments formed by spur dikes. *Annuals of Disaster Prevention Research Institute, Kyoto University B*, *45*, 2.

Namaee, & Sui. (2019a). Impact of armour layer on the depth of scour hole around side-by-side bridge piers under ice-covered flow condition. *Journal of Hydrology and Hydromechanics*, *67*(3), 240-251.

Namaee, & Sui. (2019b). Local scour around two side-by-side cylindrical bridge piers under ice-covered conditions. *International Journal of Sediment Research*, *34*(4), 355-367.

Namaee, M. R., Li, Y., & Sui, J. (2020). Effects of Ice Cover on Local Scour Around Bridge Piers—An Experimental Study. In *Estuaries and Coastal Zones in Times of Global Change* (pp. 691-706). Springer.

Namaee, M. R., & Sui, J. (2019). Effects of ice cover on the incipient motion of bed material and shear stress around side-by-side bridge piers. *Cold Regions Science and Technology*, *165*, 102811.

Namaee, M. R., & Sui, J. (2020). Velocity profiles and turbulence intensities around side-by-side bridge piers under ice-covered flow condition. *Journal of Hydrology and Hydromechanics*, *68*(1), 70-82.

Namaee, M. R., Sui, J., & Whitcombe, T. (2017). A revisit of different models for flow resistance in gravel-bed rivers and hydraulic flumes. *International journal of river basin management*, *15*(3), 277-286.

Namaee, M. R., Sui, J., Wu, Y., & Linklater, N. (2021). Three-dimensional numerical simulation of local scour around circular side-by-side bridge piers with ice cover. *Canadian Journal of Civil Engineering*, *48*(10), 1335-1353.

Nasrollahi, A., Ghodsian, M., & Neyshabouri, S. (2008). Local scour at permeable spur dikes. *Journal of Applied Sciences*, *8*(19), 3398-3406.

Nazari, A., Mccorquodale, J., & Solari, L. (2017). Numerical study on the effect of the spur dikes on sedimentation pattern. *Ain Shams Engineering Journal*. https://doi.org/http://creativecommons.org/licenses/by-nc-nd/4.0/. 10.1016/j.asej.2017.02.007.

Nelson, J. M., Shreve, R. L., McLean, S. R., & Drake, T. G. (1995). Role of near-bed turbulence structure in bed load transport and bed form mechanics. *Water Resources Research*, *31*(8), 2071-2086.

Odgaard, A. J., & Wang, Y. (1987). Scour prevention at bridge piers. Hydraulic Engineering,

Pagliara, S., Carnacina, I., & Cigni, F. (2010). Sills and gabions as countermeasures at bridge pier in presence of debris accumulations. *Journal of Hydraulic Research*, *48*(6), 764-774.

Pandey, M., Ahmad, Z., & Sharma, P. (2018). Scour around impermeable spur dikes: a review. *ISH Journal of Hydraulic Engineering*, *24*(1), 25-44.

Pandey, M., Karbasi, M., Jamei, M., Malik, A., & Pu, J. H. (2023). A comprehensive experimental and computational investigation on estimation of scour depth at bridge abutment: emerging ensemble intelligent systems. *Water Resources Management*, *37*(9), 3745-3767.

Papanicolaou, A., Diplas, P., Dancey, C., & Balakrishnan, M. (2001). Surface roughness effects in near-bed turbulence: Implications to sediment entrainment. *Journal of Engineering Mechanics*, *127*(3), 211-218.

Parola, A. (1993). Stability of riprap at bridge piers. *Journal of Hydraulic Engineering*, *119*(10), 1080-1093.

Peng, W., Hirshfield, F., & Sui, J.-y. (2015). Local scour around bridge abutments under ice covered condition–an experimental study. *International Journal of Sediment Research*, *30*(1), 39-47.

Pizarro, A., Manfreda, S., & Tubaldi, E. (2020). The science behind scour at bridge foundations: A review. *Water*, *12*(2), 374.

Prowse, T. D., & Beltaos, S. (2002). Climatic control of river-ice hydrology: a review. *Hydrological processes*, *16*(4), 805-822.

Rajaratnam, N., & Nwachukwu, B. (1983). Erosion near groyne-like structures. *Journal of Hydraulic Research*, *21*(4), 277-287.

Ranjbar-Zahedani, M., Keshavarzi, A., Khabbaz, H., & Ball, J. (2019). Flow Structures Around a Circular Bridge Pier with a Submerged Prism at Upstream.

Rankin, K. L., & Hires, R. I. (2000). Laboratory measurement of bottom shear stress on a movable bed. *Journal of Geophysical Research: Oceans*, *105*(C7), 17011-17019.

Raudkivi, A. J. (1986). Functional trends of scour at bridge piers. *Journal of Hydraulic Engineering*, *112*(1), 1-13.

Raudkivi, A. J., & Ettema, R. (1983). Clear-water scour at cylindrical piers. *Journal of Hydraulic Engineering*, *109*(3), 338-350.

Rehmel, M. (2007). Application of acoustic Doppler velocimeters for streamflow measurements. *Journal of Hydraulic Engineering*, *133*(12), 1433-1438.

Richardson, & Davis. (1995). *Evaluating scour at bridges: Federal highway administration hydraulic engineering circular no. 18*.

Richardson, Karaki, S., Mahmood, K., Simons, D., & Stevens, M. (1975). *HIGHWAYS IN THE RIVER ENVIRONMENT: HYDRAULIC AND ENVIRONMENTAL DESIGN CONSIDERATIONS. TRAINING AND DESIGN MANUAL*.

Richardson, E., & Davis, S. (2001). Evaluating scour at bridges (HEC-18). *US Department of Transportation, Federal Highway Administration, Colorado, 4th edn. FHWA NHI*, 01-001.

Richardson, E., Richardson, J., & Edge, B. (1993). Scour at highway structures in tidal waters. Hydraulic Engineering,

Richardson, E., Stevens, M., & Simons, D. (1975). The design of spurs for river training. XVIth, IAHR congress,

Sadat, S. H. (2015). *MODIFICATION OF SPUR-DIKE WITH FOOTING OR PILE-GROUP TO STABILIZE RIVER MORPHOLOGY AND REDUCE LOCAL SCOUR* [Dissertation, Nagoya Institute of Technology]. http://doi.org/10.20602/00003162

Sanadgol, E., Heidarpour, M., & Mohammadpour, R. (2021). Reduction of local scouring at round-nosed rectangular piers using a downstream bed sill. *Journal of the South african institution of civil engineering*, *63*(3), 62-70.

Saneie, M. (2011). Experimental study on effect of minor spur dike to reduce main spur dike scouring. *Watershed Engineering and Management*, *3*(3), 140-148.

Schlichting, H., & Gersten, K. (2016). *Boundary-layer theory*. Springer.

Schwimmer, R. (2006). *Calculation of Stream Discharge Required to Move Bed Material* Teaching Sedimentary Geology in the 21st Century Retrieved Jul 3, 2006 from https://serc.carleton.edu/download/images/11032/shields.gif

Shahmohammadi, R., Afzalimehr, H., & Sui, J. (2021). Assessment of critical shear stress and threshold velocity in shallow flow with sand particles. *Water*, *13*(7), 994.

Shen, H. T. (2010). Mathematical modeling of river ice processes. *Cold Regions Science and Technology*, *62*(1), 3-13.

Sheppard, D. M., & Miller Jr, W. (2006). Live-bed local pier scour experiments. *Journal of Hydraulic Engineering*, *132*(7), 635-642.

Shields, A. (1936). Application of similarity principles and turbulence research to bed-load movement.

Shields Jr, F. D., Bowie, A., & Cooper, C. (1995). CONTROL OF STREAMBANK EROSION DUE TO BED DEGRADATION WITH VEGETATION AND STRUCTURE 1. *JAWRA Journal of the American Water Resources Association*, *31*(3), 475-489.

Shvidchenko, A. B., & Pender, G. (2000). Flume study of the effect of relative depth on the incipient motion of coarse uniform sediments. *Water Resources Research*, *36*(2), 619-628.

Singh, N. B., Devi, T. T., & Kumar, B. (2022). The local scour around bridge piers—a review of remedial techniques. *ISH Journal of Hydraulic Engineering*, *28*(sup1), 527-540.
Smith, B. T., & Ettema, R. (1995). *Ice-cover influence on flow and bedload transport in dune-bed channels*. Iowa Institute of Hydraulic Research, the University of Iowa.
Smith, B. T., & Ettema, R. (1997). Flow resistance in ice-covered alluvial channels. *Journal of Hydraulic Engineering*, *123*(7), 592-599.
Sohrabi, M., Keshavarzi, A., & Javan, M. (2019). Impact of bed sill shapes on scour protection in river bed and banks. *International journal of river basin management*, *17*(3), 277-287.
Sontek, A. D. V. (1997). Operation manual, firmware version 4.0. (Sontek, San Diego.)
SonTek, M. (2017). SonTek-IQ Series Intelligent Flow Featuring Smart Pulse HD User's Manual. *Xylem brand SmartPulse HD User's Manual*(Firmware Version 3.0
Sui, J., Faruque, M., & Balachandar, R. (2009). Local scour caused by submerged square jets under model ice cover. *Journal of Hydraulic Engineering*, *135*(4), 316-319.
Sui, J., Hicks, F. E., & Menounos, B. (2006). Observations of riverbed scour under a developing hanging ice dam. *Canadian Journal of Civil Engineering*, *33*(2), 214-218.
Sui, J., Jun, W., Yun, H., & Faye, K. (2010). Velocity profiles and incipient motion of frazil particles under ice cover. *International Journal of Sediment Research*, *25*(1), 39-51.
Sui, J., Karney, B. W., & Fang, D. (2005). Variation in water level under ice-jammed condition–Field investigation and experimental study. *Hydrology Research*, *36*(1), 65-84.
Sui, J., Wang, D., & Karney, B. W. (2000). Suspended sediment concentration and deformation of riverbed in a frazil jammed reach. *Canadian Journal of Civil Engineering*, *27*(6), 1120-1129.
Sukhodolov, A., Uijttewaal, W. S., & Engelhardt, C. (2002). On the correspondence between morphological and hydrodynamical patterns of groyne fields. *Earth Surface Processes and Landforms*, *27*(3), 289-305.
Tafarojnoruz, A., Gaudio, R., & Dey, S. (2010). Flow-altering countermeasures against scour at bridge piers: a review. *Journal of Hydraulic Research*, *48*(4), 441-452.
Tanaka, S., & Yano, M. (1967). Local scour around a circular cylinder.
Telionis, D., Yang, Y., & Rediniotis, O. (2009). Recent developments in multi-hole probe (mhp) technology. 20th international congress of mechanical engineering,
Teraguchi, H., Nakagawa, H., KAWAIKE, K., BABA, Y., & ZHANG, H. (2010). Morphological Changes induced by River Training Structures: Bandal-like structures and Groins.
Teraguchi, H., Nakagawa, H., MUTO, Y., BABA, Y., & ZHANG, H. (2008). Flow and sediment transport around impermeable or permeable groins. *PROCEEDINGS OF HYDRAULIC ENGINEERING*, *52*, 175-180.
Thomas, Z. (1967). An interesting hydraulic effect occurring at local scour.
Tominaga, A., NAKANO, Y., & FUJITA, T. (2000). Visualization analysis of flow structures in submerged spur dikes. *PROCEEDINGS OF HYDRAULIC ENGINEERING*, *44*, 1041-1046.
Tsujimoto, A., Cardoso, A., & Saito, A. (1990). Open channel flow with spatially varied bed shear stress. *J of Hydroscience and Hydr. Eng*, *8*(2), 1-52.
Tu, W., Deng, Q., Zhang, P., Chen, H.-P., & Liu, Z. (2022). Evaluation of the lateral bearing characteristics of composite caisson-pile foundation considering the scour-hole dimensions. *Marine Georesources & Geotechnology*, *40*(5), 538-553.
Umbrell, E. R., Young, G. K., Stein, S. M., & Jones, J. S. (1998). Clear-water contraction scour under bridges in pressure flow. *Journal of Hydraulic Engineering*, *124*(2), 236-240.
Unger, J., & Hager, W. H. (2006). Riprap failure at circular bridge piers. *Journal of Hydraulic Engineering*, *132*(4), 354-362.
Vaghefi, M., Solati, S., & Abdi Chooplou, C. (2021). The effect of upstream T-shaped spur dike on reducing the amount of scouring around downstream bridge pier located at a 180 sharp bend. *International journal of river basin management*, *19*(3), 307-318.

Valela, C., Sirianni, D. A., Nistor, I., Rennie, C. D., & Almansour, H. (2021). Bridge Pier Scour under Ice Cover. *Water*, *13*(4), 536.
Vijayasree, B., Eldho, T., Mazumder, B., & Ahmad, N. (2019). Influence of bridge pier shape on flow field and scour geometry. *International journal of river basin management*, *17*(1), 109-129.
Vittal, N., Kothyari, U., & Haghighat, M. (1994). Clear-water scour around bridge pier group. *Journal of Hydraulic Engineering*, *120*(11), 1309-1318.
Vollmer, S., & Kleinhans, M. G. (2007). Predicting incipient motion, including the effect of turbulent pressure fluctuations in the bed. *Water Resources Research*, *43*(5).
Wahl, T. L. (2000). Analyzing ADV data using WinADV. In *Building partnerships* (pp. 1-10).
Wang, Sui, J.-y., & Karney, B. W. (2008). Incipient motion of non-cohesive sediment under ice cover—an experimental study. *Journal of Hydrodynamics*, *20*(1), 117-124.
Wang, C., Yu, X., & Liang, F. (2017). A review of bridge scour: mechanism, estimation, monitoring and countermeasures [User's Manual

]. *Natural Hazards*, *87*, 1881-1906.
Wang, h., Zhao, J., & Chen, Z. (2008). Experimental investigation of ice and snow melting process on pavement utilizing geothermal tail water. *Energy Conversion and Management*, *49*(6), 1538-1546.

Wardhana, K., & Hadipriono, F. C. (2003). Analysis of recent bridge failures in the United States. *Journal of performance of constructed facilities*, *17*(3), 144-150.
Warren, L. P. (2011). Scour at bridges: stream stability and scour assessment at bridges in massachusetts. *US Geological Survey*.
Wei, K., Qiu, F., & Qin, S. (2022). Experimental and numerical investigation into effect of skirted caisson on local scour around the large-scale bridge foundation. *Ocean Engineering*, *250*, 111052.
Weitbrecht, V., Kühn, G., & Jirka, G. (2002). Large scale PIV-measurements at the surface of shallow water flows. *Flow Measurement and Instrumentation*, *13*(5-6), 237-245.
Wiberg, P. L., & Smith, J. D. (1987). Calculations of the critical shear stress for motion of uniform and heterogeneous sediments. *Water Resources Research*, *23*(8), 1471-1480.
Wilcock, P. R. (1996). Estimating local bed shear stress from velocity observations. *Water Resources Research*, *32*(11), 3361-3366.
Wilcock, P. R., Barta, A. F., Shea, C. C., Kondolf, G. M., Matthews, W. G., & Pitlick, J. (1996). Observations of flow and sediment entrainment on a large gravel-bed river. *Water Resources Research*, *32*(9), 2897-2909.
Wörman, A. (1989). Riprap protection without filter layers. *Journal of Hydraulic Engineering*, *115*(12), 1615-1630.
Wu, Hirshfield, & Sui. (2014). Further studies of incipient motion and shear stress on local scour around bridge abutment under ice cover. *Canadian Journal of Civil Engineering*, *41*(10), 892-899.
Wu, Hirshfield, Sui, Wang, & Chen. (2014). Impacts of ice cover on local scour around semi-circular bridge abutment. *Journal of Hydrodynamics*, *26*(1), 10-18.
Wu, Peng, Hirshfield, F., & Sui, J. (2014). Further studies of incipient motion and shear stress on local scour around bridge abutment under ice cover. *Canadian Journal of Civil Engineering*, *41*(10), 892-899.
Wu, P., Balachandar, R., & Sui, J. (2016). Local scour around bridge piers under ice-covered conditions. *Journal of Hydraulic Engineering*, *142*(1), 04015038.
Wu, P., Hirshfield, F., & Sui, J.-y. (2015). Local scour around bridge abutments under ice covered conditions-an experimental study. *International Journal of Sediment Research*, *30*(1), 39-47.
Wu, P., Hirshfield, F., & Sui, J. (2015). Armour layer analysis of local scour around bridge abutments under ice cover. *River research and applications*, *31*(6), 736-746.
Wu, P., Sui, J., Hirshfield, F., Wang, J., & Chen, P.-p. (2014). Impacts of ice cover on local scour around semi-circular bridge abutment. *Journal of Hydrodynamics*, *26*(1), 10-18.

Yang, S., Belkin, I., Belkina, A., Zhao, Q., Zhu, J., & Ding, P. (2003). Delta response to decline in sediment supply from the Yangtze River: evidence of the recent four decades and expectations for the next half-century. *Estuarine, Coastal and Shelf Science*, *57*(4), 689-699.

Yazdi, J., Sarkardeh, H., Azamathulla, H. M., & Ghani, A. A. (2010). 3D simulation of flow around a single spur dike with free-surface flow. *Intl. J. River Basin Management*, *8*(1), 55-62.

Yoon, T., Yoon, S., & Yoon, K. (1995). Design of riprap for scour protection around bridge piers. PROCEEDINGS OF THE CONGRESS-INTERNATIONAL ASSOCIATION FOR HYDRAULIC RESEARCH,

Yossef, M. M., & Klaassen, G. J. (2002). Reproduction of groynes-induced river bed morphology using LES in a 2-D morphological model. River Flow,

Zabilansky, L. J. (1996). *Ice force and scour instrumentation for the White River, Vermont*.

Zabilansky, L. J., Hains, D. B., & Remus, J. I. (2006). Increased bed erosion due to ice. In *Current Practices in Cold Regions Engineering* (pp. 1-12).

Zarrati, A., Nazariha, M., & Mashahir, M. (2006). Reduction of local scour in the vicinity of bridge pier groups using collars and riprap. *Journal of Hydraulic Engineering*, *132*(2), 154-162.

Zarrati, A. R., Gholami, H., & Mashahir, M. (2004). Application of collar to control scouring around rectangular bridge piers. *Journal of Hydraulic Research*, *42*(1), 97-103.

Zdravkovic, S. K., & Tsiampousi, A. (2023). INTERNATIONAL SOCIETY FOR SOIL MECHANICS AND GEOTECHNICAL ENGINEERING.

Zhang, H., & Nakagawa, H. (2008). *Scour around spur dyke: recent advances and future researches*.

Zhang, H., Nakagawa, H., ISHIGAKI, T., & MUTO, Y. (2005). Prediction of 3D flow field and local scouring around spur dykes. *PROCEEDINGS OF HYDRAULIC ENGINEERING*, *49*, 1003-1008.

Zhang, H., Nakagawa, H., Kawaike, K., & Yasuyuki, B. (2009). Experiment and simulation of turbulent flow in local scour around a spur dyke. *International Journal of Sediment Research*, *24*(1), 33-45.

Zhang, L., Wang, P., Yang, W., Zuo, W., Gu, X., & Yang, X. (2018). Geometric characteristics of spur dike scour under clear-water scour conditions. *Water*, *10*(6), 680.

3 CHAPTER THREE: Velocity Field and Turbulence Structure around Spur Dikes with Different Angles of Orientation under Ice-Covered Flow Conditions

(*Published @ Water (2021)13(13)-1844)*

3.1 Introduction

When multiple spur dikes are used, close spacing can provide continuous protection along a riverbank or around a bridge pier. Spur dikes are extended structures where one end is at the riverbank, and the other is projected toward the river flow (Kuhnle et al., 1999). These constructions have been widely used for many purposes, such as river bank protection, flood control, improvement of a navigational course, control of scour process, landscape improvement, and ecosystem restoration (Sadat, 2015). Regardless of the different types of spur dikes, they redirect flow from the river bank and affect the flow regime, flow velocity, sediment transportation, and, consequently, the scour process (Giglou et al., 2018).

If a spur dike allows the flow to pass through it, that is called permeable. It is impermeable if the dikes block and then repel the river flow. Since impermeable spur dikes reduce the channel width, the energy gradient becomes steeper, and flow velocity increases. Consequently, the riverbed will be eroded. The shape and size of the spur dike will affect the scouring process and flow conditions (Pandey et al., 2018). Zhang et al. (2005) investigated bed morphology, sediment distribution, and flow field in a channel with a series of impermeable spur dikes on both sides of the channel. They claimed that the flow field and local scour around the most upstream pairs of spur dikes are affected the most. Teraguchi et al. (2008) studied flow field and scour patterns around spur dikes using laboratory experiments and numerical simulations. They pointed out that the scour holes on the upstream side of the impermeable spur dikes are larger and deeper than those of permeable ones. Mizutani et al. (2011) investigated the impact of the spur dike height and grain size of riverbed material on the morphology and topography around an impermeable spur dike. It was found that the maximum scour depth is reduced with the increase of the median particle size of bed materials. Furthermore, field observations regarding the bed deformation around stone-lined spur dikes in the Akashi River indicate that the maximum scoured depth around the permeable spur dikes is reduced to 40% compared to the impermeable ones (Kanda et al., 2019). Clearly, the local scour depth around the impermeable spur dikes is much deeper than the permeable ones.

The spur dikes in channels can be classified as submerged and non-submerged, depending on the flow conditions and water depth. Normally, the impermeable spur dikes are designed as non-submerged spur dikes because the overflow on the top of a dike can form a vertical jet just behind the spur dike. This vertical jet moves downstream and causes a significant erosion of the downstream bank along with the body of the spur dike itself (Yossef & Klaassen, 2002). Moreover, in terms of the orientation angle of a spur dike, defined as the angle between the dike axis and the river flow direction, spur dikes are divided into three groups: Attracting, deflecting, and repelling dikes. The attracting spur dike, which points downstream, averts the river flow toward the middle of the channel and protects the region on its downstream side. Deflecting spur dike is a well-known type that changes the direction of the river flow by not repelling it; this type is usually used to protect the banks locally against erosion. They create a turbulent flow, cause more sediment transportation in the middle of the rivers and make the main channel deeper (Sadat, 2015). Muto et al. (2002) conducted two experimental studies about the effects of the opening ratio and water depth on the velocity distributions. Their first study was based on experiments in the Yodo River in Japan using large-scale particle image velocimetry. The second one was conducted in a laboratory flume with a downscaled spur dike. They pointed out that the flow was highly unsteady inside the scour hole based on the experiment in the field. However, laboratory results did not show the same characteristics. The authors concluded that the difference in the result of the field experiment from that of the laboratory was caused by the complex bathymetry of the natural river and lower Reynolds numbers of flows in the laboratory.

Further research shows that models developed from a steady, uniform flow cannot be applied to nonuniform flows (Jennifer et al., 2011; Nelson et al., 1995). Duan et al. (2009) construe that dikes increase shear stress and turbulence intensities at the riverbed by converging water flow, which initiates the local scour process around the dikes. A two-dimensional (2D) experimental model has been used to evaluate the effect of turbulence intensities on the entrainment of bed material (coarse sand and gravel). The instantaneous streamwise velocity has a higher rate than the instantaneous vertical velocity (Papanicolaou et al., 2001). An experimental study on a three-dimensional (3D) flow illuminates that the local scour around the dike causes more complexity of the flow field (Huai et al., 2009). Dey and Barbhuiya (2006) assessed the turbulent flow field around a vertical-wall abutment. They reported that the near-bed Reynolds stress played a significant role in transporting sediment and the scour process.

Many researchers have investigated the turbulence structure in an open channel flow since it is essential to the flow characteristics and the local scour process around the dike. However, nearly all reported research has been conducted under the condition of open channel flow. The impact of an ice cover on the local scour process around the spur dikes has not been investigated. In cold regions, such as Canada, ice covers appear on rivers' surfaces and may last six months, such as the Fraser River's upper and middle reaches. During an ice-covered flow condition, the river hydrology will be dramatically changed compared to an open flow condition. An ice cover adds an extra hydraulic boundary to the flow in a river, which leads to considerable changes in the velocity profile, flow rate, bed shear stress distribution, sediment transport, and consequently scour pattern (Sui et al., 2000).

Under an ice-covered flow condition, the location of the maximum flow velocity gets closer to the channel bed, which increases the bed shear stress (Namaee & Sui, 2020; Sui et al., 2010; P. Wu et al., 2014). In conclusion, the presence of ice on the water surface makes the flow condition much more complicated than an open flow condition. Namely, the existence of an ice cover leads to an increase in the turbulence kinetic energy at the riverbed. Thus, the Reynolds shear stress under an ice-covered flow condition differs from that under an open flow condition. This change affects the incipient motion of bed material, rate of sediment transportation, and sediment suspension loads, making evaluating (predicting) local scour more complex (Sui et al., 2010). To our knowledge, there is no research regarding the effect of an ice cover on the local scour process around the spur dikes. Moreover, measurements of the turbulence flow fields inside scour holes around the spur dikes have never been conducted under an ice-covered flow condition.

Many factors affect the design of a spur dike, such as the river width and depth, flow velocity, channel sinuosity, grain size of bed material, sediment transport rate, bank cohesiveness, the length and shape of a spur dike, the orientation angle of the spur dike to the flow, and construction materials. Understanding the characteristics of the flow in the vicinity of a spur dike under an ice cover will help to develop formulas that can accurately estimate the scour depth and elaborate models for the design of spur dikes. Additionally, it can provide a better understanding of the turbulence structure around obstacles equivalent to spur dikes, such as boulders. The specific objectives of the present experimental study are summarized as follows:

- The impact of an ice cover, including ice cover roughness, on the turbulence intensities, 3D flow fields, shear velocity, and Reynolds stress around the spur dikes.

- The dependence of the scour morphology and turbulence structure around spur dikes on the orientation angle of the spur dike, ice cover roughness, and hydraulic condition.

3.2 Materials and Methods

3.2.1 Site Description

The present experimental study was conducted in a large-scale outdoor flume in the Quesnel River Research Center, BC, Canada. The flume was 38.2 m long, 2.0 m wide, and 1.3 m deep. The longitudinal slope of the flume bed was 0.2%. A holding tank feeds water into the flume to have a constant discharge throughout each experimental run. The holding tank upstream of the flume had a volume of 90 cubic meters and was 40 m long, 2 m wide, and 1.3 m deep. Three valves provided a wide range of flow rates for various experimental runs (Figure 3.1). By adjusting three valves, the following three different flow rates were generated in this experimental study: 0.055 m^3/s, 0.105 m^3/s, and 0.12 m^3/s.

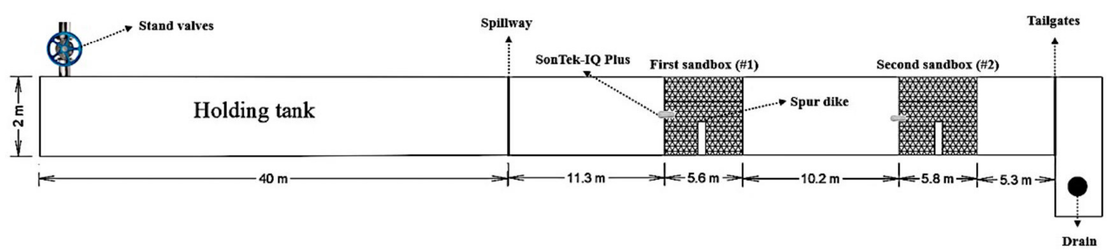

(**a**) Plan view

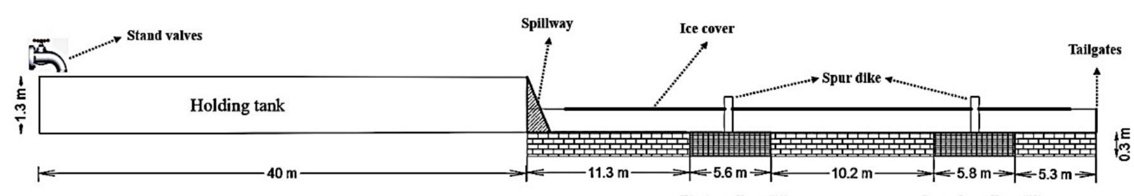

(**b**) Vertical view

Figure 3. 1:The layout of the experimental flume: (a) Plan view; (b) vertical view

Due to the slope of the flume, water levels varied gradually from upstream to downstream. Therefore, the flow was classified as a nonuniform flow. Another important feature that influences the flow is the aspect ratio B/H (where *B* is the channel width and *H* is the flow depth), which is used to classify the channel (flume) either as a narrow (B/H < 5) or wide (B/H > 5) channel. A flow in a narrow channel is affected by the secondary currents from the banks (flume side walls). It causes the dip phenomena (the maximum velocity occurs below the flow surface). However, in the wide channel, the strength of secondary currents is reduced in the flume's lateral direction (Sui et al., 2010). In this experimental study, since the deepest flow depth was 35 cm and the flume width was 200 cm, all flows in this flume belong to wide channel flows (B/H > 5).

Two sandboxes were spaced 10.2 m from each other. These sandboxes were 2 m wide and 0.3 m deep. The upstream sandbox was 5.6 m long, and the downstream was 5.8 m long (Figure 3.2). Three types of nonuniform sands with a median grain size (D_{50}) of 0.9 mm, 0.6 mm, and 0.48 mm were used in the sandboxes. One side of the flume wall along each sandbox was made of plexiglass to have a clear view of the scour process. A staff gauge was located in the middle of each sandbox to measure the water depth during experimental runs. The impermeable model spur dike, made of marine plywood (had a dimension of 80 cm height, 5 cm width, and 50 cm length), was installed in the middle of each sandbox. The model dike was placed at the bottom of each sandbox (30 cm buried in the sand) so that 50 cm of the dike was exposed to the flow. Of note, the model spur dike was non-submerged for all experimental runs in this study.

Figure 3. 2:The view of the original site (experimental flume)

The tailgate at the downstream end of the flume was used to control the water depth and flow velocity (Figure 3.2). Since the flume was very long with a longitudinal slope of 0.2%, water depths differed in these two sandboxes for each experimental run, creating a wide range of water depths for this experimental study. Since the roughness of the ice cover was one of the main factors affecting the local scour process, two types of model ice cover (smooth and rough) were used. Styrofoam panels were used to model the smooth cover, while the rough cover was made by attaching small 2.5 cm Styrofoam cubes to the bottom of the Styrofoam panels. Sixteen panels with 1.99 × 2.4 m dimensions covered almost the entire flow surface. For the experiments with ice cover, before each experimental run, the sixteen Styrofoam panels were put side by side on the flume bed. By opening the valves very slowly, water feeds inside the flume gradually. The Styrofoam started to float on the surface of the water. There were ropes at the flume's end to keep the Styrofoam panels floating side by side on the water surface throughout the experiment. Li

(2012) proposed the equation for calculating the roughness coefficient of an ice cover. He found that Manning's coefficient for ice-covered rivers averages from 0.013 to 0.04. To calculate the roughness coefficient of the ice cover, a reverse engineering approach was employed. The effect of the ice cover on the vertical velocity profile and the ice-affected layer was analyzed, and Equation 3.2 was applied to determine the roughness coefficient, which was found to average 0.02 for the rough ice cover. The roughness coefficient for the smooth ice cover was considered 0.013, derived from Manning's value for smooth concrete (Mays, 1999).

$$k_s = 30\, y_i \exp[-(1 - v_i/v_{max})] \tag{3.1}$$

where, y_i is the thickness of the ice-affected layer, v_i is the average velocity of the ice-affected layer, v_{max} is the maximum velocity of the velocity profile.

$$n_i = 0.039\, k_s^{1/6} \tag{3.2}$$

where, k_s is the average roughness height of the ice underside in meters.

3.2.2 Apparatuses for Measurements

There are many different apparatuses or devices for measuring flow velocities, such as Laser Doppler velocimeter (LDV), Particle Image velocimeter (PIV), Particle Tracking velocimeter (PTV), Acoustic Doppler velocimeter (ADV), Electro Magnetic velocimeter (EMV), Pitot Static Tube (PST), etc. (Kadota & Suzuki, 2010; Kuhnle et al., 2008; Weitbrecht et al., 2002). LDV, ADV, EMV, and PST are all point instruments. Some of them, such as the LDV and PIV, have limitations in their working range (Telionis et al., 2009). As pointed out by researchers in the literature, the ADV is accurate for measuring the turbulence properties of flows (Martin et al., 2002; Rehmel, 2007; Wahl, 2000). Thus, for 3D measurements of instantaneous velocity components, a 10-MHz SonTek ADV (SonTek-A Xylem Brand, San Diego, CA, USA) was used in this research. The ADV includes one probe (transmitter) and three receivers. It acquires the instantaneous velocity components by the sampling volume positioned at the intersection of the transmitted and received acoustic beams located 10 cm beneath the probe head. The sample volume was a cylinder with a diameter of 0.61 cm and a height of 0.72 cm. The ADV's sampling volume is larger than those of the Laser-based velocimetry devices, such as the LDV and PIV (Duan et al., 2009). The ADV cannot acquire the velocity very close to the flow surface, and the velocity profiles were not continuous to the top layer of the flow. However, this limitation does not affect the velocity analysis because the significant change in the velocity distribution occurs from the mid-water depth toward the flume bed, particularly inside the scour hole.

The ADV measures the scattering particles' velocities in the flow. Therefore, the accuracy of the measurements depends on the quality and quantity of particles inside the sampling volume. Two auxiliary parameters provided in the ADV files, the signal-to-noise ratio (SNR) and the correlation (COR), should be evaluated to acquire robust data from ADV measurements (Rehmel, 2007). The SNR represents the relative density of the particulate matter in the flow. The COR, which varies from 0 to 100, indicates the relative consistency of the particle velocity scattering within the sampling period (Wahl, 2000). According to the user manual for ADV and previous studies, to achieve the most accurate data in this experimental study, these two parameters were set as follows: SNR > 15 and COR > 70% (Martin et al., 2002; Rehmel, 2007). The Water Resources Research Laboratory of the US Bureau of Reclamation developed a software program known as Win ADV for filtering the ADV data files. This study used Win ADV for data filterings like SNR and COR. Regarding previous research, to obtain the most accurate data at each measuring location, the data sampling rate of ADV was set with the highest frequency (25 Hz) with a duration of 120 to 150 s (Martin et al., 2002; Rehmel, 2007). Following the proper setting of ADV and filtering data spikes, the velocity measurements were reliable within the range of 0.25 cm/s, with an error of ±1.5% of the measurement scale (Namaee & Sui, 2020; Sontek, 1997).

The present study used a SonTek-IQ Plus (SonTek-A Xylem Brand, San Diego, CA, USA) to measure the approaching flow rate, average velocity, and water depth. There are two types of SonTek-IQ (standard and plus); the Plus edition contains advanced post-processing functions, providing deeper insight into approaching flow and volume data, making it very precise and robust (Manual, 2017). The SonTek-IQ Plus contains six measuring beams (sensors); four are velocity beams, which monitor the flow velocity along the longitudinal and latitudinal axis to secure the best possible coverage and most accurate depiction of the velocity field. The remaining two measuring beams, the pressure sensor and vertical acoustic beams work together to measure the water level precisely (Manual, 2017). According to the SonTek-IQ Series User's Manual, the data collected using the SonTek-IQ Plus is subjected to a 1% error in the range of measurement scale. The SonTek-IQ Plus was installed on the flume bed in front of each sandbox (the location of the SonTek-IQ is depicted in Figure 3.1). The flume shape, size, and exact location of the device were set in the SonTek-IQ software. Then, based on these inputs and using the data collected by sensors, the software calculates the average flow velocity, water depth, and flow rate during each experimental run.

3.2.3 Data Collection

Before each experimental run, the surfaces of the sandboxes were levelled. Then, the flume was slowly filled with water to avoid initial scouring around the spur dikes. The valves opened completely after reaching the desired water levels, and the experimental run began. The initiation of the local scour process at the dike tip was observed from the first minute of each run. A scour hole slowly develops and surrounds the upstream side of the dike to the flume wall. Then, as time passes, the scour hole becomes deeper and wider and extends downstream of the dike.

One of the critical factors affecting the scour process is the time needed to reach the equilibrium condition. Equilibrium scour is defined as the condition when the dimensions of the scour hole do not change with time. Zhang et al. (2009) studied the local scour process around a spur dike and reported that 90% of the equilibrium depth happened about 2 hours after the experiment started. Other researchers claimed that 80% of the maximum scour depth occurred during the experiment's first two hours (Vijayasree et al., 2019). Namaee and Sui (2020) conducted experimental research on local scour around side-by-side piers. They indicate that the equilibrium depth of a scour hole could be achieved within the first 6 hours, although all their experimental runs lasted 24 hours. In the present study, no change in scour depth was observed after about 12 hours, and the scour hole reached its equilibrium condition. Therefore, each experimental run lasted for 24 hours to make sure that the scour process was entirely completed. Some experiments were conducted for 48 and 72 hours to investigate the time needed to achieve the equilibrium condition. Results confirm that after 24 hours, there was no change in the scour hole around the spur dike comparing to those of experiments that lasted for 48 and 72 hours.

After the scour process reached equilibrium, velocity components in all three dimensions around the dike and inside the scour hole were recorded using a 10-MHZ ADV. Regardless of the dike layout, water surface condition, and flow depths, the velocity measurements were taken from the bottom of the scour hole to the water surface with intervals of 1 cm for shallower flow depths and 2 cm for other flow depths (Figure 3.3).

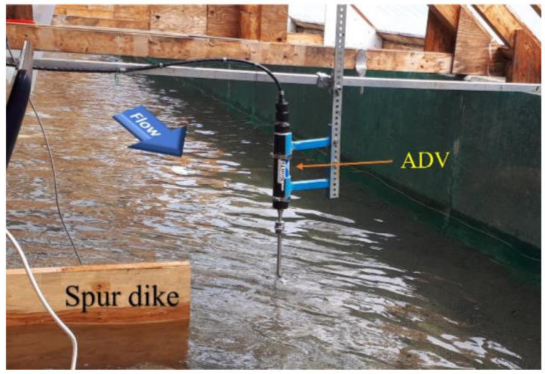

Figure 3. 3:3D Velocity data collection using the 10-MHz SonTek ADV

Results showed that the highest turbulence intensity of the flow occurred in the center of the scour hole, where the maximum scour depth occurred. Therefore, the ADV locale for the velocity measurements of all experimental runs was at the deepest part of the scour hole, which was very close to the tip of the spur dike. For this experimental study, U_x (x-axis) is used to describe the streamwise velocity in the downstream direction, U_y (y-axis) is used to denote the lateral velocity in the transverse direction pointing to the left bank, and the vertical velocity is expressed as U_z in the z-axis (towards the water surface). Under an ice-covered flow condition, a small part of the Styrofoam panel around the spur dike was cut to place the ADV probe in the flow to acquire velocity data. After 24 h, all valves were closed completely, and the flume was drained gradually. Then, the scour pattern was measured (Figure 3.4). Some of the experimental runs were repeated to validate the recorded data.

Figure 3. 4:Plan view of the scour hole

3.3 Results and Discussions

Throughout the scouring process, several horseshoe vortexes were detected inside the scour hole. This vortex system has been observed in a clockwise direction. Some small bow waves on the surface of the upstream side of the dike were also observed (Figure 3.5). Since bow waves had opposite rotation directions to those of horseshoe vortexes, these two eddy systems were interfering with each other. Results indicate that these interferences become less noticeable with the increase in water depth. Moreover, decreasing the dike orientation angle inclined to the downstream direction makes the bow waves smaller and less frequent. Moreover, these waves can hardly be observed for a dike with an orientation angle of 45° (toward downstream), and their effect on the horseshoe vortex was negligible.

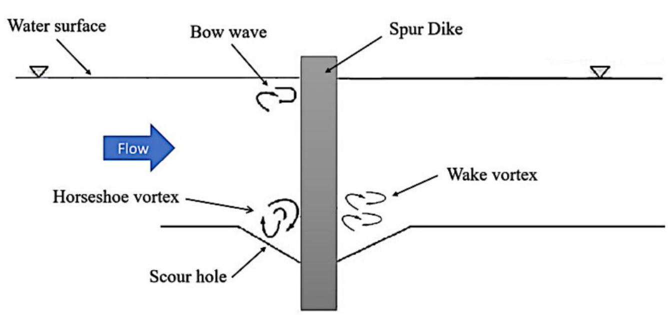

Figure 3. 5:Development of the vortex system around the spur dike (Ghaderi & Abbasi, 2019)

The horseshoe vortexes are created because of the flow separation at the dike tip and the formation of a powerful downflow at the upstream side of the dike. Consequently, a scour hole around the spur dike will be developed. The wake vortex system develops behind the spur dike, which results in the extension of the scour hole downstream of the dike. As pointed out by other researchers, wake vortexes are smaller and weaker than horseshoe vortexes, and they cannot carry sediment load that eroded from the scour hole (Melville et al., 2002; Namaee & Sui, 2020). This fact explains the development of the deposition ridge downstream of the dike (Figure 3.6).

Figure 3. 6:Deposition ridge on the downstream side of the spur dike

Inside the scour hole, horseshoe vortexes were created by the intense turbulence and a high level of instantaneous velocity fluctuation. Therefore, the bottomless hole that developed around the dike tip was the one where the horseshoe vortex flow and downflow were stronger. By studying the 3D velocity inside a scour hole, the effects of different flow conditions and the dike setups on the local scour pattern should be assessed.

The relationships between different parameters should be expressed using dimensionless variables to effectively translate laboratory findings to practical applications, such as rivers, spur dikes, and bridge piers. Furthermore, normalizing variables (making them dimensionless) will enable us to compare results under different experiment conditions. Therefore, in all figures in the present study, both velocity components and water depth (h, the vertical distance at which 3D velocity data was collected) were normalized by average approaching flow velocity (U) and total water depth in the sandbox (H), respectively.

3.3.1 Streamwise Velocity Component (Ux)

Among all 3D velocity components, the streamwise velocity (U_x) plays a crucial role in developing the scour hole and the turbulence structure. The streamwise velocity has the maximum value and highest fluctuation compared to the other two velocity components (Uy, Uz). Results show that regardless of the flow conditions and the orientation angle of the dike, velocity distributions inside the scour hole are less regular (or completely irregular). Moreover, the magnitudes of the streamwise velocity components inside the scour hole are smaller than those outside. However, in most cases, the highest level of fluctuation and the maximum velocity magnitude occur in the center of a scour hole, which is close to the dike tip.

In terms of the boundary conditions for the water surface, there were three different types: open flow, smooth covered condition, and rough covered condition. As indicated in Figure 3.7, the streamwise velocity (U_x) inside the scour hole is minimal at the bottom of the scour hole and increases with the distance from the scour hole bottom. The maximum streamwise velocity happens at the mid-water depth, and the streamwise velocity profile shows a convex shape. Of note is that the ADV measuring volume is located at 0.10 m from the probe head. Due to this limitation, the velocity profile cannot fully cover up to the water surface, as shown in Figure 3.7. Moreover, when a high level of turbulence existed at the measuring point using the ADV, the Doppler noise often appeared (McLelland & Nicholas, 2000). These noises decrease with the data collection process and create data spikes. Moreover, sediment movement near the scour hole bed interferes with data collection during the ADV measurements (Muste et al., 2000). By using Win ADV software, these ambiguous data were filtered. Therefore, velocity profiles can sometimes not cover the bottom of the hole.

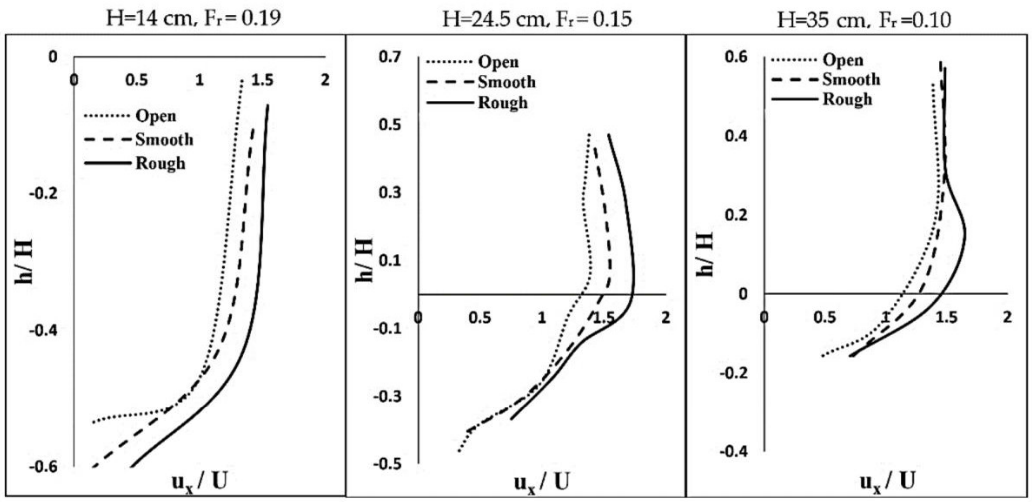

Figure 3. 7: u_x under different surface cover conditions, spur dike with an orientation angle of 90°

Regardless of the orientation angle of the dike and flow properties, under an ice-covered flow condition, the maximum velocity is located at the mid-depth of water. By increasing the cover's roughness coefficient, the maximum velocity's location is further shifted toward the channel bed. Additionally, cover conditions not only influence the location of U_{max} but also affect the magnitude of the velocity (Figure 3.7). Results indicate that rough ice cover can increase streamwise velocity values by nearly 25%. These findings agree with previous studies (Namaee & Sui, 2020; Sui et al., 2010; Sui et al., 2000). One can conclude that regardless of the shape and location of the barriers in an ice-covered river, the locale and magnitude of the maximum velocity depend on the features of an ice cover.

Under an ice-covered flow condition, the streamwise velocity (U_x) depends on the flow properties, such as water depth, cover roughness, and approaching velocity. In the present study, velocity profiles have been evaluated for all experiments. The flow Froud number (Fr) is one of the most essential dimensionless parameters, and the effect of Fr on U_x was examined.

$$F_r = \frac{U}{\sqrt{gH}} \tag{3.3}$$

where, U is the average approaching velocity, g is the gravitational acceleration, and H is the water depth.

The result indicates that with the decrease in the flow Froud number, the streamwise velocity distributions under different surface conditions (open channel, smooth cover, and rough cover) become closer, especially for velocity distributions under both open channel and smooth covered flow conditions. Figures 3.7 and 3.8 show that the Froud numbers for water depths of 14 cm, 24.5 cm, and 35 cm are 0.19, 0.15, and 0.10, respectively. The effect of ice cover condition on the velocity distributions appears to intensify with the increase in the flow Froud number. Moreover, as the dike orientation angle decreases from 90° to 45°, this effect becomes more tangible (Figures 3.7 and 3.8).

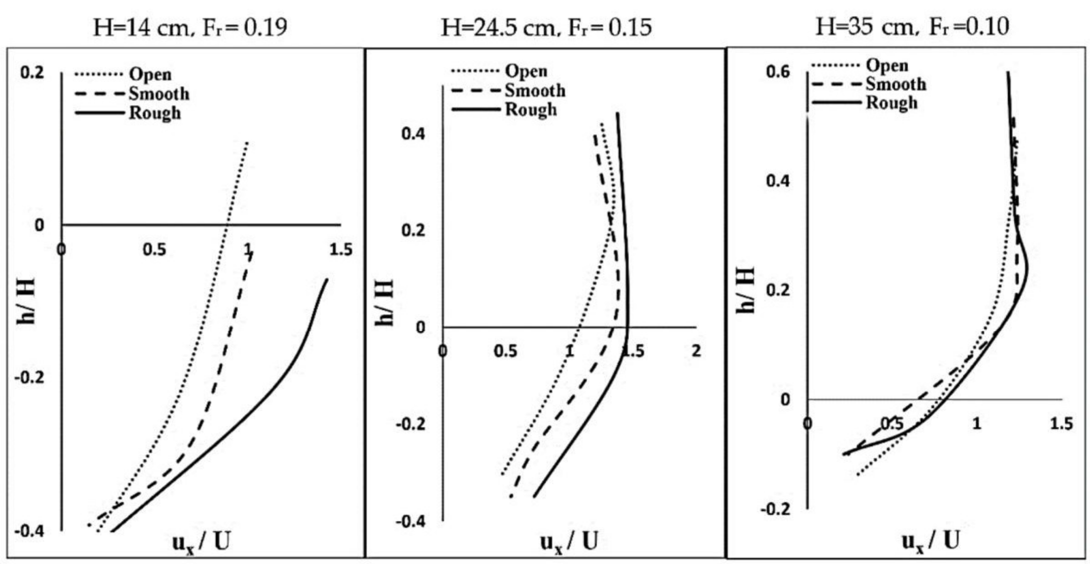

Figure 3. 8: u_x inside and outside the scour holes under different surface conditions with a 45° dike

As the dike orientation angle decreases, the magnitude of the streamwise velocity diminishes, and the scour hole becomes smaller. As indicated in Figures 9 and 10, regardless of the water depth and surface cover conditions, decreasing the dike orientation angle from 90° to 45° shifts the velocity profiles upward, implying a decrease in the scour hole depth. These findings are consistent with the continuity theory (Equation (3.4)). Since the spur dike reduces the cross-section area of the flow, the velocity should increase. As the dike orientation angle decreases, the cross-section area increases, and velocity decreases.

$$(\rho AU)_{inlet} = (\rho AU)_{outlet} \tag{3.4}$$

where, ρ is the mass density of water, A is the cross-section area of the flow, and U is the average approaching velocity.

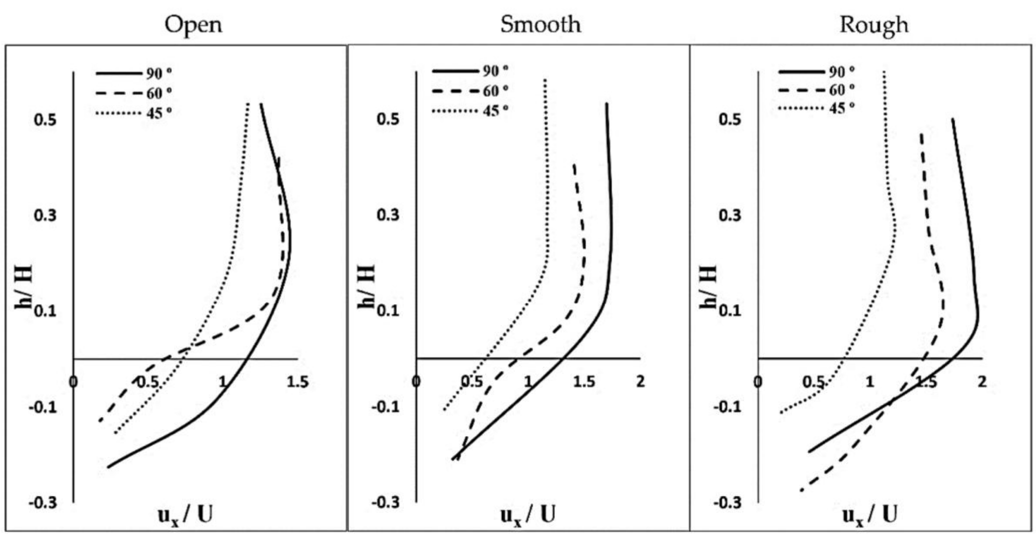

Figure 3. 9: u_x inside and outside the scour holes for different dike orientation angles (water depth: 31 cm)

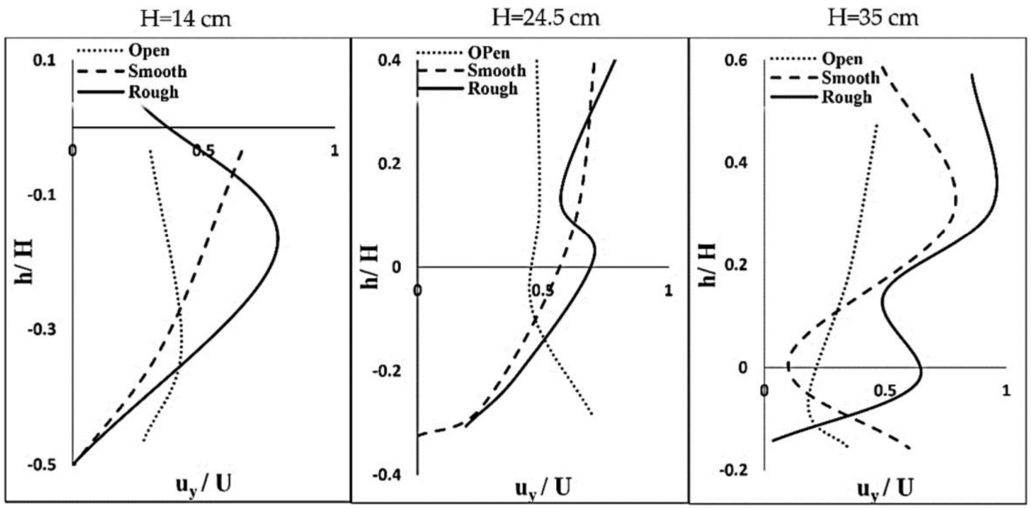

Figure 3. 10: u_y inside and outside the scour holes under different surface conditions with a 90° dike

With the decrease in the dike orientation angle (from 90° to 45°), the blockage ratio of the flow cross-section decreases. Therefore, both the downflow and horseshoe vortex become weaker. This leads to the formation of a smaller scour hole. Of note, these effects are independent of the surface cover condition, water depth, and flow rate (Figure 3.9).

3.3.2 Lateral Velocity Component (Uy)

When multiple spur dikes are used, close spacing can provide continuous protection along a riverbank or around a bridge pier. Two significant characteristics of the lateral velocity component (U_y) are their irregularity and much smaller values than the streamwise velocity component (U_x). After scrutinizing U_y profiles (under different conditions of surface cover, flow rate, water depth, and dike orientation angle), results reveal that the vertical distribution of the lateral velocity component was nonmonotonic. Compared to the streamwise velocity component (U_x), the lateral velocity component (U_y) is considerably smaller and primarily positive. Some non-negligible effects have been observed in the vertical distribution profiles of the lateral velocity component (U_y). It is noted that the presence of an ice cover increases the magnitude of the lateral velocity regardless of the flow rate, water depth, and dike orientation angle. With the increase in the cover roughness coefficient, the value of U_y increases (Figure 3.10). This result indicates that the ice cover plays an essential role in the value of U_y.

To determine the effects of the dike orientation angle on U_y, the vertical distribution profiles of the lateral velocity component (U_y) were evaluated. As indicated in Figure 11, with the decrease in the dike orientation angle, the magnitude of U_y decreases, similar to the effect of the dike orientation angle on the streamwise velocity. Furthermore, results indicate that only for the dike orientation angle of 90°, a semi-consistent pattern has been noticed for the vertical distribution profiles of the lateral velocity component (Figure 3.11). No clear or meaningful trend was detected for the dike orientation angles of 60° and 45° (despite different flow rates, surface conditions, and bed materials). Nevertheless, in all cases, the vertical distribution profiles of the lateral velocity component (U_y) were positive inside and outside the scour holes with an equivocal pattern. Thus, the locales of the maximum lateral velocity component in the vertical distribution profiles remain unknown (Figures 3.10 and 3.11).

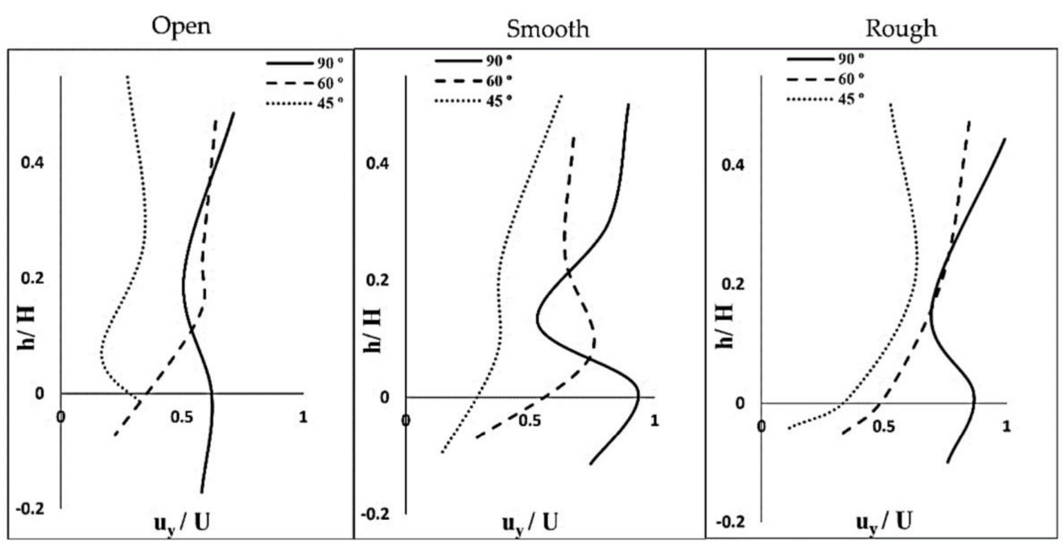

Figure 3. 11: u_y inside and outside the scour holes under different surface conditions, water depth: 35 cm

3.3.3 Vertical Velocity Component (Uz)

To evaluate the vertical velocity component (U_Z) under different experimental conditions, its vertical distribution in the center of the scour hole (the location of the maximum scour depth) has been examined. Results show that the values of the vertical velocity component are mostly negative inside and outside the scour holes (Figure 3.12). These negative values signify the existence of the powerful downflow around the dike, created due to the obstruction of the flow by the spur dike. This downflow plays an essential role in the local scour process because the downward velocity increases and strengthens the horseshoe vortex system, which leads to a deeper scour hole. This fact is consistent with the local scour morphology around the spur dike. As illustrated in Figure 3.13, for the dike perpendicular to the flume wall (with an orientation angle of 90°), the scour hole is the deepest compared to those of dikes with other orientation angles (60° and 45°). Thus, it can be concluded that by increasing the blockage ratio of the obstacle (such as piers and spur dikes), downward velocity will increase and create a more powerful vertical velocity component inside the scour hole.

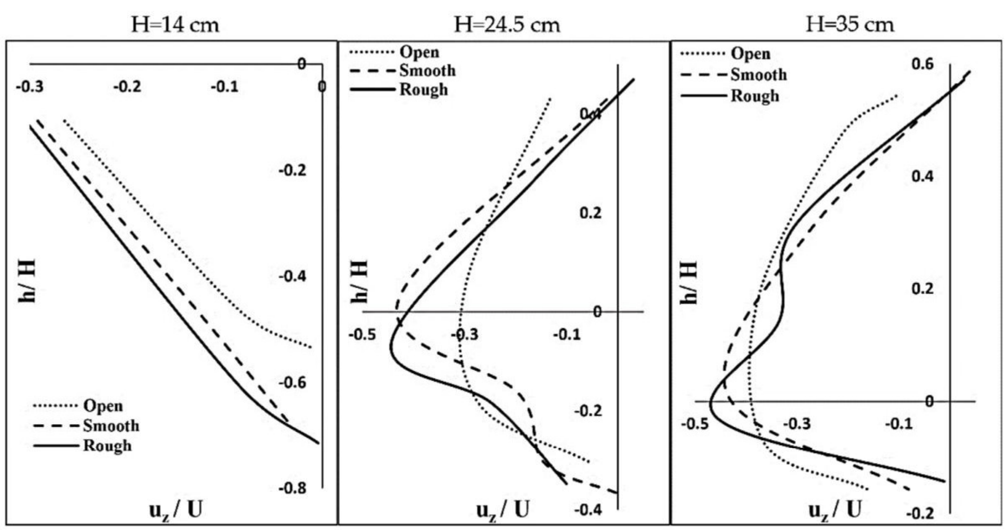

Figure 3. 12: u_z inside and outside the scour holes under different flow conditions with a dike of 90°

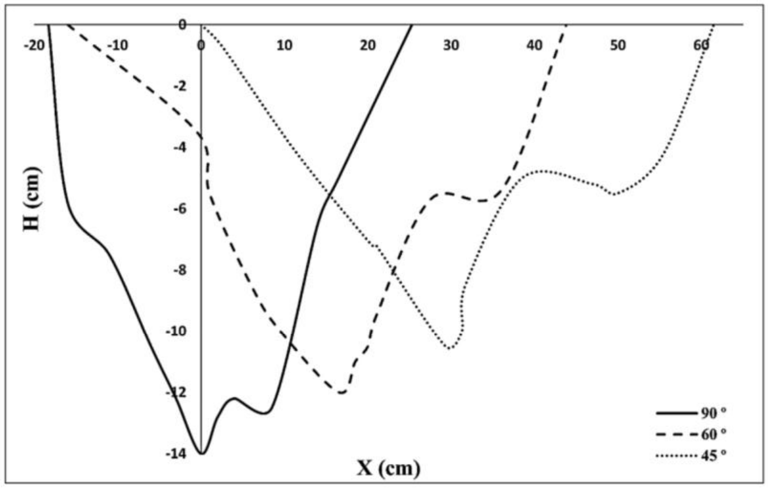

Figure 3. 13:Scour hole profiles around the dike with different angles (water depth: 11 cm, open channel flow)

Considering the absolute value of the vertical velocity, the U_z values reach their minimum at the bottom of the scour hole and increase with the distance from the bottom. The maximum value of U_z occurs around the initial level of the sand bed (before the scouring process starts), and then it reduces toward the flow surface. Uz becomes very small (close to zero) close to the water surface, and in some cases, it turns positive. The vertical velocity distribution shows a parabolic shape (Figure 3.12). Results show that vertical velocity vectors change their direction near the flow surface.

As shown in Figure 3.12, the ice cover significantly impacts the value of U_z. The presence of an ice cover on the surface of the flow results in apparent changes in the shape of the vertical velocity distribution. One can also notice that under open flow conditions, the minimum values of U_z are always negative. However, by adding an ice cover to the flow surface, the minimum values of U_z are closer to zero and are positive in some cases. Furthermore, the absolute magnitude of the U_z increases with the increase in the roughness coefficient of the cover. Therefore, it can be concluded that under an ice-covered flow condition, the vertical velocity component (U_z) is the most critical velocity component for developing scour holes compared to other velocity components (U_x and U_y). Moreover, results indicate that the presence of an ice cover influences the locale of the maximum vertical velocity. As the ice cover becomes rougher, the location of the maximum vertical velocity moves closer toward the channel bed. However, compared to the streamwise velocity component (U_x), this effect on the location of the maximum vertical velocity component is less noticeable (Figures 3.7 and 3.12).

Results reveal that by increasing the flow rate, the value of U_z increases, and velocity profiles shift toward the water surface. The water depths are 14 cm, 24.5 cm, and 35 cm, and the average approaching velocity (U) is 21, 24, and 17 cm/s, respectively. One can see that the differences in the average approaching velocity are small. However, as shown in Figure 3.14, the difference in the vertical velocity distribution is remarkable. Therefore, one can say that the flow rate is one important factor responsible for the change in the vertical velocity component (U_z) profile. Results also showed that the maximum value of Uz under rough-covered flow conditions is higher than that under open and smooth-covered flow conditions.

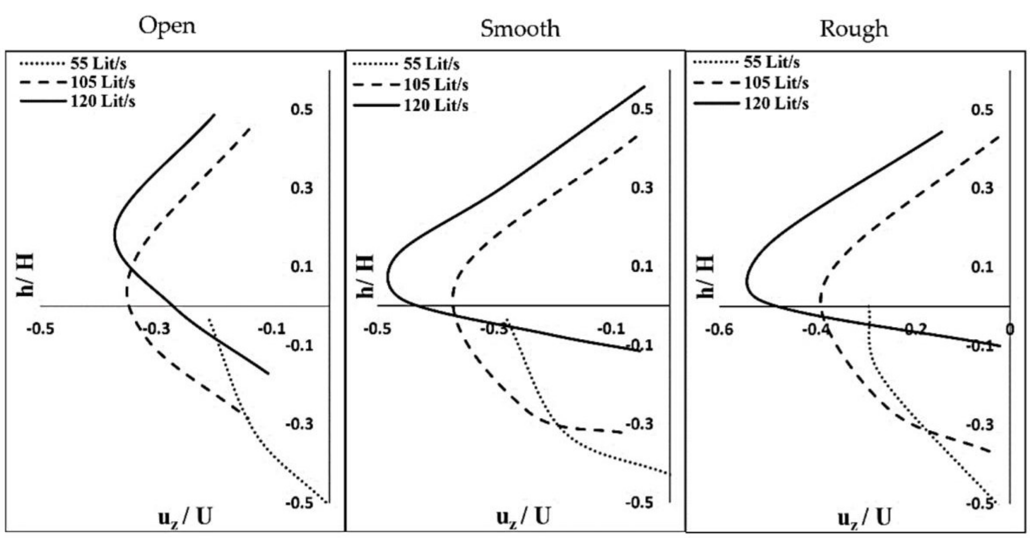

Figure 3. 14: u_z inside and outside the scour holes under different flow rates with a dike of 90°

Further studies have been conducted to assess the impact of the dike orientation angle on the U_z distributions. Results reveal that by reducing the blockage ratio of the dike (namely, by decreasing the dike orientation angle), the effect of the ice cover on the vertical velocity profile became less noticeable. The presence of an ice cover on the flow surface leads to a considerable change in the shape of the Uz profile. However, by reducing the dike orientation angle from 90° to 45°, the vertical velocity profiles for a flow under an open channel become more similar to that under an ice-covered flow condition. Likewise, by reducing the dike orientation angle, the absolute value of U_z decreases (Figure 3.15). Results indicated that when the dike orientation angle is reduced, the vertical velocity component will be significantly affected in two ways: (1) the effect of an ice cover will be counteracted, and (2) the downward velocity vectors will be weakened. Of note, this effect is more noticeable regarding scour hole depth than the surface area.

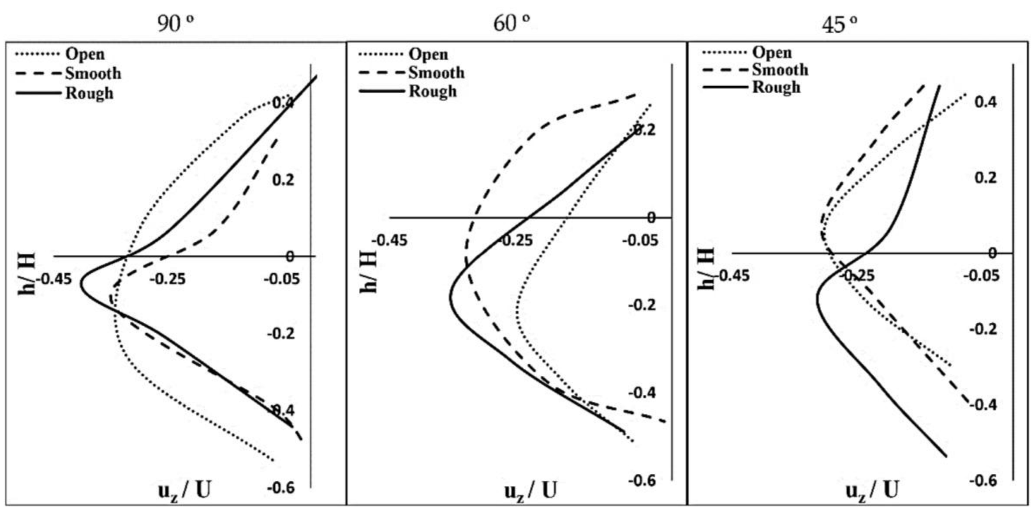

Figure 3. 15: u_z inside and outside the scour holes under different surface conditions; water depth: 21.5 cm

3.3.4 Turbulence Intensities and Reynolds Shear Stress

It is noted that inside the scour holes, the flow is a combination of the downflow and horseshoe vortexes, which cause a complex turbulence structure. Turbulent eddies generate velocity fluctuations, referred to as turbulence strength (u_{rms}). u_{rms} was defined as the standard deviation (root mean square (RMS)) of the instantaneous velocity fluctuations. As Equation (3.5) described, u_{rms} were calculated based on 3D velocity components measured by ADV. A larger u_{rms} signifies a higher level of turbulence.

$$u_{rms} = \sqrt{\frac{1}{N}\sum_{i=1}^{N}(u_i^{'})^2} \tag{3.5}$$

where, u_{rms} is the root-mean-square of the turbulent velocity fluctuations, u_i' is the instantaneous fluctuations of velocity components.

Because turbulent bursts are the main mechanism that entrains sediment and initiates the scouring process (Jennifer et al., 2011; Sui et al., 2010), the distribution patterns of the turbulence strength of 3D velocity components (u_x', u_y', u_z') have been examined. To accurately assess different instantaneous velocity fluctuations, the turbulence strength has been normalized by the average approach velocity (U). Results reveal that in most cases, the highest level of fluctuation occurs in the center of the scour holes (very close to the dike tip) and the exit of the hole (flume bed) due to the exposure of a larger flow field. As indicated in Figure 3.16, the streamwise turbulence intensity (u_x') is generally the largest, and the vertical turbulence intensity is the least, namely, $u_x' > u_y' > u_z'$. Moreover, the streamwise and vertical turbulence intensity generally followed a distinct pattern—they are small (close to zero) at the scour hole bottom and increase with the distance from the scour hole bottom. Usually, u_x' and u_z' become slightly above the scour hole (flume bed) and decrease toward the water surface, creating the reverse C shape profiles. Nonetheless, no consistent trend has been observed for the lateral turbulence intensity (Figure 3.16).

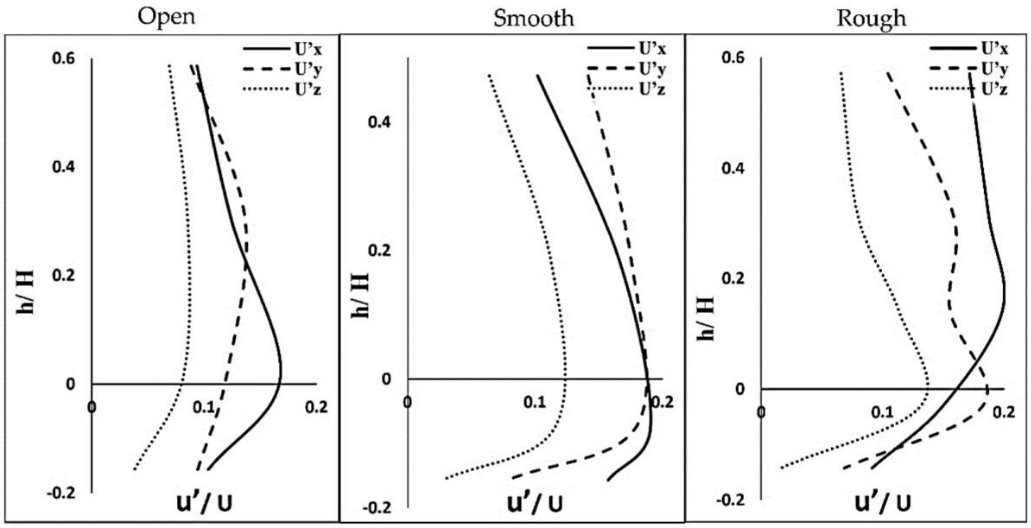

Figure 3. 16:Turbulence intensity in three directions with the 90° dike (water depth: 35 cm)

In terms of the impact of an ice cover on the turbulence strength, results indicate that the presence of an ice cover increases the turbulence intensities. With the increase in the roughness coefficient of an ice cover, the maximum fluctuation amount increases (Figure 3.16). Additionally, the approaching velocity plays an important role in the turbulence intensity. Regardless of the surface cover condition or the dike orientation angle, the maximum instantaneous velocity fluctuations happen when the approaching velocity is the highest. Experiments clearly show that with a high approaching velocity, the maximum depth of the scour hole will be reached in a shorter amount of time. Moreover, the scour hole becomes larger with a higher approaching velocity.

The local scour process starts with the increase in the shear stress resulting from the accelerating flow around the spur dike. The shear stress refers to the Reynolds stress (τ), which can be illuminated as the transport of the streamwise momentum through a surface normal to the z-axis. Based on instantaneous velocity fluctuations collected using the ADV, the Reynolds shear stress can be calculated (Equation (3.6)) (Zhang et al., 2009). The Reynolds stress plays a key role in the entrainment and movement of sediment particles.

$$\tau = -\rho < u_x^{'} u_z^{'} > \tag{3.6}$$

where, τ is the Reynolds stress, ρ is the mass density of water, $u_x^{'}$ is the streamwise turbulence strength and $u_z^{'}$ is the vertical turbulence strength.

To better understand the Reynolds stress distribution inside scour holes, the Reynolds stress values were normalized by the shear velocity (friction velocity) u_*^2. The Shear velocity was calculated based on the boundary layer characteristic method (BLCM) (Afzalimehr et al., 2019), as illustrated in Equation (3.7).

$$\frac{\tau}{\tau_b} = \frac{-< u_x^{'} u_z^{'} >}{u_*^2} \tag{3.7}$$

where, τ is the Reynolds stress, $u_x^{'}$ is the streamwise turbulence strength, $u_z^{'}$ is the vertical turbulence strength, τ_b is the bed shear stress, and u_* is the shear velocity or friction velocity.

$$u_* = \frac{(\delta_* - \theta)\, u_{max}}{C\delta_*} \tag{3.8}$$

where, δ_* is the displacement thickness, θ is the momentum thickness, which is defined by (Schlichting & Gersten, 2016), C is a constant which was estimated as 4.4 for Canadian rivers (Afzalimehr & Rennie, 2009).

As shown in Figure 3.17, the Reynolds stress is zero at the scour hole bottom and gradually decreases to the least negative value, and it becomes zero again in the middle of the scour holes; then, it increases with the distance from the scour hole bottom. Afterward, it decreases toward the water surface. Inside the scour hole, the distribution of the Reynolds stress has a parabolic shape. Outside the scour hole, the Reynolds stress value becomes positive, reaching its maximum slightly above the initial level of the sand bed (flume bed). Then, it reduces again toward the flow surface and becomes negative close to the surface, creating a convex shape distribution (Figure 3.17).

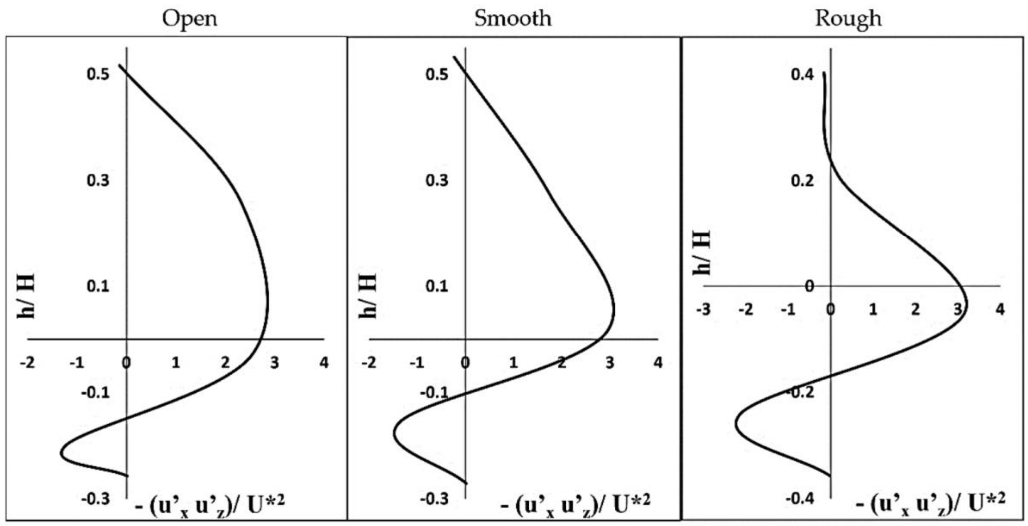

Figure 3. 17:Reynolds stress, under different surface conditions for the dike with 90° (water depth: 31 cm)

The negative Reynolds stress inside the scour hole demonstrates an upward vertical momentum transport caused by a negative velocity gradient ($\frac{du}{dz} < 0$). Similarly, the negative Reynolds stress close to the flow surface indicates the impact of the adverse pressure gradient at the upper portion of the flow, which also has a negative velocity gradient.

Results show that the value of Reynolds stress under an ice-covered flow condition is greater than that under an open flow condition. With an ice cover's roughness increase, the Reynolds stress's absolute value rises (Figure 3.17). It can be concluded that higher shear stress at the sand bed will be generated under the ice-covered flow conditions. This increase in shear stress leads to more sediment movement around the dike, creating a larger scour hole.

3.4 Conclusions

The three-dimensional velocity components and turbulence structure inside and outside scour holes around the spur dikes in a large-scale flume have been investigated. The model spur dikes are impermeable and non-submerged, with orientation angles of 90°, 60°, and 45°, respectively. Experiments have been conducted under open channel, smooth-covered, and rough-covered flow conditions to comprehensively study flow characteristics near a dike. Based on data collected from laboratory experiments, the impacts of the spur dike on the 3D velocity distributions, Reynolds shear stress, and turbulence intensities have been investigated. Overall, the following results were obtained in this experimental study.

The presence of an ice cover on the water surface causes a considerable change in the bed shear stress. It raises the turbulence intensities inside the scour holes, significantly affecting sediment transportation. To be more specific, the presence of an ice cover increases the maximum values of the 3D velocity components average by 10% to 25% for smooth and rough ice cover, respectively. The rough ice cover shifts the location of the maximum velocity further close to the sandbed, which leads to the increase in the Reynolds shear stress inside the scour hole and, accordingly, results in a deeper scour hole. These effects are independent of flow rates and dike orientation angle.

The dike with an orientation angle of 90° generates the strongest downflow around the dike compared to those resulting from the orientation angles of 45° and 60°. Thus, the dike with an orientation angle of 90° creates high turbulence and powerful horseshoe vortexes inside the scour holes generate the deepest scour hole compared to those around the dike with the smaller orientation angles. Results show that reducing the dike orientation angle from 90° to 45° shifts the velocity profiles upward, and scour hole depth decreases by 5–10% for each 10° angle decrease. These results imply that changing the dike orientation angle will reduce the blockage ratio of the cross-section area. Consequently, the vortex system in the vicinity of the spur dike will become weak. Thus, the turbulence kinetic energy inside the scour hole is reduced.

Generally, the 3D velocity distributions are less regular inside the scour holes. Besides, the velocity components inside the hole are smaller than those outside the scour holes. The highest velocity fluctuation and turbulence intensity level appear immediately above the scour holes. The maximum turbulence intensity increases with the increase in the roughness coefficient of an ice cover. The smooth and rough ice cover raised turbulence intensity averages by 15% and 30%, respectively. Moreover, the instantaneous velocity fluctuation increases with the increases in the approaching velocity. The higher the flow velocity, the more influential the turbulence kinetic energy around the spur dike, and thus, the deeper the scour holes.

The streamwise velocity (U_x) is the highest among all 3D velocity components, implying that U_x contributes more to the turbulence intensities, Reynolds shear stress, and, consequently, the development of the scour holes. The lateral velocity component (U_y) has the highest level of irregularities inside and outside the scour hole. Unlike the streamwise and vertical velocity (U_z) distributions, no meaningful trend has been observed for the lateral velocity component. Moreover, the presence of an ice cover on the water surface considerably affects the lateral velocity component. The lateral velocity increased with the increase in the roughness coefficient of an ice cover.

Both the streamwise velocity component and lateral velocity component are almost always positive. However, the vertical velocity component is almost negative inside and outside the scour holes. The negative vertical velocity components indicate the powerful downflow and downward velocity near the dike. The absolute value of U_z increases proportionately with the approaching flow velocity. The higher the approaching velocity, the more the vertical velocity component absolute value. This effect has been intensified with the increase in the roughness coefficient of an ice cover. Under an ice-covered flow condition, the distribution pattern of U_z differs entirely from that under an open flow condition. Moreover, the maximum vertical velocity was observed when the dike had an orientation angle of 90°. With an increase in the dike angle of each 10° (from 45° to 90°), the absolute value of vertical velocity relatively increases by up to almost 10%, implying that the dike orientation angle is one of the important controlling factors for U_z.

The Reynolds shear stress is negative inside the scour holes and becomes positive toward the flow surface. It reaches its maximum slightly above the scour holes. The negative values of the Reynolds stress are caused by the upward vertical momentum transport generated by a negative velocity gradient. Additionally, with the increase in the roughness coefficient of an ice cover, the absolute value of the Reynolds stress increases. It can be concluded that the presence of an ice cover creates more powerful shear stress at the sand bed, which causes a deeper scour hole.

3.5 Bibliography

Afzalimehr, H., Maddahi, M. R., Naziri, D., & Sui, J. (2019). Effects of non-submerged boulder on flow characteristics–a field investigation. International Journal of Sediment Research, 34(2), 136-143.

Afzalimehr, H., & Rennie, C. (2009). Determination of bed shear stress using boundary layer parameters in a gravel-bed river. Hydrological Sciences Journal, 54(1), 147-159.

Dey, S., & Barbhuiya, A. K. (2006). Velocity and turbulence in a scour hole at a vertical-wall abutment. Flow Measurement and Instrumentation, 17(1), 13-21.

Duan, J. G., He, L., Fu, X., & Wang, Q. (2009). Mean flow and turbulence around experimental spur dike. Advances in Water Resources, 32(12), 1717-1725.

Giglou, A. N., Mccorquodale, J. A., & Solari, L. (2018). Numerical study on the effect of the spur dikes on sedimentation pattern. Ain Shams Engineering Journal, 9(4), 2057-2066.

Huai, W., Zeng, Y., Xu, Z., & Yang, Z. (2009). Three-layer model for vertical velocity distribution in open channel flow with submerged rigid vegetation. Advances in Water Resources, 32(4), 487-492.

Jennifer, D., Li, H., Guangqian, W., & Xudong, F. (2011). Turbulent burst around experimental spur dike. International Journal of Sediment Research, 26(4), 471-523.

Kadota, A., & Suzuki, K. (2010). Local scour and development of sand wave around T-type and L-type groynes. In Scour and Erosion (pp. 707-714).

Kanda, K., Samoto, Y., & Li, Z. (2019). Study on morphodynamics around stone-lined spur dikes in the Akashi river. In River, Coastal and Estuarine Morphodynamics: RCEM 2007, Two Volume Set (pp. 1176-1182). CRC Press.

Kuhnle, R. A., Alonso, C. V., & Shields, F. D. (1999). Geometry of scour holes associated with 90 spur dikes. Journal of Hydraulic Engineering, 125(9), 972-978.

Kuhnle, R. A., Jia, Y., & Alonso, C. V. (2008). Measured and simulated flow near a submerged spur dike. Journal of Hydraulic Engineering, 134(7), 916-924.

Li, S. S. (2012). Estimates of the Manning's coefficient for ice-covered rivers. Proceedings of the Institution of Civil Engineers-Water Management, Manual, S.-I. S. U. s. (2017). SonTek-IQ Series Intelligent Flow Featuring Smart Pulse HD User's Manual [User's Manual]. Xylem brand, SmartPulse HD

User's Manual(Firmware Version 3.0), 135. https://doi.org/SonTek-IQ Series

Intelligent Flow (Xylem Inc)

Martin, V., Fisher, T., Millar, R., & Quick, M. (2002). ADV data analysis for turbulent flows: Low correlation problem. Hydraulic Measurements and Experimental Methods 2002,

Mays, L. W. (1999). Hydraulic design handbook. McGraw-Hill Education.

McLelland, S. J., & Nicholas, A. P. (2000). A new method for evaluating errors in high-frequency ADV measurements. Hydrological processes, 14(2), 351-366.

Melville, B. W., Coleman, S., & Hoe, D. (2002). Countermeasures for Scour at Spill-Trough Bridge Abutments. First International Conference on Scour of Foundations. November 17-20, 2002, College Station, USA,

Mizutani, H., Nakagawa, H., Kawaike, K., Baba, Y., & Zhang, H. (2011). STUDY ON LOCAL SCOUR AND VARIATION OF BED COMPOSITION AROUND NON-SUBMERGED SPUR DYKE. Journal of Japan Society of Civil Engineers, Ser. B1 (Hydraulic Engineering), 67.

Muste, M., Braileanu, F., & Ettema, R. (2000). Flow and sediment transport measurements in a simulated ice-covered channel. Water Resources Research, 36(9), 2711-2720.

Muto, Y., Baba, Y., & Aya, S. (2002). Velocity measurements in open channel flow with rectangular embayments formed by spur dikes. Annuals of Disaster Prevention Research Institute, Kyoto University B, 45, 2.

Namaee, M. R., & Sui, J. (2020). Velocity profiles and turbulence intensities around side-by-side bridge piers under ice-covered flow condition. Journal of Hydrology and Hydromechanics, 68(1), 70-82.

Nelson, J. M., Shreve, R. L., McLean, S. R., & Drake, T. G. (1995). Role of near-bed turbulence structure in bed load transport and bed form mechanics. Water Resources Research, 31(8), 2071-2086.

Pandey, M., Ahmad, Z., & Sharma, P. (2018). Scour around impermeable spur dikes: a review. ISH Journal of Hydraulic Engineering, 24(1), 25-44.

Papanicolaou, A., Diplas, P., Dancey, C., & Balakrishnan, M. (2001). Surface roughness effects in near-bed turbulence: Implications to sediment entrainment. Journal of Engineering Mechanics, 127(3), 211-218.

Rehmel, M. (2007). Application of acoustic Doppler velocimeters for streamflow measurements. Journal of Hydraulic Engineering, 133(12), 1433-1438.

Sadat, S. H. (2015). MODIFICATION OF SPUR-DIKE WITH FOOTING OR PILE-GROUP TO STABILIZE RIVER MORPHOLOGY AND REDUCE LOCAL SCOUR [Dissertation, Nagoya Institute of Technology]. http://doi.org/10.20602/00003162

Schlichting, H., & Gersten, K. (2016). Boundary-layer theory. Springer.

Sontek, A. D. V. (1997). Operation manual, firmware version 4.0. (Sontek, San Diego.)

Sui, J., Jun, W., Yun, H., & Faye, K. (2010). Velocity profiles and incipient motion of frazil particles under ice cover. International Journal of Sediment Research, 25(1), 39-51.

Sui, J., Wang, D., & Karney, B. W. (2000). Suspended sediment concentration and deformation of riverbed in a frazil jammed reach. Canadian Journal of Civil Engineering, 27(6), 1120-1129.

Telionis, D., Yang, Y., & Rediniotis, O. (2009). Recent developments in multi-hole probe (mhp) technology. 20th international congress of mechanical engineering,

Teraguchi, H., Nakagawa, H., MUTO, Y., BABA, Y., & ZHANG, H. (2008). Flow and sediment transport around impermeable or permeable groins. PROCEEDINGS OF HYDRAULIC ENGINEERING, 52, 175-180.

Vijayasree, B., Eldho, T., Mazumder, B., & Ahmad, N. (2019). Influence of bridge pier shape on flow field and scour geometry. International journal of river basin management, 17(1), 109-129.

Wahl, T. L. (2000). Analyzing ADV data using WinADV. In Building partnerships (pp. 1-10).

Weitbrecht, V., Kühn, G., & Jirka, G. (2002). Large scale PIV-measurements at the surface of shallow water flows. Flow Measurement and Instrumentation, 13(5-6), 237-245.

Wu, P., Sui, J., Hirshfield, F., Wang, J., & Chen, P.-p. (2014). Impacts of ice cover on local scour around semi-circular bridge abutment. Journal of Hydrodynamics, 26(1), 10-18.

Yossef, M. M., & Klaassen, G. J. (2002). Reproduction of groynes-induced river bed morphology using LES in a 2-D morphological model. River Flow,

Zhang, H., Nakagawa, H., ISHIGAKI, T., & MUTO, Y. (2005). Prediction of 3D flow field and local scouring around spur dykes. PROCEEDINGS OF HYDRAULIC ENGINEERING, 49, 1003-1008.

Zhang, H., Nakagawa, H., Kawaike, K., & Yasuyuki, B. (2009). Experiment and simulation of turbulent flow in local scour around a spur dyke. International Journal of Sediment Research, 24(1), 33-45.

4 CHAPTER FOUR: Channel deformation around non-submerged spur dikes with different alignment angles under ice cover

(Accepted for publication by the Journal of Hydrology and Hydromechanics)

4.1 Introduction

The flowing water in rivers and streams plays a pivotal role in sustaining human life while serving as a habitat for various aquatic vegetation and animals. Human activities have modified river flows by constructing various channels and structures (Giglou et al., 2018). The in-stream infrastructures, such as spur dikes and bridge piers, significantly affect flow characteristics and riverbed deformation. The flow characteristics in the presence of in-stream infrastructures have been investigated by many researchers (Namaee et al., 2021; Wu, Hirshfield, Sui, et al., 2014).

Spur dikes are one of the in-stream infrastructures widely used in river engineering and water ecological restoration projects for various purposes such as bank protection, the maintenance of navigation channels, flood control, improvement of the habitat zone, and ecosystem rehabilitation. Spur dikes are hydraulic structures extending to the river flow from the channel bank and can be built from various materials such as riprap, concrete, and steel structures. A spur dike is described as permeable if river flow can pass through it, and it is impermeable if it completely blocks the flow (Pandey et al., 2018). A permeable spur dike usually slows down sediment transportation by reducing the velocity on its upstream side, thus reducing the scour process (Gu et al., 2011). In contrast, an impermeable spur dike can benefit riverbank protection and flood control. An impermeable spur dike protects the riverbank from erosion by repelling a turbulent flow in some parts of the river. In the event of a flood, by reducing the flow energy, an impermeable spur dike redirects and controls the rapid flows (Teraguchi et al., 2008; Zhang & Nakagawa, 2008). Spur dikes significantly change the flow patterns and bed morphology due to the decrease in the channel width and formation of a contraction section. An obvious flow separation and recirculation are generated in the vicinity of a spur dike, which raises the turbulence kinetic energy and shear velocity surrounding the spur dike and thus causes the extreme scouring process of the river bed (Yazdi et al., 2010).

The erosion process around a spur dike is one of the most critical issues in fluvial hydraulics and has been investigated to predict the geometry of the scour holes (Giglou et al., 2018). Derrick et al. (1989) studied spur dikes and pile dikes that are widely used in large river development projects. Some research focuses on the sediment deposition pattern and velocity structures behind the permeable spur dike (Tominaga et al., 2000). Ishigaki et al. (2000) claimed that the vortex development occurs aside from the dike, and the deepest hole is created at some distance from the obstacle. Also, either utilizing laboratory experiments or computational simulations, some research works have been conducted to investigate flow structures and sediment transport in the presence of different obstacles in channels such as spur dikes, bridge piers and abutments (Shahmohammadi et al., 2021; Wu et al., 2016).

As (Kuhnle et al., 2002) pointed out, a dike's flow depth and orientation angle affect the maximum erosion depth and the scour hole volume. Results showed that the ratio of the scour volume to the maximum erosion depth is variable and rises with the decrease in flow depth in shallow rivers and demonstrated that the blockage ratio significantly affected the geometric characteristics of the scour hole (Zhang et al., 2018). Ishigaki and Baba (2004) found that the downward-angled spur dike (oriented at a downstream angle) was less effective than the deflecting one (intended to deflect the flow rather than completely block it) in protecting channel banks from erosion. Most reported research works are about calculating the maximum scouring depth instead of the scour hole geometry (Kuhnle et al., 2002). Based on the morphological dimensions of scour holes, Haltigin et al. (2007) predicted the geometric features of scour holes.

In cold regions, such as northern Canada, it is pervasive for rivers to be covered by ice in winter. The presence of an ice cover emerges as an essential factor that significantly influences the morphology and scouring patterns around spur dikes (Namaee & Sui, 2019b; Peng et al., 2015). The appearance of an ice cover on the water surface enforces different geomorphological situations to flow characteristics, sediment transportation, and velocity distribution (Wu, Hirshfield, Sui, et al., 2014). al. (2002) stated that an ice cover on the water surface could increase the scour hole depth up to 35%. Sui et al. (2010) pointed out that the location of the maximum streamwise velocity depends on the ratio of roughness coefficients of the ice cover to that of the channel bed and will be shifted toward the smoother boundary. This change in the streamwise velocity contributes more kinetic energy to the riverbed and increases the bed shear stress (h. Wang et al., 2008). Therefore, the roughness coefficients of the ice cover and channel bed play an essential role in the scour morphology under an ice-covered flow condition (Ashton, 1986; Smith & Ettema, 1995). Zabilansky et al. (2006) claimed that the roughness of an ice cover is significant for the deformation of the channel bed. Hains (2004) concluded that the roughness of an ice cover considerably affects the bed shear stress, and the increase in the bed shear stress will result in amplified bed erosion and scour depth.

Numerous numerical simulations and laboratory experiments have been conducted to study the bed morphology and local scour around spur dikes. However, to the authors' knowledge, no research has been reported to investigate the effect of an ice cover on the geometrical features of channel bed deformation around non-submerged spur dikes with different alignment angles. The current research is based on laboratory experiments to investigate the geometric characteristics of channel bed deformation around spur dikes, considering different alignment angles under smooth and rough ice-covered flow conditions.

4.2 Methodology and Materials

4.2.1 Experimental setup and equipment for measurements

Experimental investigations typically occur in compact indoor hydraulic flumes due to the higher costs of constructing larger outdoor flumes. Smaller-scale flumes often have limitations in flow depths and discharge ranges, and considerations must be made regarding the impact of sidewalls within the flume. On the other hand, larger flumes offer a wider range of options for selecting hydraulic parameters and can be considered approximations of small natural rivers. Conducting simulations of scour phenomena in larger hydraulic flumes is expected to yield more accurate results (P Wu et al., 2015).

This experimental investigation was conducted in a large-scale outdoor flume at the Quesnel River Research Center in Canada. As depicted in Figure 4.1, this flume is 38.2 m long, 2.0 m wide, and 1.3 m deep. The longitudinal slope of the flume bed is 0.2%. A water holding tank with a capacity of 90 m^3 and dimension of 40.0 m × 2.0m × 1.3 m is located upstream of the flume and used to maintain a designated discharge for each experimental run. The tank is supplied by three standpipes, facilitating a maximum flow rate of 0.12 m^3/s. Notably, a gradual change in water level was observed along the flume section from upstream to downstream, attributed to the flume's slope. Consequently, the flow was classified as non-uniform. A roof covering the entire flume section was built to mitigate the influence of environmental factors, including precipitation, wind, and tree leaves.

Two sandboxes were meticulously constructed within the flume, with a spacing distance of 10.2 meters. The upstream sandbox is 5.6 m long, 2.0 m wide, and 0.3 m deep, while the downstream one spans 5.8 meters in length, 2.0 meters in width, and 0.3 meters in depth. Notably, one sidewall of each sandbox section is made of plexiglass, facilitating precise observation of the scouring process. This study selected three types of non-uniform natural sediments with median diameters (D_{50}) of 0.48 mm, 0.60 mm, and 0.90 mm with standard deviations of 1.97, 2.39, and 1.41, respectively, as the bed material. Moreover, the average sediment density of these three types of sediments was 1.7 (g/cm^3).

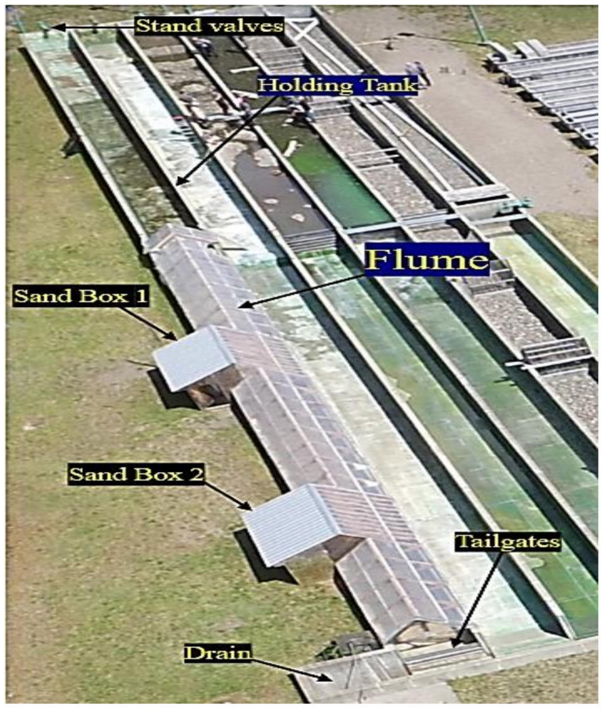

(a) Overview of the flume

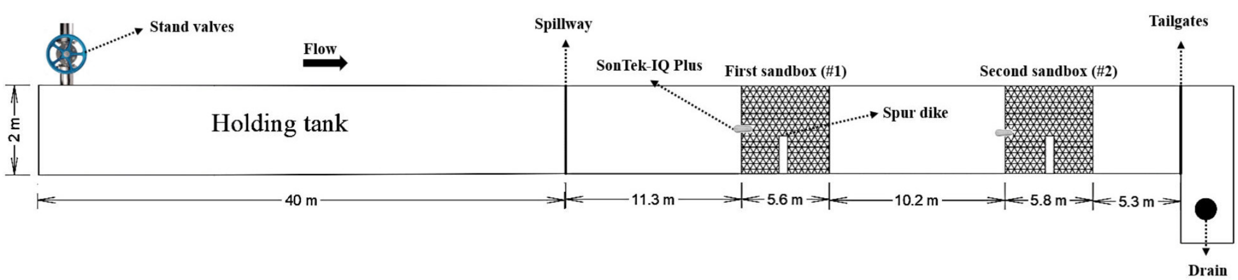

(b) Plan view

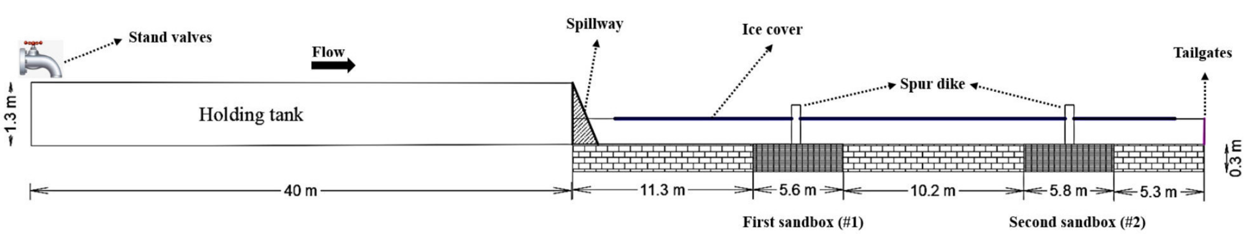

(c) Vertical view

Figure 4. 1:Flume for experiments: (a) Overview of the flume, (b) Plan view, (c) Vertical view

A staff gauge was installed in the middle of each sandbox to monitor the flow depth. The tailgate located at the downstream end of the flume was used to control the flow depth and, consequently, the flow velocity within the channel. The mean approaching flow velocity ranged from 15 cm/s to 30 cm/s. The model spur dike is made of impermeable marine plywood, standing at a total height of 80 cm, with a width of 5 cm and a length of 50 cm. Positioned centrally within each sandbox, the dike was partially submerged, with 30 cm of its height buried beneath the sand bed while the remaining 50 cm protruded above the initial bed surface (Figure 4.1). For each inflow and cover condition, the model spur dike was placed at three alignment angles (inclined to the downstream sidewall): 90º, 60º, and 45º. Consequently, the dike positioned perpendicular to the flume sidewall exhibited the highest blockage ratio at 25%, and the blockage ratio for the dike alignment angles of 60º and 45º reduced to 20% and 15%, respectively.

Styrofoam panels, 1.99 m wide and 2.4 m long, were utilized to replicate the ice cover floating on the water surface. Two distinct types of model ice covers were used to assess the impact of the ice cover roughness coefficient on channel bed deformation, namely smooth and rough ice covers. The model smooth ice cover mimics the sheet ice typical of natural rivers, while the model rough ice cover replicates an ice jam formed by accumulated ice floes. The smooth ice cover was modelled using untreated Styrofoam panels. To create the model rough ice cover, numerous Styrofoam cubes with the dimensions of 2.5 cm × 2.5 cm × 2.5 cm were affixed to the bottom surface of the Styrofoam panels in a staggered arrangement, with a spacing distance of 35mm between the adjacent cubes. For experiments conducted under ice-covered flow conditions, the entire flow surface in the flume was covered by the model ice cover (Figure 4.2).

A SonTek-IQ Plus, an optimum apparatus for flow measurement in natural rivers, was used to measure the approaching flow velocity, water depth, and incoming discharge into the flume.

The data collection process of the IQ Plus is exposed to an error of 1% in the range of measurement scale (Manual, 2017). An IQ Plus was fixed to the flume bed in front of each sandbox.

Figure 4. 2:A cover condition experiment under smooth ice cover with a 45º inclination angle

An Acoustic Doppler velocimeter (ADV) was used to measure the flow velocities. To ensure reliable measurement data using the ADV, assessing both the signal-to-noise ratio (SNR) and the correlation (COR) is imperative. According to the user manual for ADV, these two parameters were set as follows: SNR > 15 and COR >70% to achieve the most accurate data in this experimental study. The software program WinADV was used to filter the ADV data files, such as SNR and COR. To obtain the most accurate data at each measuring location, the data sampling rate of ADV was set with the highest frequency (25 Hz) for 120 to 150 seconds. After configuring the ADV appropriately and implementing data spike filtering, velocity measurements in the current study were reliable within the range of 0.25 cm/s, with an error margin of ±1.5% of the measurement scale.

4.2.2 Data Acquisition Procedures

Experimental runs have been carried out in the same flume on local scour around bridge piers and abutments under ice-covered flow conditions (Namaee & Sui, 2020; Namaee et al., 2021; Wu, Hirshfield, & Sui, 2014; Wu, Hirshfield, Sui, et al., 2014; P Wu et al., 2015). Time is one of the essential factors in studying channel bed deformation around in-stream infrastructures such as spur dikes. The scouring process is complete when the scour hole reaches its equilibrium condition, such that the dimensions of scour holes and deposition dunes remain constant over time. It was found that the quasi-equilibrium scour process can happen within the first 6 hours of the experiment, and there was hardly a scour hole pattern after 12 hours (M. R. Namaee & J. Sui, 2019). Thus, the duration of all experimental runs in this study was 24 hours, which ensured an equilibrium scour condition was achieved. In this study, the following procedures for data acquisition were followed:

1) Before initiating each experimental run, verification of the fullness of the upstream water holding tank is essential. Subsequently, the initial step involves levelling each sandbox's entire surface. Following this, all Styrofoam panels (or model ice cover) are systematically and carefully arranged on the flume bed to facilitate experiments under ice-covered flow conditions.
2) Then, the valves were slowly opened to allow the gradual inflow of water from the upstream holding tank into the flume, preventing initial erosion at the spur dikes. The flow depth in the flume increased gradually, and concurrently, the model ice cover began to float on the water surface. Once the flow attained the desired depth, the valves were fully opened to achieve the required flow rate. Throughout each experimental run, monitoring and calculating water level, flow rate, and approaching velocity were conducted using IQ Plus.

In the meantime, the flow depth was also monitored using a staff gauge located at the midpoint of the sandboxes.

3) The experiment was completed after 24 hours. Then, ADV was carefully positioned within the flow to measure the velocity field around the spur dikes at diverse locations.

After all required measurements for flow velocity were completed, all valves were turned off. Then, the model ice cover was carefully removed from the water surface. The flume slowly drained by lowering the tailgate to avoid disturbance of the deformation patterns of the sand bed. The geometry of scour holes and deposition dunes around spur dikes was carefully measured using a calliper. The Surfer Golden Software was used to process all measured data for the geometry of scour holes and deposition dunes to generate 3D plotting of the profile and contour lines for scour holes and deposition dunes.

4.3 Results

Channel bed scour initiates when shear stresses around an obstacle, such as a spur dike, exceed the critical shear stress of riverbed material. In the early stages, intense scouring predominantly occurs at the dike toe, leading to rapid development and deepening of the scour hole. However, as time progresses, typically after approximately 2 hours, the scouring process gradually slows down as bed shear stresses diminish. Eventually, when shear stresses become insufficient to displace significant bed material, the scouring process reaches an equilibrium state, indicating the maximum scour depth (Richardson & Davis, 1995). In channels with finer bed material, smaller flow depths and higher flow velocities tend to result in larger maximum scour hole depths. This phenomenon occurs because higher velocities generate stronger downflow on the upstream side of the dike, leading to intensified horseshoe vortex activity, a primary scouring mechanism.

Moreover, as flow depths decrease while maintaining a constant flow velocity, downflow and vortex activity within the scour hole are enhanced. This relationship is further amplified by an increase in the flow Froude number, which elevates turbulence kinetic energy within the scour hole, consequently expanding the erosion process (Jafari & Sui, 2021). Consequently, the maximum depth of scour holes tends to be lesser in deeper flows with lower flow Froude numbers.

Notably, during the evolution of a scour hole, the quantity of coarse particles within the scour hole progressively augmented. These larger sediment particles settled on the scour hole's surface, forming what is commonly known as an armour layer, which impedes further scouring. The presence of an armour layer indicates that the scouring process is approaching an equilibrium state. Additionally, the formation of an ice cover on the water surface and variations in the alignment angle of the dike were found to influence the maximum depth of a scour hole around the dike.

The presence of a spur dike in a river modifies the flow dynamics by obstructing the streamflow and redirecting the incoming flow in a different direction. As a result of the contraction caused by a spur dike, the flow velocity at the dike tip increases significantly. Additionally, the flow is separated into two segments. One portion of the flow experienced acceleration and displacement towards the flume's central region. The velocity can be increased by up to 60% of the approaching flow velocity to the dike, depending on the dike alignment angle and the flow surface cover condition (Jafari & Sui, 2021). The other part of the flow goes toward the channel bed, creating an intense downflow at the dike's upstream side, eroding around the dike toe and forming a scour hole. There are three crucial factors for assessing the scour: the location of the initial scour hole, the development of the scour pattern, and the maximum depth of scour holes after reaching the equilibrium state (Namaee et al., 2020; Valela et al., 2021; Zhang et al., 2018).

4.3.1 Vortex system at the dike

It was observed that the local scour was initiated at the upstream side of the dike toe once an experiment started. Due to the local flow acceleration around the dike and strong vertical downward flow, a primary vortex was formed within the initial scour hole. The two most important factors influencing the primary vortex are the dike orientation angle and the approaching velocity. For the dike with an alignment angle of 90º, the primary vortices were more substantial and lasted longer. By reducing the dike alignment angle, the primary vortex became less noticeable. As the approaching velocity increased, the downflow interaction strengthened, and these vortices exhibited greater intensity. Additionally, an adverse pressure gradient formed within the scour hole, leading to the development of a secondary vortex system known as a horseshoe vortex. These vortices were visible within the scoured zone and developed clockwise inside the scour hole around a spur dike.

The horseshoe vortex's strength depends on flow rate, blockage ratio, and surface condition. By increasing the flow rate and blockage ratio (increasing the dike alignment angle from 30º to 90º), the scour hole around the spur dike became deeper, implying that the intensity of the horseshoe vortex was increased. Under an ice-covered flow condition, flow circulations are intensified, leading to powerful vortices inside the scour hole at a spur dike. With the increase in the roughness coefficient of an ice cover, the scour hole around a spur dike became wider and deeper, indicating a more powerful horseshoe vortex inside the scour hole. Thus, the bed shear stress under an ice-covered flow condition was raised above the critical shear stress for the incipient motion of bed materials under an open flow condition. Consequently, an increased sediment movement was observed, leading to the further development of the scour hole under an ice-covered flow condition.

After a couple of hours, the primary vortex faded and was no longer visible. The horseshoe vortex system continued to be the primary cause for the expansion of the scour hole. Sediment particles in the scour hole were transported downstream by the vortex system and deposited in the low-velocity zone behind the spur dike. In this low-velocity zone, the streamflow mixed with the separated flow downstream of the dike generated another vortex system called the wake vortex. Following the dispersal of the primary vortex, the final scour process resulted from these two remaining vortex systems, namely, horseshoe and wake vortex. The scour hole surrounding the dike progressively increases in width and depth over time, expanding in the upstream, downstream, and lateral directions toward the middle of the channel. Due to the difference in strength and rotation direction of the vortices, the shape and slope of scour holes located upstream of a spur dike differ significantly from those downstream.

4.3.2 Scour morphology

4.3.2.1 Features of scour holes

The process of channel bed deformation around a spur dike is influenced by various factors, including flow characteristics, grain size of bed material, water surface cover condition, spur dike layout and alignment angle. The configurations of scour holes and deposition dunes can be effectively depicted using contour maps, which provide two-dimensional representations of three-dimensional data, as depicted in Figure 4.3. Lines of equal "Z" values in contour maps portray channel bed deformation around the dike. The shape of scour holes and deposition dunes can be comprehended by analyzing a contour map.

The results showed that an ice cover on the water surface leads to a wider scour hole in the lateral direction compared to an open channel flow condition. One can see from Figure 4.3 that the scour hole around a dike under an open flow condition exhibited a circular shape, while the scour hole extended toward another side of the channel wall under an ice-covered condition. This effect was accentuated under a rough-covered flow condition, implying that an increase in the ice cover roughness corresponds to an enlargement in the size of the scour hole around a dike. This finding aligns with Sui et al. (2009), who investigated the local scour caused by submerged jets under ice-covered flow conditions.

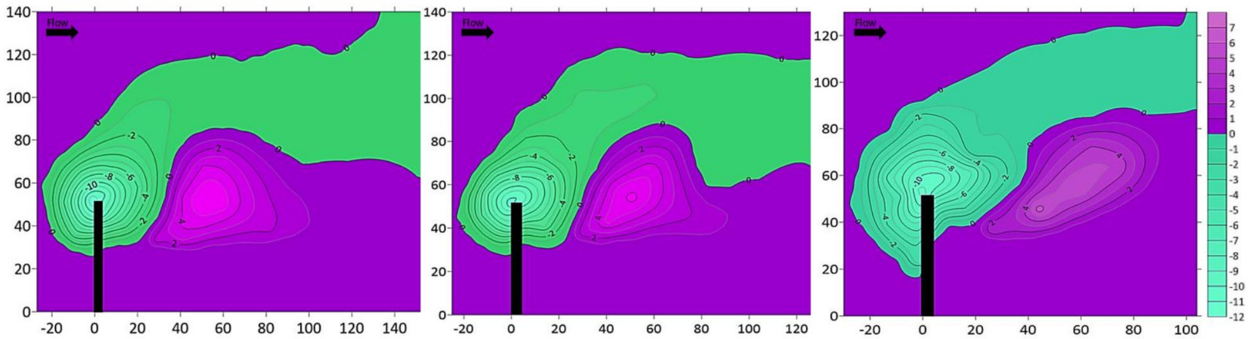

Open channel Smooth ice cover Rough ice cover

Figure 4. 3:Scour holes under various water surface conditions (Fr=0.19, and 90º-dike alignment)

In addition to the cover roughness, the dike alignment angle also significantly influences the local scour process around a dike. As depicted in Figure 4.4, reducing the dike alignment angle from 90º to 45º resulted in an elongated scour hole shape in the streamwise direction. The quasi-semicircular scour hole associated with the 90º alignment angle was changed to an elliptical shape.

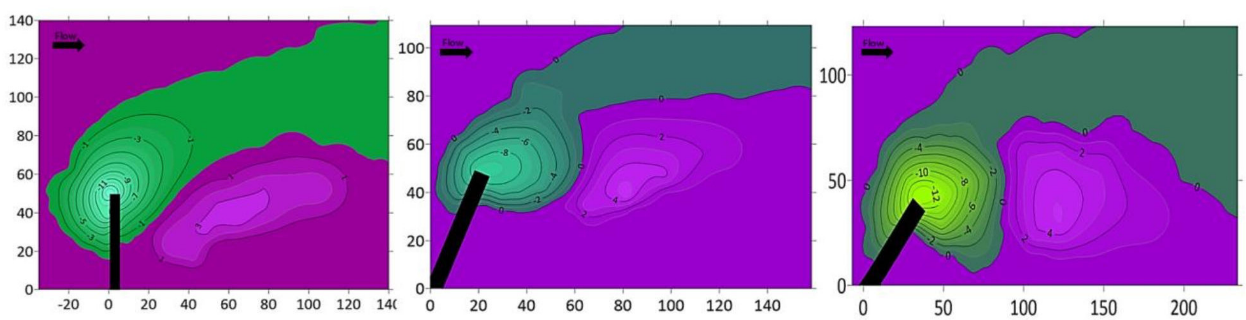

90°-alignment angle 60°-alignment angle 45°-alignment angle

Figure 4. 4:Scour holes under different dike alignment angles and an open flow condition (Fr=0.19)

4.3.2.2. Scour hole geometry

The scour hole pattern around a spur dike is another essential factor for studying the scouring process. To provide a more comprehensive portrayal of the experimental results and enhance their applicability to real-world scenarios, this study employed the following dimensionless variables to assess the development of scour holes and deposition dunes around spur dikes. In this context, the dimensions of scour holes in all directions were normalized by the spur dike length (Figure 4.5).

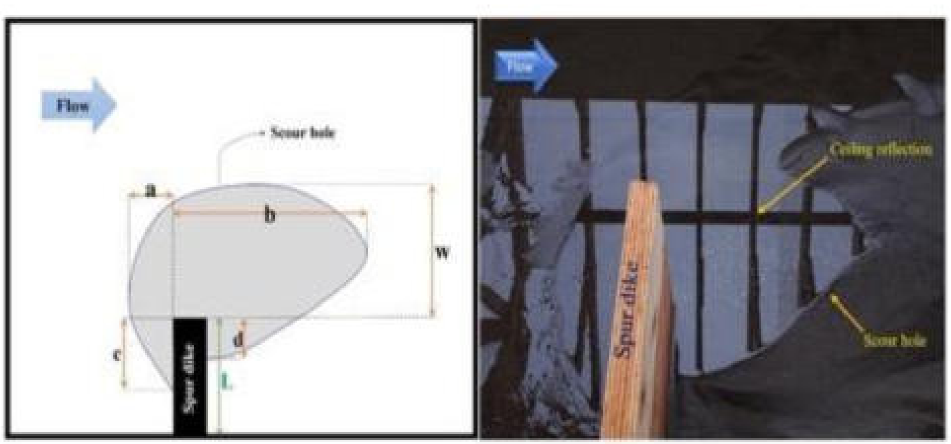

(a) Schematic plan view of a scour hole (b) Actual plan view of a scour hole

Figure 4. 5:Plan view of the scour hole

1) The upstream and downstream lengths (*a/L* and *b/L*) of a scour hole are used to examine the extent of a scour hole in the streamwise direction. Their combination, *(a+b)/L*, represents the maximum scour hole length in the streamwise direction.
2) The maximum outward width, measured from the dike tip to the outer boundary of a scour hole (*w/L*), is used to express the maximum outward scour width in the transverse direction. By utilizing this variable, one can evaluate whether the maximum outward width of a scour hole can be extended to the opposite channel sidewall.

3) The maximum inward width of a scour hole along the front side of a spur dike (*c/L*) is the distance measured from the dike tip to the inner boundary of the scour hole in the transverse direction. Along the rear side of a spur dike, the maximum inward width of a scour hole in the transverse direction is expressed as (*d/L*). These two ratios (*c/L* and *d/L*) can be used as indicators for assessing the extension of a scour hole toward the channel wall where the dike is attached. By examining these maximum inward scour widths, one can evaluate whether the scouring process around the dike can induce channel bank erosion, thereby carrying the risk of detrimental consequences such as landslides and spur dike failure.

These ratios are influenced by various factors, including flow surface conditions (open channel, smooth ice-covered, and rough ice-covered flow), hydraulic parameters (flow depth and velocity), dike alignment angles and dimensions, and the grain size of bed materials. In the following section, the influence of the distinct experimental setups on the scour hole geometry has been evaluated by assessing these ratios.

a). Upstream length of a scour hole (a/L)

The experimental results demonstrate that hydraulic conditions substantially impact the upstream length of a scour hole (*a/L*). As the approaching flow depth decreases, the upstream length of a scour hole (*a/L*) increases. With every 10 cm increase in the flow depth, there is an approximately 20% reduction in the upstream length of a scour hole (*a/L*). The finer the bed material (D_{50}), the larger the upstream length of a scour hole (*a/L*). Moreover, the upstream length of a scour hole (*a/L*) was expanded by elevating the approaching flow velocity. This means the experimental scenario with the largest flow Froude number and finest bed material will generate the most significant upstream length of a scour hole (*a/L*).

As depicted in Figure 4.6, the upstream length of a scour hole (*a/L*) exhibited marginal expansion under a smooth-covered condition compared to an open-flow condition. However, a rough ice cover led to a pronounced increase in the upstream length of a scour hole (*a/L*) by 25%. Hence, the roughness coefficient of an ice cover plays a crucial role in the initiation and development of a scour hole toward the upstream zone of a spur dike. Under the same covered flow condition, an elevation in the flow depth diminishes the influence of the ice cover on the scouring process toward the upstream of the spur dike.

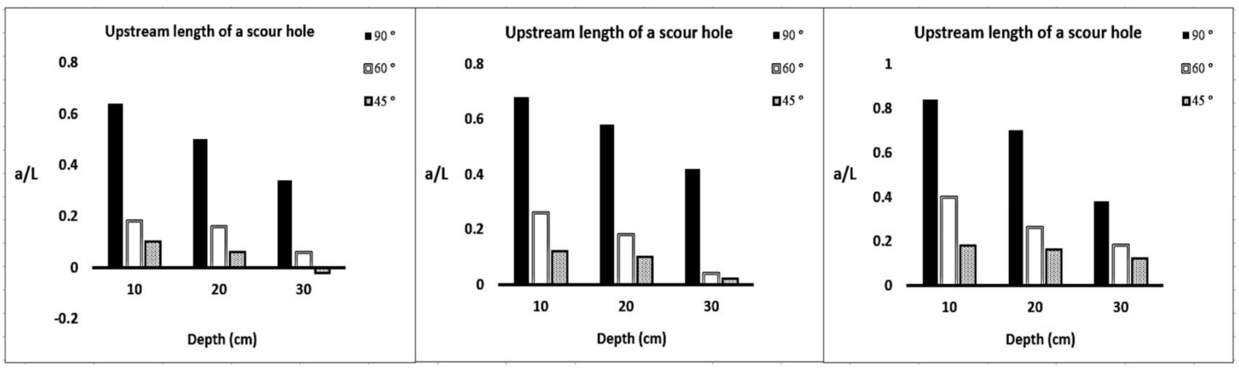

Open channel   Smooth ice cover   Rough ice cover

Figure 4. 6:Effect of experimental conditions on the upstream length of a scour hole (a/L)

The findings indicate that a reduction in the dike alignment angle led to an immense decrease in the upstream length of a scour hole (*a/L*), as shown in Figure 4.6. Decreasing the dike alignment angle from 90º to 60º reduces approximately 60% in the upstream length of a scour hole (*a/L*). A marginal reduction of the dike alignment from 60º to 45º exhibited a less noticeable impact on the upstream length of a scour hole (*a/L*). By increasing the approaching flow velocity, the impact of the dike alignment angle on the upstream length of a scour hole (*a/L*) will intensify.

b). Downstream length of a scour hole (b/L)

Results showed that the influences of pertinent factors on the downstream length of a scour hole (*b/L*) differ from those on the upstream length of a scour hole (*a/L*). In particular, the water surface cover condition has a much less impact on the downstream length of a scour hole (*b/L*), namely, just caused a slight increase in the downstream length of a scour hole (*b/L*) compared to that under an open flow condition. Also, the impact of a rough ice cover on the downstream length of a scour hole (*b/L*) is not clearly different from that of a smooth ice cover. Furthermore, by increasing the flow depth, the downstream length of a scour hole (*b/L*) decreases slightly but is observable.

Results also showed that the downstream side of a scour hole expanded as the approaching velocity increased, but it is less noticeable compared to the impact of the flow rate. With an increase of about 50% in the flow rate (from 55 lit/s to 120 lit/s), the downstream length of a scour hole (*b/L*) increased by about 20%.

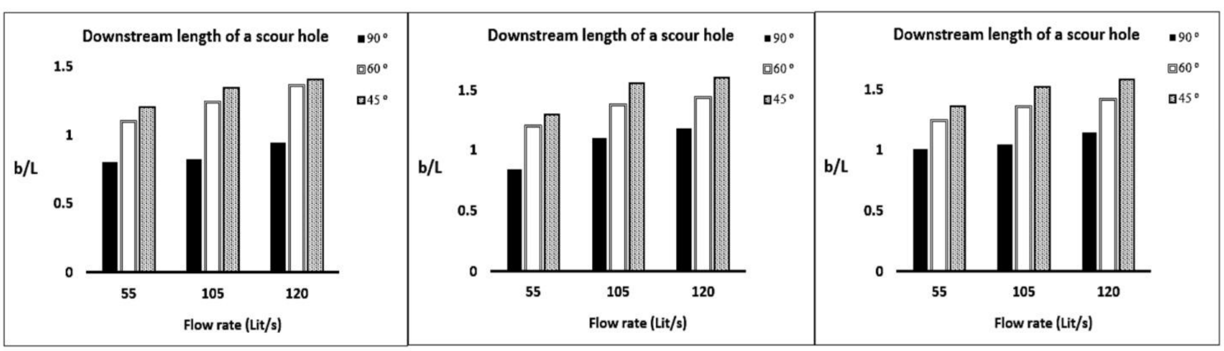

Open channel Smooth ice cover Rough ice cover

Figure 4. 7:Effect of experimental conditions on the downstream length of a scour hole (b/L)

By changing the dike alignment angle, the shape of scour holes changes substantially. With the decrease in the dike alignment angle, the downstream length of a scour hole (*b/L*) expanded. As shown in Figure 4.7, the reduction of the dike alignment angle from 90º to 60º resulted in a significant change in the downstream length of a scour hole (*b/L*). However, a further decrease in the dike alignment angle from 60º to 45º had a less conspicuous effect on the downstream length of a scour hole (*b/L*). In summary, as the flow rate increases and the dike alignment angle decreases simultaneously, the downstream length of a scour hole (*b/L*) will substantially increase in streamwise and lateral directions under an ice-covered flow condition.

c). Maximum outward width of a scour hole (w/L)

The flow velocity considerably impacts the width of the scour hole around a spur dike. Increasing the flow velocity from 0.15 m/s to 0.30 m/s increases the maximum outward scour width (w/L) by about 8%. The depth of the approaching flow is another factor that significantly influences the maximum outward scour width (*w/L*). As the approaching flow depth increases, a noticeable decrease in the maximum outward scour width (*w/L*) results. An increase of each 10 cm in the water depth leads to a decrease of 15% in the maximum outward width of a scour hole (*w/L*).

Given that the maximum outward width of a scour hole (*w/L*) increases with the approaching flow velocity but decreases with the flow depth, the flow Froude number (*Fr*) can be employed to represent the influences of flow velocity and water depth on the maximum outward scour width (*w/L*). Results showed that, with an increase of each 30% in the Froude number, the maximum outward scour width (*w/L*) increases by 15%~20%. The findings reveal that an ice cover on the water surface amplifies the influence of the flow Froude number on the maximum outward scour width (*w/L*). A higher Froude number under the rough ice-covered flow condition led to a larger maximum outward scour width (*w/L*).

As illustrated in Figure 4.8, the maximum outward scour width (*w/L*) also depends on the dike alignment angle. Decreasing the dike alignment angle changes the scour hole shape from semi-circular to elliptical. Hence, the maximum outward scour width (*w/L*) decreased with the decrease in the dike alignment angle. Depending on the cover condition and flow Froude number

(F_r), a decrease in the dike alignment angle from 90º to 60º reduces 20%~30% in the maximum outward scour width (*w/L*). A further reduction in the dike angle from 60º to 45º had a marginal effect on the maximum outward scour width (*w/L*). In this study, the maximum outward scour width (*w/L*) reached the smallest when the dike was placed at an alignment angle of 45º.

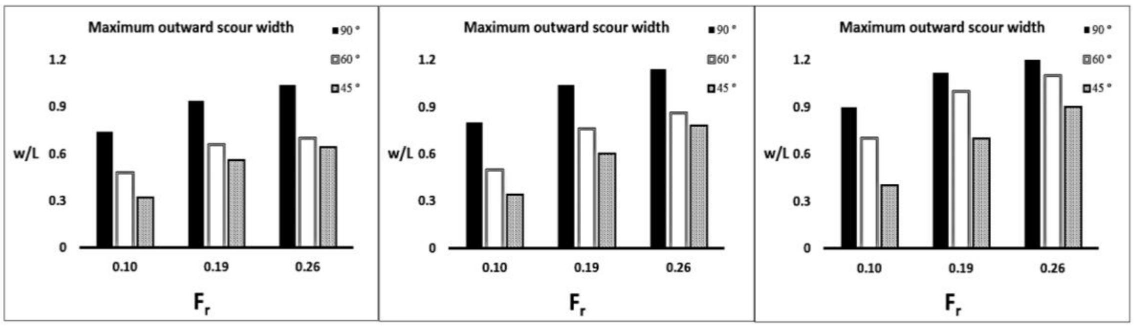

Open channel Smooth ice cover Rough ice cover

Figure 4. 8:Effect of experimental conditions on the maximum outward scour width (w/L)

It has been observed that the maximum outward scour width (*w/L*) increases by adding an ice cover on the water surface. Also, the rougher the ice cover, the larger the maximum outward scour width (*w/L*). As the water depth increases, the effects of the ice cover on the maximum outward scour width (*w/L*) become mitigated. Furthermore, an increase in flow velocity amplifies the impact of an ice cover on the development of a scour hole. Throughout all experimental runs, the maximum outward scour width never extended to the opposite side wall of the flume, reaching a maximum of 62 cm (from the tip of the dike to the outside boundary of the scour hole). Consequently, the far sidewall does not influence the development of the scour hole and the maximum outward scour width.

d). Maximum frontal inward width of a scour hole (c/L)

If the inside boundary of a scour hole extends to the channel bank to which the dike is attached, it can induce bank erosion, landslides, and dike failure. Thus, assessing the maximum frontal inward scour width of a scour hole is necessary for the spur dike design. Results indicate that an increase in the flow depth decreases the maximum frontal inward scour width (*c/L*). The higher the approaching flow velocity, the larger the maximum frontal inward scour width (*c/L*). Combining the impact of flow depth and velocity on the maximum frontal inward scour width (*c/L*), it can be concluded that an increase in the Froude number caused an increase in the maximum frontal inward scour width (*c/L*). Notably, as the particle size of the bed material decreases and the Froude number increases, a substantial increase in the maximum frontal inward scour width of a scour hole (*c/L*) will result.

Based on all experimental runs conducted under different conditions, it has been found that the maximum frontal inward scour width (*c/L*) is hardly close to one, namely, $c/L<1$. This result indicates that the likelihood of bank erosion and landslides is extremely low when the criteria of $c/L<1$ is ensured in the spur dike design. As shown in Figure 4.9, the presence of an ice cover on the water surface is another factor that significantly affects the maximum frontal inward scour width (*c/L*). The appearance of an ice cover on the water surface increases the maximum frontal inward scour width (c/L) by 40~50% compared to that under an open flow condition. Nevertheless, an increase in the roughness coefficient of an ice cover has little impact on the maximum frontal inward scour width (*c/L*).

The dike alignment angle influences the maximum frontal inward scour width (*c/L*). As the dike alignment angle decreases, the maximum frontal inward scour width (*c/L*) decreases accordingly. This finding suggests that the maximum frontal inward scour width (*c/L*) with the 90º alignment angle clearly differs from that around a dike with the 60º alignment angle. This effect becomes less prominent by further reducing the dike alignment angle.

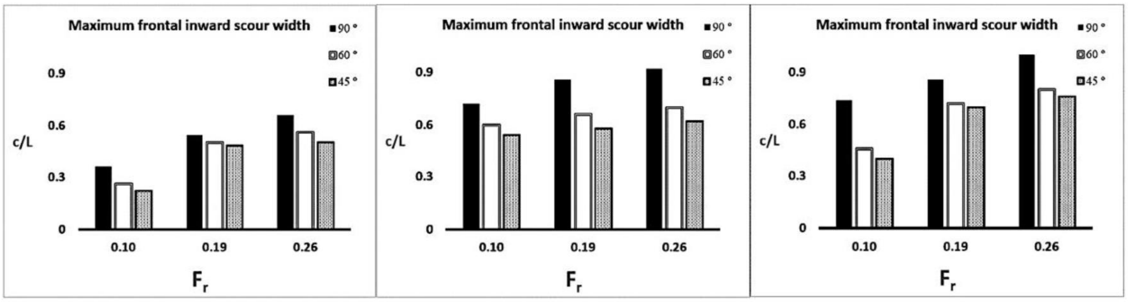

Open channel Smooth ice cover Rough ice cover

Figure 4. 9:Effect of experimental conditions on the maximum frontal inward scour width (c/L)

e). Maximum rear inward width of a scour hole (d/L)

The maximum rear inward width of a scour hole (*d/L*) is as crucial as the maximum frontal inward scour width (*c/L*). However, as illustrated in Figure 4.10, the maximum rear inward scour width (*d/L*) was consistently less than the maximum frontal inward scour width (*c/L*) in all experimental runs and never reached one. Results showed that the maximum rear inward scour width (*d/L*) increases with the increase in the Froude number. However, the Froude number had a minor impact on the maximum rear inward scour width (*d/L*) compared to the maximum frontal inward scour width (*c/L*).

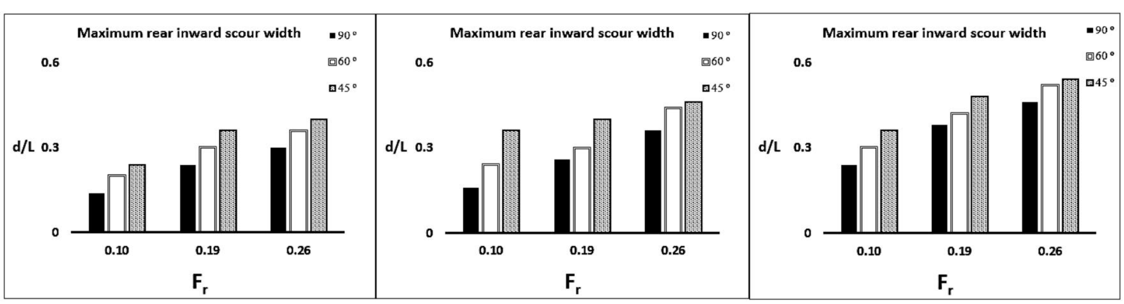

Open channel Smooth ice cover Rough ice cover

Figure 4. 10:Effect of experimental conditions on the maximum rear inward scour width (d/L)

Similarly, an ice cover on the water surface causes a larger maximum rear inward scour width (*d/L*) than that under an open flow condition. Results showed that the maximum rear inward scour width (*d/L*) slightly increases as the cover roughness increases. In addition, under an ice-covered flow condition, the maximum rear inward scour width (*d/L*) increases with the decrease in flow depth and particle size of the bed material. The impact of the ice cover is more pronounced in the case of shallow flow depth and finer bed material (D_{50}=0.48 mm).

The dike alignment angle has an entirely reverse impact on the maximum rear inward scour width (*d/L*) compared to the maximum frontal inward scour width (*c/L*). The maximum rear inward scour width (*d/L*) exhibits a noticeable increase with the decrease in the dike alignment angle. Furthermore, an increase in the flow velocity under an ice-covered condition magnifies the impact of the dike alignment angle on the maximum rear inward scour width (*d/L*). Under the same flow and cover conditions, the maximum rear inward scour width (*d/L*) with an alignment angle of 45º is more than that with the larger alignment angles of 60º and 90º (Figure 4.10)

4.3.3 Maximum scour depth

Understanding a scour hole's maximum depth and location is crucial for designing in-stream infrastructures like spur dikes, bridge piers, and abutments. To ensure structural integrity and longevity, foundations must be situated at a certain depth below the riverbed to mitigate the detrimental effects of hydraulic forces induced by flowing water and river ice. Understanding the influence of hydraulic factors and channel conditions, particularly in the presence of ice cover and ice jam, is essential for accurately predicting scour holes' maximum depth and locations around in-stream infrastructures.

Experimental observations revealed no discernible impact of different flow conditions (flow velocity and depth) on time required to develop a scour hole to reach an equilibrium condition. Notably, under rough ice-covered flow conditions, the local scour around a dike with a 90º alignment angle took the longest time to reach an equilibrium state. A significant difference in the maximum scour depth was clearly noticed among a wide range of the flow Froude numbers from 0.10 to 0.26. With the increase of each 15% in the Froude number, the maximum depth of a scour hole increased by 5%~10%. For most experimental runs, the maximum scour depth was located near the toe of the dike with an alignment angle of 90º. With the decrease in the flow Froude number, the location of the maximum depth of a scour hole was observed to shift a marginal amount downstream. As illustrated in Figure 4.11, the cross-section profile of the scour hole was transformed from a narrow "V" shape to a broader "V" shape. Additionally, a substantial reduction in the scour hole volume was observed as the Froude number decreased. For an increase of 30% in the Froude number, the volume of a scour hole increased by approximately 12%.

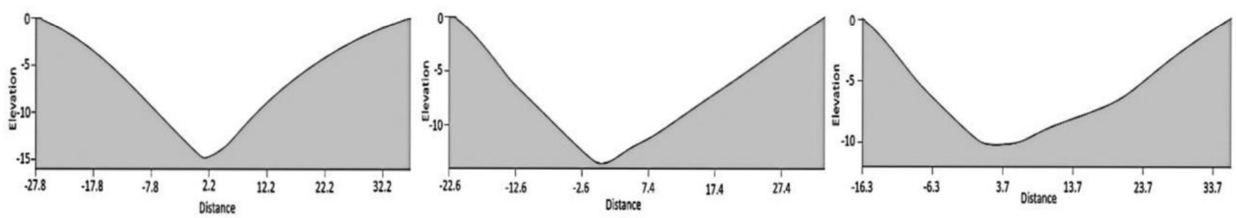

$F_r = 0.26$ $F_r = 0.19$ $F_r = 0.10$

Figure 4. 11:Cross-section profile of scour holes around a dike with the alignment angle of 90º for different Froude numbers under an open flow condition

The augmentation of the scour area was the most prominent effect induced by an ice cover on the development of scour holes around the dikes. An ice cover on the water surface resulted in a broader scour hole in streamwise and transverse directions, particularly in rough ice cover. This implies that the water surface cover conditions mainly influence the maximum depth of scour holes. The outcomes indicate that, under a smooth ice-covered condition, the maximum depth of a scour hole increases by about 10% compared to that under an open flow condition, and it increases by about 15% under the rough ice-covered condition. The effect of an ice cover on the location of the maximum depth of scour holes does not demonstrate a consistent trend. As the scour hole enlarged, the slopes of the hole's entrance and exit sections became steeper, but with a milder slope of the exit section compared to that of the entrance section, regardless of water surface cover conditions. Under a rough ice-covered flow condition, the slope of the entrance section of a scour hole is much steeper than that of the exit section compared to that under an open flow condition.

The dike alignment angles significantly influence the size and shape of the scour holes. By reducing the dike alignment angle, the geometric patterns of scour holes were different. One significant impact is the scouring depth. Under the same flow and cover conditions, the maximum depth of scour holes is observed at the dike with an alignment angle of 90°. The depth of the scour hole decreases significantly as the dike alignment angle reduces. In general, regardless of the dike alignment angle, the position of the maximum depth of scour holes appears proximate to the dike toe. As the dike alignment angle decreases, the location of the maximum scour depth is shifted away from the dike toe, and the scouring process progresses from upstream to downstream.

The key parameters that affect the depth of scour holes around an in-stream infrastructure should include flow velocity, turbulence intensity, water depth, sediment characteristics (such as grain size), structure geometry, and roughness coefficients of the riverbed and ice cover. The following essential parameters influencing the maximum depth of scour holes (Y_{max}) should be considered in this experimental study:

$$Y_{max} = f\,(H, V, L_e, B, D_{50}, n_i, n_b, \sin\theta) \quad (4.1)$$

Where, H is the approaching water depth, V is the approaching flow velocity, L_e is the dike effective length, which is defined as the vertical distance from the dike tip to the sidewall to which the dike is attached, B is the channel width, D_{50} is the median particle size of the bed material, n_i is the roughness coefficient of an ice cover, n_b is the roughness coefficient of the riverbed, θ is the dike alignment angle.

To precisely assess the impact of each parameter on the maximum depth of scour holes and obtain a more detailed depiction of the laboratory results, the essential parameters mentioned in Equation 1 are represented as dimensionless variables as follows:

$$\frac{Y_{max}}{H} = f\left(F_r, \frac{L_e}{B}, \frac{D_{50}}{H}, \frac{n_i}{n_b}, \sin\theta\right) \tag{4.2}$$

This experimental study regarding local scour around non-submerged dikes with different alignment angles has been conducted under ice-covered flow conditions compared to that under open flow conditions. As discussed above, the influence of an ice cover on the maximum depth of scour holes around the angled dike is substantial since the distribution profiles of flow velocity and the composite roughness coefficient of the channel under an ice-covered flow condition differ significantly from those in an open flow. Thus, it is necessary to derive distinct equations for describing the maximum depth of scour holes under ice-covered and open-flow conditions, respectively. Based on data obtained from laboratory experiments, the following two equations have been derived to estimate the maximum depth of scour holes for ice-covered and open-flow conditions, respectively.

Ice-covered flow condition:

$$\frac{Y_{max}}{H} = 17.07(F_r)^{0.63}\left(\frac{L_e}{B}\right)^{0.43}\left(\frac{D_{50}}{H}\right)^{-0.26}\left(\frac{n_i}{n_b}\right)^{0.153}(\sin\theta)^{0.40} \qquad R^2 = 0.97 \tag{4.3}$$

Open channel flow condition:

$$\frac{Y_{max}}{H} = 12.66\,(F_r)^{1.04}\left(\frac{L_e}{B}\right)^{0.174}\left(\frac{D_{50}}{H}\right)^{-0.33}(\sin\theta)^{0.57} \qquad R^2 = 0.963 \tag{4.4}$$

Results of estimations using Equations 4.3 and 4.4 reveal that, under both open channel and ice-covered flow conditions, a larger flow Froude number (Fr) corresponds to a deeper maximum depth of scour holes. However, under ice-covered flow conditions, the exponent of the Froude number in Equation 3 is approximately 60% of that under open flow conditions. This suggests that the impact of the flow Froude number on the maximum depth of scour holes under ice-covered flow conditions is less pronounced than that under open channel conditions.

Under both open channel and ice-covered flow conditions, the negative exponent of the ratio of the median particle size of bed material to the flow depth (or relative particle size) indicates that the maximum depth of scour holes increases as the relative particle size decreases. This negative exponent of the relative grain size means the finer the bed material, the deeper the maximum depth of scour holes. One can also see from Equations 4.3 and 4.4 that there is no significant difference in the exponents of the relative grain size between the ice-covered flow and open channel flow.

Equations 4.3 and 4.4 demonstrate that the blockage ratio (*Le/B*), representing the ratio of the effective dike length to the channel width, is a crucial factor influencing the maximum depth of scour holes. This influence is more pronounced under ice-covered flow than under open flow conditions, as indicated by the positive exponents of the blockage ratio. In this study, three dike alignment angles (90º, 60º, and 45º) resulted in the blockage ratios of 25%, 20%, and 15%, respectively. As the blockage ratio increases, with the same approaching flow rate, the flow velocity around the dike rises, suggesting higher kinetic energy and turbulence intensity. Results showed that the dike alignment angle 90º resulted in the most substantial downward vertical velocity, which created a negative velocity gradient and increased vertical momentum transport around the dike and inside the scour hole. With the decrease in the blockage ratio, a negative velocity gradient gradually reduced, thus decreasing the turbulence kinetic energy. Under ice-covered flow conditions, this contributed to developing a stronger horseshoe vortex, ultimately leading to a much deeper scour hole than that under open flow conditions. The proposed equations under both open channel and ice-covered flow conditions suggested that the dike alignment angle notably influences the maximum depth of scour holes. As indicated by the positive exponents of the sin function of the dike alignment angle, the smaller the dike alignment angle, the less the maximum depth of scour holes.

Under an ice-covered flow condition, the positive exponent of the ratio of the ice-cover roughness coefficient to the bed roughness coefficient (or relative roughness coefficient) signifies a direct relationship between the maximum depth of scour holes and the relative roughness coefficient. In other words, a deeper maximum depth of scour holes will result from an increase in the relative roughness coefficient, whether through an increase in the cover roughness coefficient (from smooth ice cover to rough ice cover) or a reduction in the bed roughness coefficient (from coarse bed particles to fine bed material).

The comparison between the calculated maximum depth of scour holes using the proposed equations and the results from laboratory experiments under both open channel and ice-covered flow conditions is presented in Figure 4.12. The substantial agreement between the calculated results and experimental data indicates the reliability and accuracy of Equations 4.3 and 4.4.

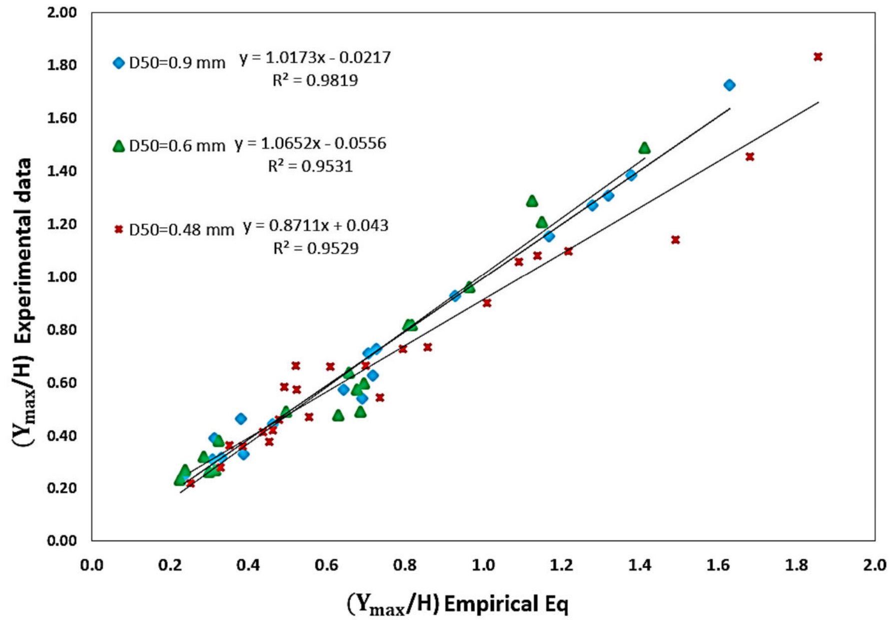

(a): ice-covered flow conditions

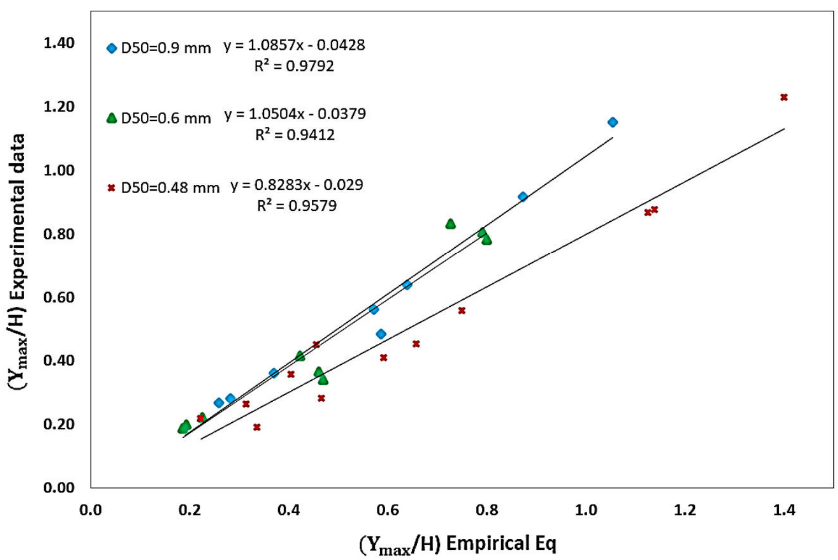

(b): open channel flow conditions

Figure 4. 12:Calculated maximum depth of scour holes using proposed equations compared to results of laboratory experiments: (a) ice-covered flow conditions, (b) open channel flow conditions.

4.4 Conclusions

In the present study, laboratory experiments have been carried out to examine the effect of ice cover with different roughness and non-submerged spur dikes with different alignment angles on the morphological features of scour holes around spur dikes by changing bed materials and hydraulic conditions. The following results have been drawn from this study:

1) The scouring was initiated with the primary vortex, and the channel bed deformation around a dike continued with the horseshow vortex and wake vortex. The horseshoe vortices last the longest among different vortex systems. The orientation of spur dikes and flow Froude number emerged as the primary determinants of the vortex system. Notably, the system's most robust downflow and vertical velocity was generated in the flow with a higher Froude number around the spur dike with the 90º alignment angle.
2) The upstream length of the scour hole (*a/L*) is significantly affected by the dike alignment angles, flow Froude number and the presence of an ice cover. Among them, the dike alignment angle is the controlling factor for the scour hole's upstream length (a/L) and downstream length (b/L). On average, the upstream length of scour holes (*a/L*) decreased by 60% when the dike angle was changed from 90º to 60º. The presence of a rough ice cover on the water surface led to an increase in the upstream length of a scour hole (*a/L*). For flow with high flow Froude number under the rough ice cover, the upstream length of scour holes (*a/L*) and the frontal inward scour width (*c/L*) around the 90º-angled dike reached the most significant values. With an increase of about 50% in the flow rate, the downstream length of a scour hole (*b/L*) increased by about 20%. The change of the dike alignment angle from 90º to 60º resulted in a significant change in the downstream length

of a scour hole (*b/L*). However, a further decrease in the dike angle from 60º to 45º had less effect on the downstream length of a scour hole (*b/L*).

3) An increased flow Froude number corresponds to greater scour hole depths around a dike in both open channel and ice-covered flow scenarios. A finer bed material contributes to deeper scour holes regardless of flow surface cover conditions. The impact of the flow Froude number on the maximum scour depth under ice-covered conditions is less pronounced than that under open channel conditions. Under an ice-covered flow condition, a larger relative roughness coefficient leads to a larger maximum depth of scour holes.

4) The proposed equations under the open channel and ice-covered flow conditions are derived to compute the maximum depth of scour holes around angled, non-submerged spur dikes. These equations consider factors such as dike alignment angle, flow Froude number, dike blockage ratio, particle size of bed material, and relative roughness coefficient (for covered flow conditions). The calculated maximum depths of scour holes using the proposed formula agree well with those of laboratory experiments, indicating that the performance of the proposed equations is reliable.

4.5 Bibliography

Ackermann, N., Shen, H.T., Olsson, P., 2002. Local scour around circular piers under ice covers, International Symposium on Ice: 02/12/2002-06/12/2002. Dep. of Physic, Univ. of Otago, pp. 149-155.

Derrick, D.L., Gernand, H.W., Crutchfield, J.P., 1989. Inventory of river training structures in shallow-draft waterways, ARMY ENGINEER WATERWAYS EXPERIMENT STATION VICKSBURG MS HYDRAULICS LAB.

Giglou, A.N., Mccorquodale, J.A., Solari, L., 2018. Numerical study on the effect of the spur dikes on sedimentation pattern. Ain Shams Engineering Journal, 9(4): 2057-2066.

Gu, Z.-p., Akahori, R., Ikeda, S., 2011. Study on the transport of suspended sediment in an open channel flow with permeable spur dikes. International Journal of Sediment Research, 26(1): 96-111.

Hains, D.B., 2004. An experimental study of ice effects on scour at bridge piers.

Haltigin, T.W., Biron, P.M., Lapointe, M.F., 2007. Predicting equilibrium scour-hole geometry near angled stream deflectors using a three-dimensional numerical flow model. Journal of Hydraulic Engineering, 133(8): 983-988.
Ishigaki, T., Baba, Y., 2004. Local scour induced by 3D flow around attracting and deflecting groins, Proceedings 2nd International Conference on Scour and Erosion (ICSE-2). November 14.–17., 2004, Singapore.
Ishigaki, T., Baba, Y., Muto, Y., 2000. Vortex motion around a plate with footing in open channel flow and its effect on local scouring. Advances in Hydro Science and-Engineering, 4: 169-176.
Jafari, R., Sui, J., 2021. Velocity Field and Turbulence Structure around Spur Dikes with Different Angles of Orientation under Ice Covered Flow Conditions. Water, 13(13): 1844.
Kuhnle, R.A., Alonso, C.V., Shields Jr, F.D., 2002. Local scour associated with angled spur dikes. Journal of Hydraulic Engineering, 128(12): 1087-1093.
Manual, S.-I.S.U.s., 2017. SonTek-IQ Series Intelligent Flow Featuring Smart Pulse HD User's Manual. Xylem brand, SmartPulse HD
Namaee, M., Sui, J., 2019a. Local scour around two side-by-side cylindrical bridge piers under ice-covered conditions. International Journal of Sediment Research, 34(4): 355-367.
Namaee, M.R., Sui, J., 2019b. Effects of ice cover on the incipient motion of bed material and shear stress around side-by-side bridge piers. Cold Regions Science and Technology, 165: 102811.
Namaee, M.R., Sui, J., 2020. Velocity profiles and turbulence intensities around side-by-side bridge piers under ice-covered flow condition. Journal of Hydrology and Hydromechanics, 68(1): 70-82.
Namaee, M.R., Sui, J., Wu, Y., Linklater, N., 2021. Three-dimensional numerical simulation of local scour around circular side-by-side bridge piers with ice cover. Canadian Journal of Civil Engineering, 48(10): 1335-1353.
Pandey, M., Ahmad, Z., Sharma, P., 2018. Scour around impermeable spur dikes: a review. ISH Journal of Hydraulic Engineering, 24(1): 25-44.
Richardson, E., Davis, S., 1995. Evaluating scour at bridges: Federal highway administration hydraulic engineering circular no. 18, Publication FHWA-IP-90-017.
Smith, B.T., Ettema, R., 1995. Ice-cover influence on flow and bedload transport in dune-bed channels. Iowa Institute of Hydraulic Research, the University of Iowa.
Sui, J., Faruque, M., Balachandar, R., 2009. Local scour caused by submerged square jets under model ice cover. Journal of Hydraulic Engineering, 135(4): 316-319.
Sui, J., Jun, W., Yun, H., Faye, K., 2010. Velocity profiles and incipient motion of frazil particles under ice cover. International Journal of Sediment Research, 25(1): 39-51.
Teraguchi, H., Nakagawa, H., MUTO, Y., BABA, Y., ZHANG, H., 2008. Flow and sediment transport around impermeable or permeable groins. PROCEEDINGS OF HYDRAULIC ENGINEERING, 52: 175-180.
Tominaga, A., NAKANO, Y., FUJITA, T., 2000. Visualization analysis of flow structures in submerged spur dikes. PROCEEDINGS OF HYDRAULIC ENGINEERING, 44: 1041-1046.
Valela, C., Sirianni, D.A., Nistor, I., Rennie, C.D., Almansour, H., 2021. Bridge Pier Scour under Ice Cover. Water, 13(4): 536.
Wang, h., Zhao, J., Chen, Z., 2008. Experimental investigation of ice and snow melting process on pavement utilizing geothermal tail water. Energy Conversion and Management, 49(6): 1538-1546.
Wu, P., Balachandar, R., Sui, J., 2016. Local scour around bridge piers under ice-covered conditions. Journal of Hydraulic Engineering, 142(1): 04015038.
Wu, P., Hirshfield, F., Sui, J., 2014a. Further studies of incipient motion and shear stress on local scour around bridge abutment under ice cover. Canadian Journal of Civil Engineering, 41(10): 892-899.
Wu, P., Hirshfield, F., Sui, J., 2015a. Local scour around bridge abutments under ice covered condition–an experimental study. International Journal of Sediment Research, 30(1): 39-47.
Wu, P., Hirshfield, F., Sui, J., 2015b. Armour layer analysis of local scour around bridge abutments under ice cover. River research and applications, 31(6): 736-746.

Wu, P., Hirshfield, F., Sui, J., Wang, J., Chen, P., 2014b. Impacts of ice cover on local scour around semi-circular bridge abutment. Journal of Hydrodynamics, 26(1): 10-18.
Yazdi, J., Sarkardeh, H., Azamathulla, H.M., Ghani, A.A., 2010. 3D simulation of flow around a single spur dike with free-surface flow. Intl. J. River Basin Management, 8(1): 55-62.
Zabilansky, L.J., Hains, D.B., Remus, J.I., 2006. Increased bed erosion due to ice, Current Practices in Cold Regions Engineering, pp. 1-12.
Zhang, H., Nakagawa, H., 2008. Scour around spur dyke: recent advances and future researches.
Zhang, L., Wang, P., Yang, W., Zuo, W., Gu, X., Yang, X., 2018. Geometric characteristics of spur dike scour under clear-water scour conditions. Water, 10(6): 680

5 CHAPTER FIVE: Evaluating the Impact of Spur Dike Alignment and Ice Cover Roughness on Local Scour at Bridge Abutments

5.1 Introduction

Scouring around bridge piers and abutments is a significant and pervasive challenge in hydraulic engineering, posing a critical threat to the stability and safety of bridge structures worldwide (Dargahi, 1990). The phenomenon of scour refers to the removal of sediment from around bridge foundations due to the erosive action of flowing water (Sui et al., 2006). This process can progressively undermine the structural integrity of bridges, leading to potential failures and catastrophic collapses, with severe implications for transportation networks, economic activities, and public safety (Pizarro et al., 2020). Several factors, including the velocity and turbulence of water flow, sediment transport characteristics, and the geomorphological features of the riverbed, drive the occurrence of scour (Namaee & Sui, 2019b). During high-flow events, such as floods, the increased water velocity and turbulence can intensify the scour process, rapidly eroding the sediment around bridge piers and abutments. This erosion creates scour holes, which can compromise the Bridge's stability by exposing and weakening its foundations (Arneson, 2013)

Understanding and mitigating scour have evolved significantly over the years, with extensive research conducted to develop effective methods for reducing or preventing scour around bridge piers and abutments (Zarrati et al., 2006). Early studies primarily focused on understanding the mechanics of scour and the factors influencing its development (Gupta & Gangadharaiah, 1992). These foundational studies provided valuable insights into the flowing water and sediment interaction behaviour around bridge foundations, forming the basis for developing mitigation measures (Pandey et al., 2023). As research progressed, various structural, geotechnical, and hydraulic approaches were proposed and implemented to address scour

(Lagasse, 2007). Structural measures, such as riprap and concrete aprons, aim to directly protect the riverbed and foundations. Geotechnical measures focus on enhancing the resilience of the foundations themselves. In contrast, hydraulic measures involve altering the flow patterns to reduce the erosive forces acting on the bridge piers and abutments (Zdravkovic & Tsiampousi, 2023).

One of the most common structural methods involves placing rock ripraps or gabions around bridge piers and abutments. Riprap consists of large stones that are resistant to erosion and can dissipate the energy of flowing water, thus reducing its erosive potential (Wörman, 1989). Gabions, which are wire mesh filled with stones, provide similar protection. Both methods have been widely studied and implemented due to their effectiveness and simplicity (Richardson & Davis, 1995). Early studies by Chiew (1992) highlighted the effectiveness of riprap in reducing scour around bridge piers by disrupting the flow patterns that contribute to erosion. Concrete aprons and mats provide a solid, erosion-resistant layer around the foundation of bridge structures. These can be prefabricated or cast in place and are designed to protect the underlying soil from being washed away by water flow. Studies have shown that concrete aprons effectively prevent scour, particularly in areas with high flow velocities (Melville & Coleman, 2000). More recent research by Briaud et al. (2011) supports the use of concrete aprons in combination with other methods to improve scour protection.

Designing foundations that can withstand significant scour depths is a critical geotechnical approach. This method often involves using deep foundations with piles that extend well below the expected scour depth (Sadat, 2015). This approach maintains the Bridge's structural integrity even if the surrounding soil is eroded. Research has demonstrated the effectiveness of deep foundations in various riverine environments (Briaud et al., 2011). Additionally, (Ettema et al.,

1998) studied the scale effects in pier-scour experiments, highlighting the importance of considering foundation depth in scour-prone areas. This method involves injecting grout into the spaces between riprap stones to lock them together, creating a more cohesive and durable protective layer. Grouted riprap has been found to be particularly effective in areas with hydraulic solid forces that could dislodge ungrouted stones (Ettema et al., 1998). Subsequent studies by Heibaum and Trentmann (2010) demonstrated grouted riprap's long-term stability and effectiveness in reducing scour.

Hydraulic Measures are another method that has been used to reduce local scour. Various devices, such as vanes, baffles, or flow deflectors, are placed upstream of the bridge piers to alter the water flow and reduce its velocity around the critical areas (Brice et al., 1978). These structures help redirect or slow the flow, reducing the scour potential. Studies have shown that these flow-altering devices can significantly reduce the extent of local scour (Rajaratnam & Nwachukwu, 1983). More recent research by Melville and Coleman (2000) has further refined the designs and placements of these structures for optimal performance. Research has shown that planting vegetation can reduce stream bank erosion and scour around hydraulic structures. Vegetation stabilizes the soil through root reinforcement and dissipates the flowing water's energy, reducing erosion (Shields Jr et al., 1995). A study by the Agricultural Research Service investigated the resistance of three riparian species in the Platte River Basin to removal by drag forces and scour. The research found that vegetation significantly mitigates the effects of local scour, emphasizing the importance of incorporating vegetation into river management practices (Fotherby & Randle, 2007). This method has been particularly emphasized in recent environmental engineering studies for its dual benefits of erosion control and habitat creation.

Spur dikes, also known as groynes, extend from the riverbank into the river. They are designed to alter the flow patterns of the water to protect bridge piers and abutments from scour (Li et al., 2005). Kehe (1984) provided early evidence of flow diversion's benefits in altering river morphology through spur dikes. Spur dikes obstruct the direct water flow toward the bridge piers and abutments, redirecting the high-velocity flow away from these structures and reducing the erosive forces acting on the foundations (Fang et al., 2006). Kuhnle et al. (1999) demonstrated that spur dikes reduce the flow velocity around bridge piers, thus minimizing scour. The altered flow patterns created by spur dikes encourage sediment deposition between the dikes and the protected structure. This sediment build-up further reinforces the riverbed and reduces the likelihood of scouring. Studies have shown spur dikes promote sediment accumulation in the desired areas, enhancing their protective effect (Duan & Nanda, 2006).

Spur dikes dissipate the kinetic energy of the water, lowering its capacity to erode the riverbed and the structural foundations. This energy dissipation is crucial for reducing the impact of flowing water on hydraulic structures (Nazari et al., 2017). Research by Markovic (2012) supports the effectiveness of spur dikes in energy dissipation and scour reduction. The effectiveness of spur dikes depends on their strategic placement and design. Engineers must consider the river's hydrodynamics, sediment transport patterns, and the specific vulnerabilities of the bridge piers and abutments when designing and positioning the dikes (Esmaeli et al., 2022). Karami et al. (2011) provide detailed guidelines on the optimal design and placement of spur dikes to maximize their effectiveness in scour protection. Basser et al. (2014) also contributed valuable insights into the effects of spur dike location on flow structures, which are critical for designing effective scour mitigation systems.

The literature on scour prevention and reduction methods at bridge piers and abutments reveals various effective strategies, each with strengths and suitable applications. Structural measures like riprap and concrete aprons, geotechnical measures such as scour-resistant foundations, and hydraulic measures including flow-altering structures and vegetative stabilization, all contribute to mitigating the risks associated with scour (Beg & Beg, 2013; Deng & Cai, 2010; Wang et al., 2017). Among these, spur dikes have shown considerable promise in altering flow patterns, promoting sediment deposition, and dissipating energy, thereby providing robust protection against scour (Saneie, 2011; Vaghefi et al., 2021). To the best of the authors' knowledge, no previous research has investigated the application of non-submerged spur dikes with varying alignment angles under ice cover with different roughness coefficients. This study utilizes laboratory experiments to determine the optimal configuration of protective spur dikes for minimizing local scour at the abutment.

5.2 Experimental Procedures

5.2.1 Research Site and Flume Setup

This experimental study was conducted at the Quesnel River Research Center in Likely, British Columbia, Canada. The research employed a large-scale outdoor hydraulic flume specifically designed to replicate the natural dynamics of river systems. The flume, with dimensions of 38.5 meters in length, 2 meters in width, and 1.3 meters in depth, included a longitudinal bed slope of 0.2%. This setup allowed for the simulation of natural flow conditions with sufficient spatial scale to capture relevant hydrodynamic and sediment transport processes. An upstream holding tank with a volume of 90 cubic meters (40 meters in length, 2 meters in width, and 1.3 meters in depth) was used to maintain a steady and controlled discharge throughout the experimental runs. This tank was equipped with three valves facilitating a wide range of flow rates, which is crucial for simulating various riverine conditions. These valves supplied water to the flume, ensuring a controlled and adjustable inflow. The flume's design induced a non-uniform flow characterized by longitudinal variations in water depth, thus creating a more realistic model of river environments (Figure 5.1).

Within the flume, two distinct sandboxes were constructed to simulate riverbed conditions. These sandboxes, each 2 meters wide and 0.3 meters deep, were positioned 10.2 meters apart. The upstream sandbox was 5.6 meters long, while the downstream sandbox extended to 5.8 meters, providing sufficient space for observing sediment dynamics and scour development around the spur dike and the abutment (Figure 5.1). The sandboxes were filled with three types of natural sediments to replicate riverbed conditions. These sediments had median grain sizes (D_{50}) of 0.60 mm and 0.90 mm, with respective standard deviations of 2.39 and 1.41. The sediments' average density was approximately 1.7 g/cm^3. Plexiglass sidewalls were installed on one side of each sandbox to enable detailed visual observation and monitoring of the scouring process.

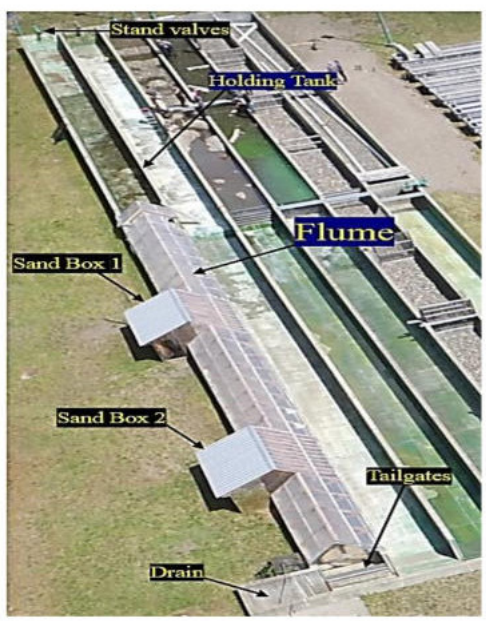

(a) Overview of the flume

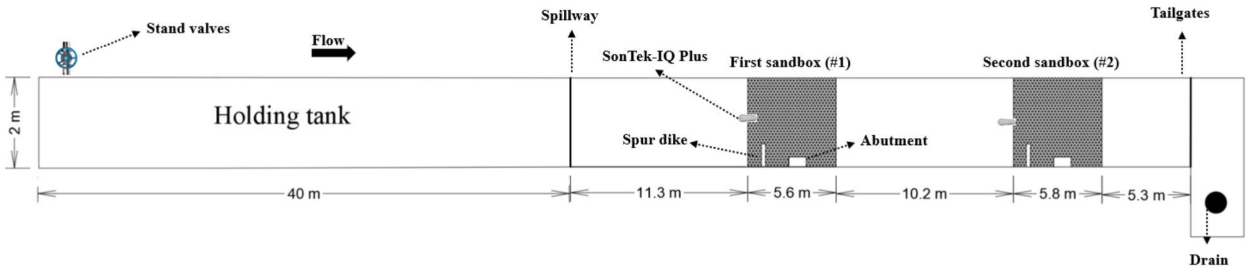

(b) Plan view

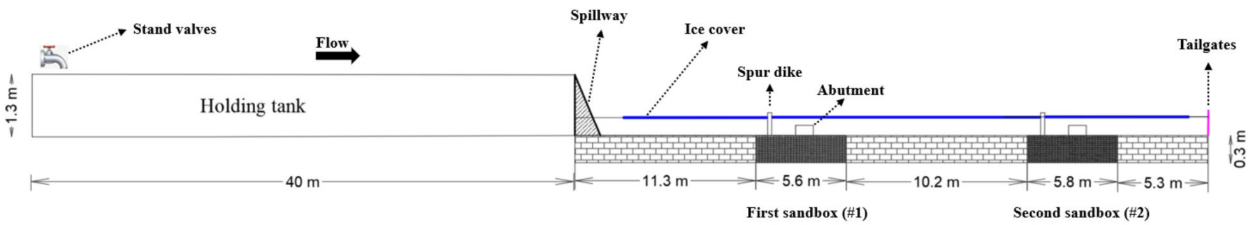

(c) Vertical view

Figure 5. 1:Experimental flume: (a) Overview of the flume, (b) Plan view, (c) Vertical view

A significant feature of the experimental setup was the installation of a spur dike and abutment in each sandbox. The dikes were constructed from marine-grade plywood, chosen for its durability and resistance to water. Each dike measured 80 cm in height, 5 cm in width, and 50 cm in length, with 30 cm of its height buried in the sand bed, leaving 50 cm exposed to the flow. The abutments were fabricated from galvanized plates designed in a rectangular shape with dimensions of 20 cm in width and 40 cm in length. The abutments were placed downstream of the dikes at 25 cm and 50 cm distances. This design aimed to simulate the impact of spur dikes on scour reduction surrounding the abutments (Figure 5.1,5.2). The dikes were tested at three different alignment angles to the downstream abutments: 90º, 60º, and 45º. These angles corresponded to blockage ratios of 25%, 20%, and 15%, respectively, providing a range of conditions to study the influence of dike orientation on flow patterns and sediment transport at the abutments.

Styrofoam panels were utilized to simulate the effects of ice cover on flow dynamics and scour processes. Smooth panels represented natural sheet ice commonly found in riverine environments during winter. Rough panels were created by affixing 2.5 cm^3 Styrofoam cubes to mimic the roughness and complexity of ice jams. Sixteen panels, each measuring 1.99 meters by 2.4 meters, were employed to cover the entire flow surface within the flume. This setup allowed for the examination of the impact of ice cover on hydraulic conditions and sediment transport, providing insights into wintertime river dynamics.

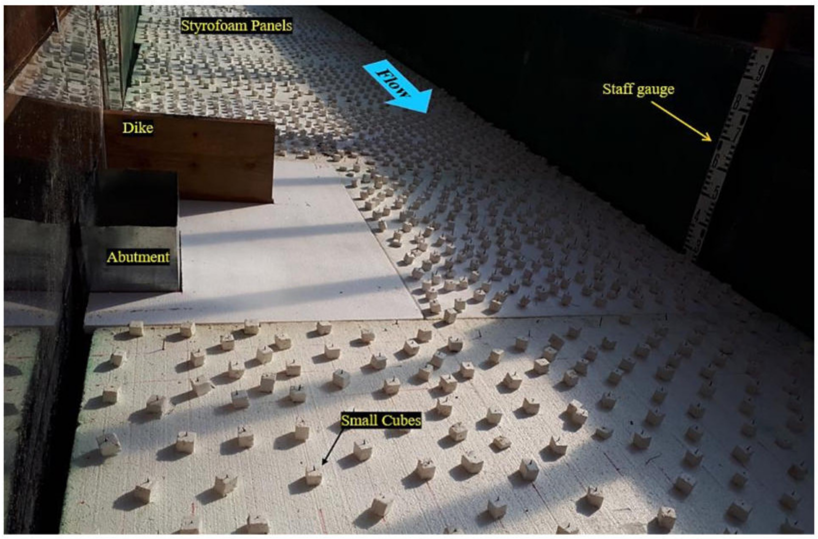

Figure 5. 2:A cover condition experiment under smooth ice cover with a 60º alignment angle

Flow measurements were primarily conducted using the SonTek-IQ Plus. The IQ Plus is an advanced instrument designed for precise flow monitoring in natural rivers and controlled environments like hydraulic flumes. It is equipped with six sensors, including four velocity beams and two additional beams for water level and vertical acoustic measurements (SonTek, 2017). These multiple sensors provide comprehensive coverage of the flow field, ensuring high accuracy and reliability in data collection. These features allow researchers to gain a deeper insight into the approaching flow characteristics and volume data, which are critical for evaluating the hydraulic performance of structures and understanding sediment transport mechanisms (SonTek, 2017). This device was strategically positioned in front of each sandbox to ensure accurate and continuous monitoring of the flow conditions (Figure 5.1).

5.2.2 Data Collection and Analysis Procedures

Prior to each experimental run, the surfaces of the sandboxes were carefully levelled. For the runs under the ice cover surface, the Styrofoam panels were gently placed on the bottom of the flume. Water was gradually introduced into the flume to prevent initial scouring around the spur dikes and abutments. Once the desired flow depth was achieved, the valves were fully opened to commence the experimental run. Flow parameters, including depth and velocity, were continuously monitored using the SonTek-IQ Plus and the staff gauges positioned at the midpoint of each sandbox. Each experimental run was conducted for 24 hours to ensure that the scouring process reached equilibrium. Equilibrium was defined as the point at which the dimensions of the scour holes and deposition dunes stabilized (Haltigin et al., 2007; Namaee & Sui, 2019b).

Upon completion of each run, the flume was carefully drained to preserve the scour patterns, and the model ice cover was removed (for the experiments under surface cover conditions). The geometries of the scour holes and deposition dunes were measured using precision callipers. Data were processed using Surfer Golden Software to generate detailed 3D profiles and contour maps of the scoured regions. To ensure the consistency and accuracy of the data, supplementary experimental runs were conducted, extending the observation periods to 48 and 72 hours. These extended experiments confirmed that equilibrium conditions were typically achieved within 24 hours, as no significant variations in scour depth were observed beyond this timeframe.

This comprehensive experimental setup and precise data acquisition provided a robust framework for understanding the impact of spur dike on the scouring dynamics around the abutment under various hydraulic and ice cover conditions, contributing valuable insights into the interactions between flow conditions, sediment transport, and protective spur dikes in fluvial systems.

5.3 Results and Discussions

At the start of each experimental run, localized scouring was initiated at the upstream corner of the abutment. This phenomenon was attributed to the intensified flow dynamics at the abutment toe and downward vertical flow velocities at the abutment's upstream side, generating a vortex system at the abutment's left corner. The erosive force of the horseshoe vortex increased the shear stress on the bed, surpassing the critical threshold needed to move sediment. As a result, the erosion of sediment around the abutment started, leading to the formation of a scour hole. This process highlights how the interaction between flow dynamics and sediment transport mechanisms influences the development of local scour at any obstacle against the river flow (namely, abutments, piers, and spur dikes). Over time, the scour hole at the left corner of the abutment gradually enlarges in all directions, with notable expansion downstream.

Sediment particles moved within the scour hole were carried downstream by the vortex system and transferred into the low-velocity zone downstream of the abutment toward the river bank. Within this zone of reduced flow velocity, the stream flow interacted with downstream eddies, forming an additional vortex system termed the wake vortex (Ishigaki et al., 2000; Namaee & Sui, 2019b). Unlike the robust horseshoe vortex, these wake vortices, originating from lower velocities, displayed weaker dynamics. Consequently, the lack of capacity to retain and transport sediment causes particles to gradually settle on the channel bed, forming deposition dune patterns (Dey & Raikar, 2007). Downstream of the right corner of the abutment, near the river bank, a sediment dune emerged.

The morphology of scour holes around abutments and the pattern of deposition dunes downstream are influenced by various factors, including flow characteristics and the condition of the water surface. Contour maps are invaluable tools for rendering three-dimensional data into a two-dimensional representation. By employing contour lines to connect points with identical elevation values, these maps provide a detailed visualization of scour hole morphology and sediment dune configuration, enabling a comprehensive analysis of riverbed deformation patterns. This section has thoroughly examined the impact of diverse factors on the formation of scour holes and deposition dunes, offering valuable insights into the complex dynamics of sediment transport and erosion processes.

5.3.1 Scour at Abutment

Open Flow Condition: In open surface conditions, scour initiation occurs at the base of the upstream corner of the abutments. The scour expands laterally and vertically as the experiment progresses, characterized by evident horseshoe vortices within the scour hole. These vortices highlight the significant role of flow dynamics in sediment transport mechanisms. Similar flow separation occurs at the downstream corner of the abutments but with lower energy levels, leading to slower sediment movement and the gradual formation of a scour hole. Over time, the downstream scour hole expands, but its depth remains relatively shallow (Figure 5.3).

The strong flow separation at the upstream corner results in a semi-circular scour hole extending downstream. Variations in flow depth have minimal influence on the scour hole, and occasional reduced flow depth enlarges the scour hole laterally and vertically. In contrast, flow depth has a negligible impact on the scour characteristics at the downstream corner of the abutment. However, the velocity of the approaching flow significantly affects the scour holes at both corners. Increased approach velocity expands the upstream scour hole in all dimensions, especially laterally, while its impact on the downstream scour hole is less noticeable.

In most experimental runs, the two scour holes at the abutment corners did not converge. However, In a few cases, the scour hole at the upstream corner extends to the opposite corner, forming a larger scour hole along the frontal side of the abutment. The scour hole depth is maximal at the upstream corner and gradually diminishes towards the downstream corner, resulting in a shallower scour hole at the right corner (Figure 5.3).

Smooth-Covered Flow Condition: The presence of an ice cover significantly influences the scour hole pattern around the abutment, leading to its enlargement and deepening in both upstream and downstream directions. The scour hole often extends to the riverbank within 8 hours, progressing upstream and forming a large hole near the abutment. Similar to open surface scenarios, scouring starts at the upstream corner early in the experiment. After about 10 hours, the scour holes at both corners converge into a large scour along the abutment's front side (Figure 5.3). The scour extends towards the channel center, resembling patterns observed downstream of a spur dike (Jafari & Sui, 2021).

Flow depth and approach velocity significantly influence the scour hole under smooth cover conditions. Reduced flow depths lead to deeper scour holes, especially at the abutments' upstream side. Higher approach velocities increase the scour hole area, extending it downstream and towards the riverbank. Consequently, the scour hole area expands with rising approach velocity and flow rate, with substantial sediment deposition forming downstream near the riverbank.

Rough-Covered Surface: Increasing the roughness coefficient of the cover surface significantly transformed the scour hole pattern around the abutment, with notable expansion in all dimensions, especially along the flow direction (x direction). Under rough cover conditions, the upstream corner scour enlarges much faster than under smooth cover, extending towards the riverbank and downstream of the abutments. In most experimental runs, the scour surrounded the abutment in all directions within the first 8 hours. The scour also extended towards the channel center, similar to smooth conditions. The larger scour hole caused the deposition dune to shift further towards the riverbank downstream of the abutment, substantially altering the sediment deposition pattern (Figure 5.3).

Flow depth significantly influenced scour dynamics in rough cover scenarios. Reduced flow depth extended the scour hole depth, especially at the abutment's front side. Approach flow velocity also impacted the scour hole, similar to smooth cover conditions. Higher velocities led to a downstream extension and overall enlargement of the scour hole around the abutment. At higher velocities, the scour hole at the channel's center showed significant enlargement and downstream extension.

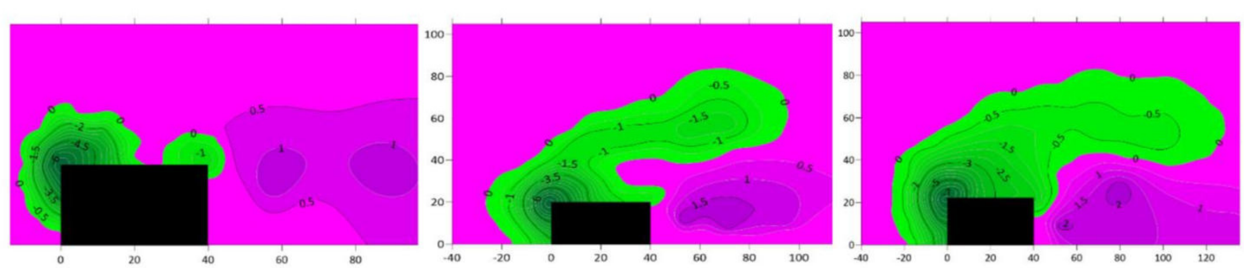

Figure 5. 3:Scour patterns around the abutment under different cover conditions (flow depth=22 cm)

5.3.2 Application of Spure Dike

The findings suggest that river flow conditions can lead to significant local scour at the abutment, potentially compromising the foundation and resulting in structural failure or bridge collapse. This section aims to thoroughly assess the effectiveness of spur dikes in mitigating and preventing scour at the abutment. The analysis includes evaluating various dike orientation angles and configurations with the abutment to determine the dike impact on reducing scour. The influence of distinct flow characteristics and ice cover conditions on local scour has also been examined. The study's ultimate goal is to identify the optimal dike layout that offers the best protection against scour for abutments, thereby minimizing the risk of structural damage.

5.3.2.1 90 alignment Spur Dike located 50 cm Upstream of the abutment

The initial spur dike layout is perpendicular to the riverbank, positioned 50 cm upstream from the abutment. The 90-degree dike effectively intercepts the river flow, redirecting it to the center of the channel and inducing turbulence flow upstream of the abutment rather than directly impacting the abutment itself. Significantly, the surface cover condition is identified as the critical factor affecting the spur dike's protective ability for the abutment. Consequently, three distinct surface conditions and several flow characteristics have been examined individually to assess the influence of ice cover and varying flow conditions on the dike's protection against local scour at the abutment.

Open Flow Condition: A small scour was observed at both outside corners of the abutment in open-flow conditions. Elevated approach velocity and higher flow rates resulted in the expansion of scour holes. While flow depth exerted a less significant influence on scour size, reductions in water depth correlated with slightly larger scour holes at the abutments. Variances in flow characteristics, including flow depth and approach velocity, widened the scour holes and expanded their area. However, scour depths at both outside corners remained constant across different runs. Generally, the upstream corner exhibited slightly larger scour than the downstream corner in most flow conditions. The sediment deposition dunes formed downstream of the dike scour hole, away from the abutments (Figure 5.4). Despite the consistent presence of scour holes at both corners of the abutment in open surface conditions, their size remained minimal, posing no threat to abutment safety.

Smooth-Covered Flow Condition: The dike scour hole enlarges under smooth cover conditions, leading to deeper scour holes and larger sediment deposition dunes. The sediment dune expands and shifts closer to the abutment but never reaches it across different runs. Scour holes form at both corners of the abutments, similar to those in open channel conditions but larger. The upstream and downstream holes are almost identical in size and shape under various flow conditions. However, the scour at the right corner tends to be slightly more prominent at higher velocities and flow rates. Reduced water depth results in deeper scour holes at the downstream corner compared to the upstream corner. As in open flow conditions, the scour holes at both corners remain relatively insignificant, posing no immediate safety risks to the structure (Figure 5.4).

Rough-Covered Surface: Under rough cover conditions, the scour hole enlarges more than under smooth cover, leading to more extensive and closer sediment deposition dunes. This expansion results in greater sediment erosion and downstream deposition toward the abutments. Consistently, deposition dunes push toward the upstream corner of the abutment. In some runs, sediment partially buries the abutment's left side, preventing local scour (Figure 5.4). Conversely, the right side of the abutment experiences more substantial scouring compared to open and smooth-covered flow conditions. Scouring at the downstream corner intensifies with increasing velocity. Water depth significantly impacts scour depth, with lower depths leading to deeper holes. Higher velocities increase the area and dimensions of the scour hole, while water depth primarily dictates its vertical extent. Despite the larger scour hole under rough cover conditions, the abutments remain structurally safe. The scour depth is insufficient to expose the abutment foundation.

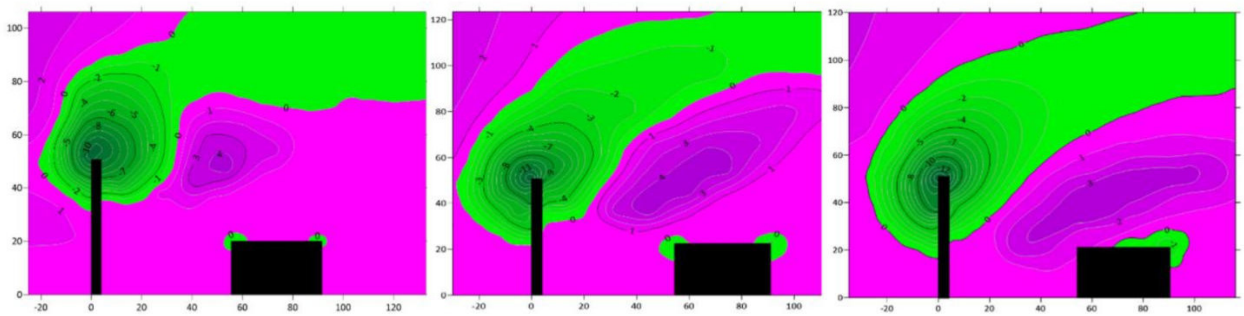

Open Smooth Rough

Figure 5. 4:Scour patterns around the abutment under different cover conditions and protective dike with 90 alignment angle (Flow depth =22 cm)

5.3.2.2 60 alignment Spur Dike located 50 cm Upstream of the abutment

The scour characteristics around a spur dike at a 60º angle differ significantly from those observed around right-angle dikes. This variance extensively influences the sediment deposition pattern, consequently impacting the scour observed at the abutment downstream of the dike. In the case of a 60-degree orientation angle, the primary controlling factor is the velocity of the approach flow. The high velocity of the flow affects the erosive forces of the eddies and vortex system in the scour hole, leading to an increase in scour depth and enlarging the sediment deposition dunes. Additionally, the flow surface condition serves as a secondary controlling factor. As a result, the research findings were assessed within two distinct scenarios: high velocity and low velocity, each under varying cover conditions and water depths. These parameters were analyzed to gain a comprehensive understanding of the interaction between flow dynamics, scour around abutments, and sediment transport processes.

5.3.2.2.1- Spur dike with alignment angle of 60º and low approaching flow velocity

Open Flow Condition: The scour hole displaces and expands towards the channel wall on the abutment side, pushing deposition dunes closer to the abutment and riverbank. Sediment deposits form extensive dunes near the upstream side of the abutment, serving as protective barriers that mitigate scouring effects. The vortex system influences the morphology of the scour hole and sediment deposition patterns. Horseshoe vortices persist around the dike, extending downstream, while wake vortices form within 50 cm of the dike, initiating downstream deposition dunes, especially near the upper left corner of the abutment. These dunes exhibit a pyramid-shaped layout, indicating that wake vortices dissipate within half a meter.

On the downstream side, scouring occurs in all runs with low approach velocity. While water depth affects scour hole dynamics, its impact is less significant than other factors. Reducing water depth sometimes correlates with slightly larger scour holes on the right side of the abutments, but the scouring depth remains relatively consistent. This highlights the complex interplay between hydraulic factors and geomorphic processes in scour hole formation, where water depth fluctuations influence the extent and dimensions of the scouring pattern.

Smooth-Covered Flow Condition: Under smooth cover conditions, sediment deposition dynamics change significantly near the abutments. Deposition dunes often encroach closer to the abutments, with the upstream corner frequently buried beneath the sediment. The highest dune elevation shifts from the upper left side in open conditions to further downstream, around the middle to lower abutment. This shift reflects changes in wake vortex strength and position, indicating altered sediment transport dynamics. In smooth cover conditions, sediment dunes caused by dike expand downstream, with deposition more dispersed and oriented downstream. Despite deposition around the abutments, scour holes at the downstream corner remain evident, more significant, and with distinct patterns compared to open conditions (Figure 5.5). While water depth influences scour dynamics more under smooth cover conditions, its impact is secondary to velocity and cover condition. Variations in water depth affect scour hole dimensions and depth, with reduced water depth often increasing the scour hole size and occasionally its depth.

Rough-Covered Surface: Under rough cover conditions, sediment deposition dynamics amplify, with dunes moving downstream and encroaching toward the abutment. Nearly half of the upstream abutment section is submerged beneath sediment deposits caused by the dike, shielding the left side from scour (Figure 5.5). Conversely, the right side remains vulnerable to large scour holes, particularly at the downstream corner, exhibiting more significant scouring than in open or smooth-covered conditions. Water depth significantly affects scour hole morphology under rough cover conditions. Reduced water depth notably increases the size and depth of the scour hole, highlighting the sensitivity of scour dynamics to water depth variations. Turbulence and eddy formation analysis reveal the intricate relationship between the vortex system and scour hole morphology. A robust horseshoe vortex is evident in rough cover conditions, especially at the downstream corner of the abutments, indicating heightened turbulence intensity compared to open conditions.

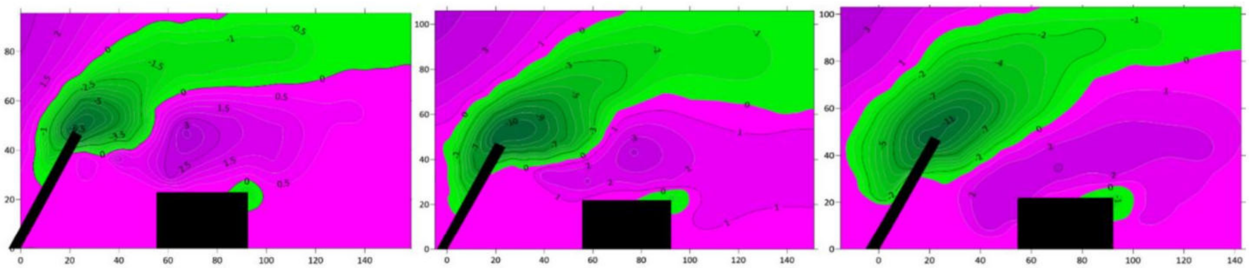

Open Smooth Rough

Figure 5. 5: Scour patterns around the abutment under different cover conditions and protective dike with 60 alignment angle (low velocity, flow depth=22 cm)

5.3.2.2.2-Spur dike with alignment angle of 60º and high approaching flow velocity

Open Flow Condition: With increased approach velocity, the vulnerability of the abutment's upstream corner becomes more noticeable. The sediment dune caused by spur dike acts as a protective barrier at lower velocities, preventing scouring. However, due to complex turbulence altering sediment deposition patterns, higher velocities lead to evident scouring at the upstream corner of the abutment. Despite extensive analysis, no clear trend in deposition dune patterns has been identified.

In open surface scenarios, scour holes form at both abutment corners, with the downstream corner exhibiting greater depth and area (Figure 5.6). Flow depth has minimal impact on scour hole size, though slight enlargement of downstream corner scour holes is noted with reduced flow depth. Elevated approach velocity transitions the scour hole morphology from semi-circular to elliptical. The deposition dune caused by the dike maintains a semi-pyramidal form, positioned away from the abutments. Higher velocity significantly impacts flow dynamics and turbulence, especially at the abutment corners. Increased kinematic energy develops a robust vortex system, enlarging scour holes, particularly at the downstream corner of the abutment.

Smooth-Covered Flow Condition: Under smooth cover conditions, sediment dunes caused by spur dike extend closer to the abutments, reducing scour hole dimensions at both corners. The upstream corner scour hole is consistently smaller compared to open flow conditions, and at the downstream corner, the scour hole also appears smaller, occasionally nearly the same size but never exceeding that under open flow conditions. Flow depth variations have minimal impact on the scour hole's dimensions, but a reduction in flow depth slightly causes an increase in the scour hole depth at the downstream corner. Increased flow velocity causes the scouring at the downstream corner to expand toward upstream, sometimes approaching the left corner. However, the two scour holes remain distinct and did not merge. A quarter of the abutment's front section consistently remains unaffected by scouring (Figure 5.6).

Detailed analysis reveals a complex interaction between flow depth, deposition dunes, and vortex dynamics. Deposition dunes near the abutments interact with the wake vortex and horseshoe vortex, reducing erosive forces at the upstream corner and limiting scour hole expansion. This effect persists even with increased approach velocity.

Rough-Covered Surface: Rough surface conditions enforce more significant scouring at spur dikes than smooth-covered and open-flow conditions. Higher flow velocities result in larger and deeper scour holes around the dike, driving them closer to the abutment. This intensified scouring alters sediment deposition patterns, causing dunes to extend further downstream. As the deposition dune moves away from the abutment, distinct scour holes form at both corners, reflecting the increased roughness coefficient's impact on scour dynamics. The scour hole at the downstream corner consistently exhibits larger and deeper scour than that at the upstream corner.

In most experiments, the upstream corner's scour hole is larger than under smooth conditions (Figure 5.6).

Water depth has a more noticeable influence under rough-covered flow conditions, with lower depths leading to larger and deeper scour holes at both corners. Similar interactions between the wake vortex and horseshoe vortex are evident. In open-flow scenarios, the horseshoe vortex is apparent at both abutment corners, especially downstream. In contrast, high-velocity flows under cover conditions lack a noticeable vortex system, suggesting complex interactions between vortices generated by the dike and abutment.

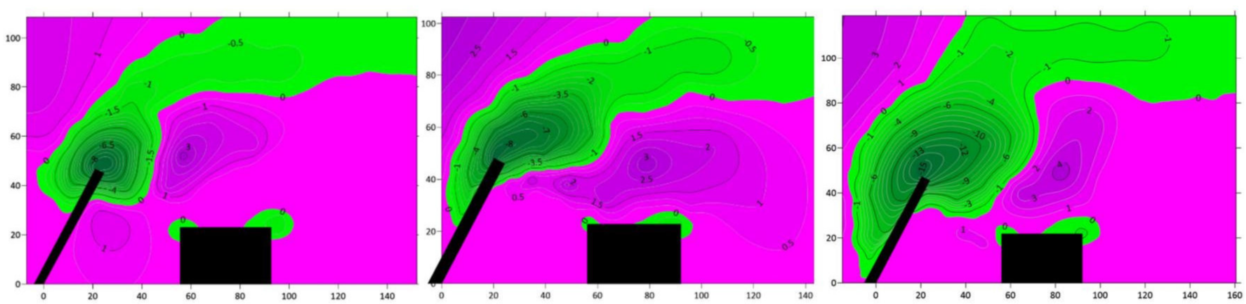

Open Smooth Rough

Figure 5. 6:Scour patterns around the abutment under different cover conditions and protective dike with 60º alignment angle (high velocity, flow depth=22cm)

5.3.2.3 45º alignment Spur Dike located 50 cm Upstream of the abutment

The scour hole pattern exhibited notable divergence at the dike with an alignment angle of 45º compared to dikes with other angles. Notably, the dike scour hole extended further downstream, displacing deposition dunes towards both the abutments and the riverbank downstream of the abutments. The primary controlling factor driving these changes was the approaching flow velocity, followed closely by the water surface cover condition and ice cover roughness coefficient, a pattern similar to the dynamics observed at the dike with an alignment angle of 60°.

However, a notable difference was observed concerning flow depth, particularly between the 45° and 60° alignment dikes. While the impact of flow depth was negligible at the dike with an alignment angle of 60°, it substantially influenced scenarios featuring a dike with an alignment angle of 45°. This consistent relationship between flow depth and velocity highlighted the significance of the Froude number as a representative indicator of both variables. The discrete effects of various factors are evaluated independently under different ranges of approaching flow velocity.

5.3.2.3.1- Spur dike with alignment angle of 45° and low approaching flow velocity

Open Flow Condition: In open flow conditions, the scour hole at the dike forms a distinct pattern, concentrates around the dike tip and extends towards the channel center. Small deposition dunes emerge downstream of the dike and in front of the abutment but remain separated, leaving the abutment exposed to vortex effects and scouring process. The downstream corner consistently experiences scour hole formation, with a horseshoe vortex becoming evident within several hours, expanding the scour hole into a semi-elliptical shape while no significant scour was observed at the upstream corner (Figure 5.7). Changes in flow depth had minimal impact on scour hole dynamics, though a slight increase in depth may occur with the decrease in flow depth. No consistent correlation has been observed between flow depth and scour hole dimensions, especially under low-velocity conditions. A small deposition dune indicates that the wake vortex was too weak to propagate far from the dike.

Smooth-Covered Flow Condition: Under smooth cover conditions, the scour hole around the spur dike extends further downstream and approaches but never touches the left corner of the abutment. A scour hole can not be developed at the abutment upstream corner. As the scour hole expands, the deposition dune also grows and occasionally reaches the frontal side of the abutment, although this effect was minimal (Figure 5.7). Despite forming a substantial deposition dune near the abutment, it fails to shield the zone around the downstream corner of the abutment, resulting in a larger scour hole similar to that around the downstream of the abutment under open flow conditions. The scour hole morphology differs notably from that under open flow conditions, with flow depth playing a significant role. The reduction in flow depth leads to larger and deeper scour holes, underscoring the importance of flow depth in shaping the scour morphology around the abutment.

Rough-Covered Surface: under conditions with low flow velocity, the scour hole around the dike favours expansion toward the channel wall and the zone downstream of the abutment rather than the center of the channel. These scour holes are larger and deeper than those under open flow and smooth-covered conditions. The dike scour hole extends to the upstream corner of the abutment, converging with the local scour around the abutment, thereby increasing the scour depth and area upstream of the abutment (Figure 5.7). Increasing the ice cover roughness coefficient plays a crucial role in affecting the velocity component, pushing the scour hole further downstream. This increase in kinetic energy makes the abutment's upstream corner more vulnerable to scour and erosion. The interaction between the dike wake vortex, and the abutment horseshoe vortex creates a complex and inconsistent influence of flow field on the scouring process at the abutment's upstream corner. Significant upstream scouring leads to sediment transport and the development of the deposition dunes. Under rough covered flow conditions with low flow velocities, these deposition dunes often extend downstream and thus protect the right side of the abutment. No scour was observed at the abutment's downstream corner under rough cover conditions. However, the upstream corner of the abutment experienced continuous scouring regardless of changes in velocity and water depth. The extent of deposition dunes increased significantly under rough cover conditions, indicating intensified kinetic energy and robust vortex systems, particularly the horseshoe and wake vortices.

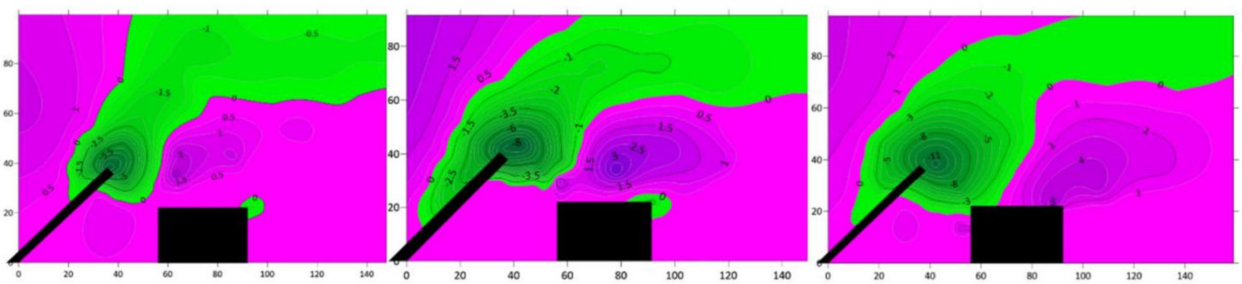

Open Smooth Rough

Figure 5. 7:Scour patterns around the abutment under different cover conditions and protective dike with 45° alignment angle (low velocity, flow depth=22cm)

5.3.2.3.1- Spur dike with alignment angle of 45º and high approach velocity

Open Flow Condition: High flow velocity significantly impacts the scouring process downstream of the dike. As velocity increases, the scour hole around the dike extends downstream and approaches the abutment and channel wall, which changes the deposition dune pattern. Sediment deposition caused by the dike moves closer to the abutment, covering a substantial portion from the upstream corner to near the downstream corner of the abutment. The deposition dunes effectively shield the zone around the abutment from erosive forces and rapid flow. In all runs under open flow conditions with high velocity, about 90% of the abutment's front side was surrounded by deposition dunes (Figure 5.8).

Water depth had no consistent impact on dune formation. Most experimental runs have observed a minor scour at the downstream corner of the abutment with a semi-circular shape and less than 1 cm deep. While water depth had little effect on scour holes, reduction in flow depth resulted in a slight increase in their dimensions without significantly affecting their depth.

Smooth-Covered Flow Condition: Under smooth cover conditions, the dike scour hole pattern is similar to that under open flow conditions but extends wider and closer to the abutment. The scour hole around the dike gets very close to the upstream corner of the abutment, but it rarely reaches the upstream corner of the abutment. Substantial scour downstream of the dike pushed the deposition dune further downstream and away from the upstream corner of the abutment. Under open flow conditions, sediment accumulated a considerable portion of the abutment's front side. The highest point of the dune was shifted downstream closer to the channel center (Figure 5.8).

As the deposition dunes were shifted away, the abutment's front face, especially the zone around the downstream corner, became more susceptible to eddies. Consequently, scour holes consistently developed at the downstream corner of the abutment under smooth cover conditions, with significant enlargement and deeper compared to open flow conditions. Water depth substantially influenced the dimensions of the scour holes; decreased flow depth led to significant horizontal expansion and vertical deepening of the scour holes.

Rough-Covered Surface: Under rough cover conditions and high approaching flow velocity, the scour hole exhibited the largest dimensions compared to other scenarios. The scour hole caused by the spur dike extended to encompass the entire abutment, causing severe scouring along the upstream corner and the front side of the abutment. In most experimental runs, the upstream corner of the abutment experienced the deepest scour, reaching approximately 4 cm. The scour zone often extends across the entire front side of the abutment, including both corners (Figure 5.8). The morphology of deposition dunes indicates the impact of surface cover conditions on flow velocity and kinematic energy. An increase in ice cover roughness redirected erosive vortices toward the abutment, extending the scour hole. A substantial scour hole at the abutment's front side under rough cover conditions indicates a dominant horseshoe vortex.

Flow depth critically affected the scour hole dimensions; with the decrease in flow depth, scour depth increases more than the scour range, highlighting the enhanced effects of ice cover roughness on the velocity gradient near the bed. Namely, the increased roughness elevated kinetic energy at lower flow layers, creating a more robust vortex system. Thus, the deposition dune was shifted further downstream, protecting the flum wall. The deposition dunes predominantly formed a pyramid shape, indicating a strong wake vortex downstream of the abutment (Figure 5.8).

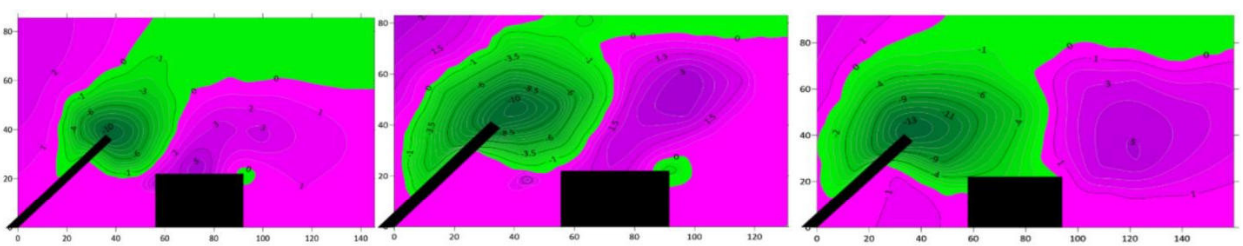

Open Smooth Rough

Figure 5. 8:Scour patterns around the abutment under different cover conditions and protective dike with 45º alignment angle (high velocity, flow depth=22cm)

5.3.2.4 90º alignment Spur Dike located 25 cm Upstream of the abutment

Based on the results of the experiment, a 90º alignment angle dike positioned 25 centimetres upstream from the abutment emerges as the optimal configuration to effectively shield against rapid flow and erosive eddies around the abutment, thereby preventing scour formation at the abutment located in the downstream region of the dike. Throughout various experimental setups involving diverse flow characteristics and water surface cover conditions, no scour has been observed surrounding the abutment, either upstream or downstream. However, it must be mentioned that sediment deposition patterns around the abutment varied significantly across different flow conditions, indicating the significant impact of water surface cover conditions and ice cover roughness coefficients on the interaction between the vortex system around the spur dike and abutment.

Open Flow Condition: In experiments under open flow conditions, the dike redirected water flow toward the channel center, developing deposition dunes away from the abutment. These dunes consistently kept an elliptical shape downstream of the dike, with the highest point in front of the abutment but at a certain distance from the abutment (Figure 5.9). Regardless of the flow conditions, the sediment dunes never reached the abutment, and no identified trend was observed in their patterns. Approaching flow velocity had minimal impact on the vortex system around the abutment and formation of the deposition dune. Occasionally, higher velocities resulted in the extension of the deposition dune towards the abutments and generated small wake vortices within the dune regions.

Smooth Covered Flow Condition: The presence of a cover significantly alters the pattern of deposition dunes compared to that under open surface conditions. Under smooth cover conditions, deposition dunes caused by the dike are extended towards the abutments, burying the front and both corners of the abutment, providing protection against the vortex systems and scouring process (Figure 5.9). The deposition dunes also extended downstream, safeguarding the channel bank. Changes in flow depth had minimal impact on the channel bed deformation dynamics, though decreased flow depth correlated with longer dunes towards the abutment. The approaching flow velocity had minimal influence; an increase in flow velocity led to slightly wider deposition dunes.

Rough-Covered Surface: The presence of a rough cover on the water surface led to an increase in the roughness coefficient, significantly changing the deposition dune pattern. The rough ice cover shifted the dunes closer to the abutments, providing additional protection against eddies. In most experiments under rough cover conditions, sediment accumulated in the upstream corner of the abutment and much of the abutment's frontal side, with the highest dune point occurred near the abutment's center, enhancing defence against vortices and erosion around the abutment (Figure 5.9). An increase in the roughness coefficient resulted in intensified kinetic energy at the lower layer, promoting a horseshoe vortex system downstream of the dike. This vortex pushed deposition dunes closer to the abutments, creating more extensive dunes at the frontal side of the abutment. A decrease in flow depth led to a further shift of the dunes toward the abutment. The influence of the approaching velocity on the deposition dunes and vortex system was observed to be similar to that of under smooth cover conditions but without a consistent trend regarding its impact on patterns of deposition dunes.

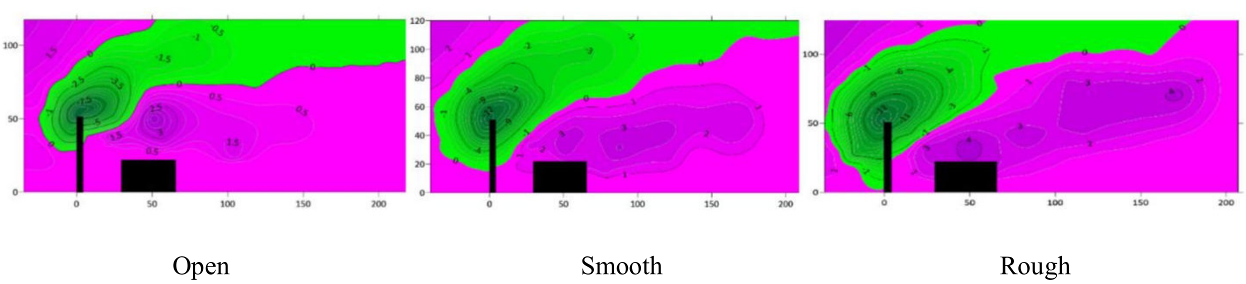

Figure 5. 9:Scour patterns around abutment scour under different cover conditions and protective dike with 90ºalignment angle, 25cm distance (flow depth=22cm)

5.3.3 Comparative Assessment of Scour Depth Variability Around Bridge Abutments

The comprehensive analysis of this chapter indicates a clear relationship between the angle of the spur dike, its distance from the abutment, and the resultant scour reduction. The results consistently show that sharper dike angles, particularly the 90° angle, are highly effective in mitigating scour. This is especially true at shorter distances (25 cm) from the abutment, where the scour reduction can reach 100%. The effectiveness of scour reduction decreases slightly as the distance increases to 50 cm. At 50 cm distance, the scour reduction remains high, ranging from 69% to 97%, but the 90° angle still outperforms the 60° and 45° angles.

The 60° angle, while still effective, does not provide as much protection as the 90° angle, indicating that the steepness of the angle plays a crucial role in the efficacy of scour reduction. The 60° dike angle also demonstrates considerable scour reduction but is less effective compared to the 90° angle, with reductions ranging from 68% to 89%. The 45° angle consistently offers the least protection, particularly in rough-covered flow conditions, suggesting that more acute angles are less effective in deflecting flow and reducing scour. The 45° dike angle provides the least protection, particularly in rough-covered conditions, where scour reduction can be as low as 25%, highlighting its limited efficacy compared to steeper angles. Table 5.1 and 5.2 compare the maximum scour depth around abutments with and without protective spur dikes under varying flow depth and flow velocity conditions.

The superior performance of the 90° dike angle, particularly at closer distances to the abutment, suggests that this configuration should be preferred in practice to maximize scour reduction. Conversely, the limited effectiveness of the 45° angle indicates that such configurations should be avoided in scenarios where significant scour protection is required. These insights contribute to a better understanding of how spur dikes can be optimally designed and positioned to mitigate the erosive forces of flowing water and protect hydraulic structures.

Table 5. 1: Comparison of maximum scour depth around abutment with and without protective dike, flow depth=11cm

Dike Angle	Distance from Dik (cm)	Flow Depth (cm)	Velocity (cm/s)	Maximum Scour Depth (cm)								
				Open Flow			Smooth-covered			Rough-covered		
				with Dike	without Dike	Scour Reduction (%)	with Dike	without Dike	Scour Reduction (%)	with Dike	without Dike	Scour Reduction (%)
90	50	11	28	0.2	7	97%	1.54	8.2	81%	2.9	9.3	69%
90	50	11	56	0.23	7.6	97%	1.61	9	82%	3.25	10.4	69%
60	50	11	28	0.8	7	89%	1.72	8.2	79%	2.5	9.3	73%
60	50	11	56	0.94	7.6	88%	2.46	9	73%	3.34	10.4	68%
45	50	11	28	0.58	7	92%	2.73	8.2	67%	6.1	9.3	34%
45	50	11	56	0.2	7.6	97%	3.81	9	58%	7.8	10.4	25%
90	25	11	28	0	7	100%	0	8.2	100%	0	9.3	100%
90	25	11	56	0	7.6	100%	0	9	100%	0	10.4	100%

Table 5. 2: Comparison of maximum scour depth around abutment with and without protective dike, flow velocity=23cm/s

Dike Angle	Distance from Dik (cm)	Flow Depth (cm)	Velocity (cm/s)	Maximum Scour Depth (cm)								
				Open Flow			Smooth-covered			Rough-covered		
				with Dike	without Dike	Scour Reduction (%)	with Dike	without Dike	Scour Reduction (%)	with Dike	without Dike	Scour Reduction (%)
90	50	13.5	23	0.17	6	97%	1.27	7.3	83%	2.3	8.4	73%
90	50	26	23	0.15	5.9	97%	0.79	6.6	88%	1.565	7.5	79%
60	50	13.5	23	0.55	6	91%	1.52	7.3	79%	2	8.4	76%
60	50	26	23	0.51	5.9	91%	1.4	6.6	79%	1.67	7.5	78%
45	50	13.5	23	0.5	6	92%	2.455	7.3	66%	5.7	8.4	32%
45	50	26	23	0.2	5.9	97%	1.6	6.6	76%	4.74	7.5	37%
90	25	13.5	23	0	6	100%	0	7.3	100%	0	8.4	100%
90	25	26	23	0	5.9	100%	0	6.6	100%	0	7.5	100%

5.3.4 Comparative Analysis of Maximum Scour Depth Around Abutments with Different Alignment Angles of Protective Spur Dikes

The analysis of results provides significant insights into the effectiveness of spur dikes in reducing scour around abutments under various hydraulic conditions. The findings highlight the critical role of dike angle and distance from the abutment in influencing the maximum scour depth. This section elaborates on the relationships and implications derived from the data, providing a complete interpretation of the findings.

The angle of the spur dike is a crucial parameter that significantly affects its ability to reduce scour. The data consistently demonstrate that the 90° dike angle is the most effective in mitigating scour across different flow conditions. At a flow depth of 22 cm (Table 5.3), the 90° dike angle achieves the lowest maximum scour depths, particularly at a 25 cm distance from the abutment, where it eliminates scour under all tested conditions. This superior performance is also evident at a distance of 50 cm, where the maximum scour depths remain significantly lower than those observed for the 60° and 45° dike angles.

Similarly, at a flow velocity of 28 cm/s (Table 5.4), the 90° dike angle maintains its effectiveness, achieving minimal scour depths at both 25 cm and 50 cm distances from the abutment. These results indicate that the perpendicular alignment of the dike to the flow direction is highly efficient in deflecting the erosive forces of the water, thereby minimizing the formation of scour holes around the abutment. The distance of the spur dike from the abutment is another critical factor influencing scour reduction. The data reveal that closer placement of the dike (at 25 cm) generally results in more effective scour mitigation. For the 90° dike angle, no scour is observed at this distance under both flow depth and flow velocity conditions, indicating optimal protection of the abutment. This suggests that placing the dike closer to the abutment enhances its ability to shield the structure from the direct impact of the flow.

In contrast, the 60° dike angle, while still providing a considerable reduction in scour depth, is less effective than the 90° angle. The scour depths for the 60° angle are consistently higher across all conditions, indicating that as the dike angle decreases, its ability to reduce scour diminishes. This trend is even more noticeable for the 45° dike angle, which shows the highest scour depths, particularly in rough-covered conditions. The 45° angle's reduced effectiveness can be attributed to its less favourable orientation relative to the flow, which likely results in less efficient deflection and more direct impact on the abutment.

The findings provide significant practical implications for hydraulic engineering and the design of protective structures around abutments. The clear superiority of the 90° dike angle suggests that this configuration should be preferred in design practices to maximize scour protection. Additionally, placing the dike closer to the abutment (at around 25 cm) offers the best protection, effectively mitigating the erosive forces and preventing the formation of deep scour holes. By optimizing both the angle and placement of spur dikes, engineers can enhance the longevity and stability of hydraulic structures, reducing maintenance costs and improving safety.

Table 5. 3:Comparison of maximum scour depth around abutment with different alignment angles of protective spur dike, flow depth=22cm

Dike Angle	Distance from Dik (cm)	Flow Depth (cm)	Velocity (cm/s)	Maximum Scour Depth (cm)		
				Open Flow	Smooth-covered	Rough-covered
90	50	22	14	0.2	0.71	1.47
90	50	22	28	0.21	1.1	1.84
60	50	22	14	0.52	1	1.15
60	50	22	28	0.79	1.65	1.95
45	50	22	14	1.03	1.13	3
45	50	22	28	0.32	1.85	5.2
90	25	22	14	0	0	0
90	25	22	28	0	0	0

Table 5. 4:Comparison of maximum scour depth around abutment with different alignment angles of protective spur dike, flow velocity=28 cm/s

Dike Angle	Distance from Dik (cm)	Flow Depth (cm)	Velocity (cm/s)	Maximum Scour Depth (cm)		
				Open Flow	Smooth-covered	Rough-covered
90	50	11	28	0.2	1.54	2.9
90	50	22	28	0.21	1.1	1.84
60	50	11	28	0.8	1.72	2.5
60	50	22	28	0.79	1.65	1.95
45	50	11	28	0.58	2.73	6.1
45	50	22	28	0.32	1.85	5.2
90	25	11	28	0	0	0
90	25	22	28	0	0	0

5.3.5 Quantitative Analysis of Maximum Scour Depth Around Abutments with Protective Spur Dikes under Ice-Covered Conditions

Quantitative descriptions of the maximum scour depth around the in-stream infrastructures are essential in hydraulic studies. The empirical formulas enable engineers and researchers to design hydraulic structures more efficiently and provide a means to predict outcomes based on observed data. This predictive capability simplifies the estimation of critical parameters, such as maximum scour depth under various conditions, including ice-covered flow conditions. In the context of this study, the empirical formula allows for estimating the maximum scour depth around abutments under different layouts of the protective spur dikes, flow conditions, grain sizes of bed material, and ice cover roughness. The following parameters, which influence the maximum depth of scour holes (Ymax) around the abutments in the presence of both ice cover on the water surface and a protective spur dike located upstream of the abutments, are considered in this study:

$$Y_{max}=f\,(H,\ V,\ L_e,\ B,\ D_{50},\ n_i,\ n_b,\ sin\theta,\ D) \tag{1}$$

Where, H is the depth of the approaching flow; V is the mean velocity of the approaching flow; Le is the effective length of the spur dike, measured distance from the dike tip to the attached sidewall; B is the channel width; D_{50} is the median particle size of the bed material; ni is the roughness coefficient of an ice cover; nb is the roughness coefficient of the channel bed, $sin\theta$ is alignment angle of spur dikes, D is the space between dike and aboutment.

To accurately evaluate the influence of each parameter on the maximum depth of scour holes around the abutment and to provide a more detailed representation of laboratory results, the key parameters are expressed as dimensionless variables as follows:

$$\frac{Y_{max}}{H} = f\left(F_r, \frac{L_e}{B}, \frac{D_{50}}{H}, \frac{n_i}{n_b}, \sin\theta, \left(\frac{D}{H}\right)\right) \tag{2}$$

Regarding the roughness of ice cover (ni), the Manning roughness coefficient for model smooth ice cover (smooth Styrofoam panel) can be treated as a smooth concrete-like surface with the Manning's roughness coefficient of 0.013 (Mays, 1999; Namaee & Sui, 2019a). The following equation suggested by Li (2012) can be used to determine Manning's roughness coefficient for the model rough ice cover:

$$\mathrm{k_s} = 30\,\mathrm{y_i}\exp[-(1 - \mathrm{v_i}/\mathrm{v_{max}})] \tag{3}$$

where, yi is the thickness of the ice-affected layer, vi is the averaged velocity of the ice-affected layer, v_{max} is the maximum velocity of the velocity profile.

$$n_i = 0.039\, \mathrm{k}_s^{1/6} \tag{4}$$

where, ks is the average roughness height of the ice underside in meters.

By using the above equation, Manning's coefficient of 0.02 has been determined for the rough ice cover. This value also agrees with the results of Wu et al. (2015). To calculate channel bed roughness coefficient (nb) for non-uniform sand bed, the following equation proposed by Hager (1999) was used:

$$n_i = 0.039\, \mathrm{k}_s^{1/6} \tag{4}$$

In this study, the roughness coefficient of the sand bed was determined to be 0.0113 for a sand bed of D50=0.60 mm and 0.012 for a sand bed of D50=0.90 mm, respectively.

$$n_b = 0.039\, D_{50}^{1/6} \tag{5}$$

From the laboratory experiment data, an equation has been developed to predict the maximum depth of scour holes around an abutment with a protective spur dike under ice-covered flow conditions. Under open flow conditions, however, because the scour holes around the abutment were minimal and negligible, it is difficult to derive an equation for determining the maximum depth of scour holes under open flow conditions. Also, to ensure the safety of in-stream infrastructures, including bridge abutments, engineers should consider the worst scenarios in practice, namely, the maximum depth of scour holes. Thus, the following expression has been derived based on data from laboratory experiments for calculating the maximum depth of scour holes around an abutment with a protective spur dike under ice-covered flow conditions:

$$\frac{Y_{max}}{H} = 0.27\,(F_r)^{0.31}\left(\frac{L_e}{B}\right)^{-0.44}\left(\frac{D_{50}}{H}\right)^{-0.4}\left(\frac{n_i}{n_b}\right)^{0.59}(\sin\theta)^{-1.18}\left(\frac{D}{H}\right)^{0.81} \qquad R^2 = 0.851 \tag{6}$$

The exponent 0.31 indicates a less-than-linear relationship, implying that doubling the Froude number will increase $\frac{Y_{max}}{H}$ ratio by approximately 23%, suggesting that more energetic flow conditions (higher Froude number) lead to a greater maximum scour depth. Since the Froude number describes the approach velocity and flow depth, this implies that increasing velocity while decreasing water depth leads to larger and deeper scour holes at the abutment.

The $\frac{L_e}{B}$, representing the blockage ratio of a spur dike, has an exponent of -0.44, indicating a considerable negative correlation. As $\frac{L_e}{B}$ increases, the dike significantly obstructs water flow, reducing turbulence kinetic energy and consequently decreasing the size and depth of the scour hole at the abutment. The magnitude of this exponent suggests an inverse effect on maximum scour depth. Doubling the blockage ratio results in an approximate 28% decrease in the $\frac{Y_{max}}{H}$ ratio.

The $\frac{D_{50}}{H}$ ratio, which normalizes the median grain size of sediment (D_{50}) by water height (H), has an exponent of -0.4. This indicates an inverse relationship between median particle size and maximum scour depth ($\frac{Y_{max}}{H}$). An exponent of -0.4 suggests a nearly linear inverse relationship, where doubling the median particle size results in approximately a 34% decrease in $\frac{Y_{max}}{H}$. This reflects a moderate effect, as larger particles resist scouring more effectively, thereby reducing the depth of the scour hole.

The $\frac{n_i}{n_b}$, representing the roughness coefficient of ice cover relative to the riverbed, has an exponent of 0.59, indicating a positive correlation. As the roughness coefficient of ice cover increases, the maximum velocity approaches the riverbed, deepening the scour hole. The high exponent implies that ice cover roughness significantly influences local scour, regardless of the protective dike. Doubling $\frac{n_i}{n_b}$ results in an approximate 50% increase in the $\frac{Y_{max}}{H}$ ratio.

The $\sin\theta$ exponent is -1.18, indicating a strong negative correlation. As $\sin\theta$ increases, it provides more protection against turbulence flow and erosive vortex system, thus significantly reducing the size and depth of scour at the abutment. The large magnitude of this exponent indicates that the sine of the spur dike angle has the most substantial negative impact on local scour at the abutment. Doubling $\sin\theta$ results in an approximate 55% decrease in the $\frac{Y_{max}}{H}$ ratio. This highlights the critical role of flow direction or the orientation of the spur dike in controlling scour processes at the abutment.

$\frac{D}{H}$ has one of the most substantial positive effects on Y_{max} among all the variables in the formula. Its large exponent of 0.81 indicates that variations in the distance between the dike and abutment can lead to significant changes in maximum scour depth, making it a critical factor in determining the extent of scouring. Doubling the $\frac{D}{H}$ ratio results in an approximate 75% increase in $\frac{Y_{max}}{H}$. This shows that $\frac{D}{H}$ is one of the most influential variables in determining the maximum scour depth at abutment. Compared to other variables, the space ratio ($\frac{D}{H}$) plays a more dominant role in increasing scour depth, surpassing factors such as the Froude number, sediment size, and blockage ratio. The only variable that rivals the space ratio in its influence on Y_{max} is $\sin\theta$, which exerts an opposite effect.

Figure 5.10 shows a strong agreement between the results calculated using the proposed equation and those of laboratory experiments, confirming the accuracy and validity of the formula.

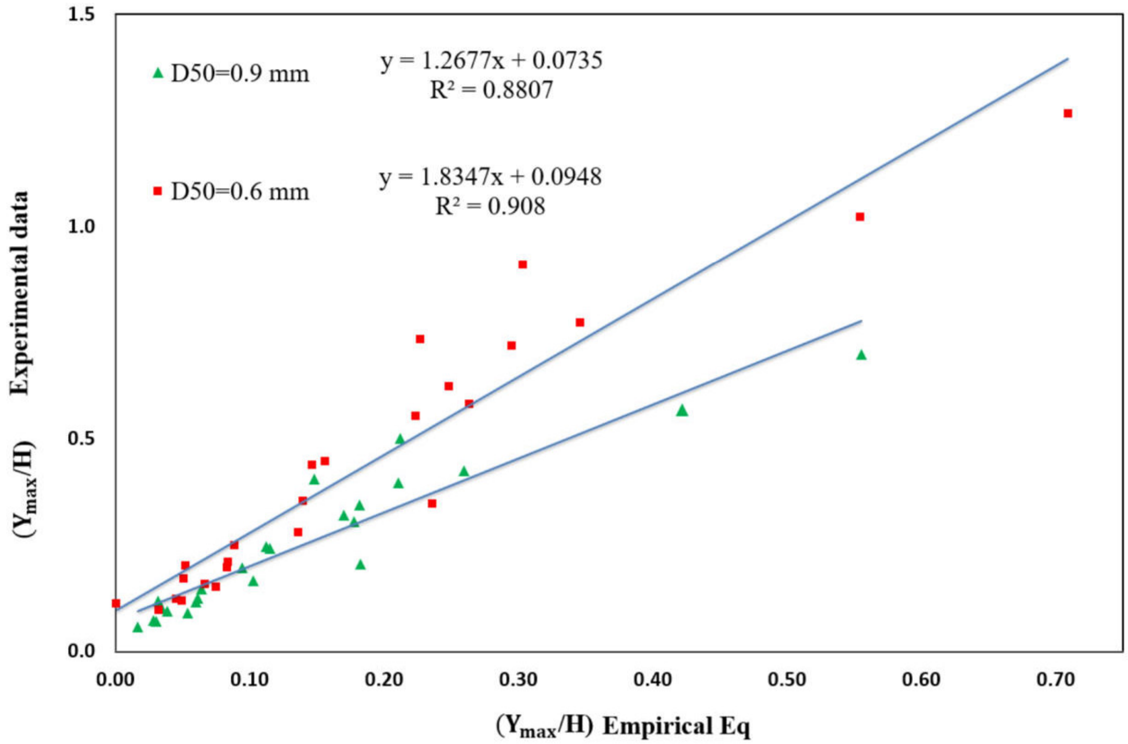

Figure 5. 10:Comparison of calculated maximum scour depth around the abutments with a protective spur dike to those of experiments under ice-covered flow conditions

Understanding the dependence of the relative maximum depth of the scour holes (Y_{max}/H) on the above-mentioned dimensionless variables provides engineers with in-depth knowledge in designing in-stream infrastructures considering the impact of ice cover on the water surface. The formula derived in this study can be used to predict how the maximum depth of the scour hole will be affected by changing flow conditions, shape and dimension of structure design, as well as the characteristics of bed material, such as grain size of sediment. By identifying the most influential variables, resources can be allocated more effectively, focusing on controlling or measuring the most critical variables, thereby facilitating better in-stream infrastructure design.

5.4 Conclusions

In this section, a comprehensive study has been conducted to investigate the effects of various flow conditions and surface cover conditions on the scouring processes around the abutments and the protective efficacy of different spur dike configurations. The results underscore the complex interplay between flow dynamics, vortex formation, and channel bed deformation mechanisms in shaping scour holes and deposition dunes. The key findings are as follows.

1. **Scour Initiation and Development at the abutment**:
    - Under open flow conditions, scouring was initiated at the upstream corner of the abutment due to intensified flow dynamics and the formation of a robust horseshoe vortex. This initial scour gradually expanded downstream, forming a semi-circular scour hole and indicating the critical role of flow dynamics in sediment transport mechanisms.
    - Under both smooth and rough ice-covered flow conditions, the presence of an ice cover significantly influenced the scour hole patterns, typically enlarging and deepening the scour holes. The presence of rough ice cover led to faster and more extensive development of scour holes around the abutment, highlighting the substantial impact of the ice cover roughness on scouring processes around the abutment.

2. **Application of Spur Dike and the Effects of dike alignment angle**:
    - A 90^{o} alignment dike positioned 25 cm upstream of the abutment proved to be the most effective configuration in preventing local scour around the abutments under

different flow and water surface cover conditions. This configuration successfully redirected the rapid flow, created a tranquil zone downstream of the abutment, and diminished the erosive impact of the vortex system. Even under rough ice-covered conditions, the shear stress remained below the critical threshold required to remove sediment from the channel bed, thereby preventing the development of scour holes around the abutment.

- The 90°-alignment dike positioned 50 cm upstream of the abutment effectively redirected river flow, minimizing the direct impact on the abutment. This configuration consistently reduced local scour around the abutment regardless of water surface cover conditions. Scour holes remained small and did not compromise the abutment safety, even under higher flow velocities and lower flow depths. Overall, this setup effectively mitigated the local scour and ensured the stability of the abutment.
- The 60°-alignment dike influenced scour dynamics under both low and high approaching flow velocities. The low velocities resulted in the formation of deposition dunes close to the upstream side of the abutment, serving as protective barriers and effectively preventing scouring at the upstream side of the abutment. Scour at the downstream corner of the abutment remained evident but relatively minor, showcasing the dike's effectiveness in reducing overall scour impact. The high velocities caused notable scouring at the abutment corners, with the greater depth and area of the scour holes at the downstream corner. Despite the increased scouring, the dike provided substantial protection against local scour surrounding the abutment. Overall, the presence of the 60°-alignment dike successfully

redirected the erosive forces and facilitated the development of protective deposition dunes, ensuring the stability of the abutment and reducing the risk of structural damage.

- The impact of the 45º-alignment dike on scour dynamics varied significantly with respect to the magnitudes of the approaching flow velocities. At low velocities, the dike effectively minimized the scouring process at the upstream corner of the abutment. Scouring was consistently observed at the downstream corner of the abutment, with the extension of the scour hole to the upstream corner of the abutment under rough cover scenarios. In contrast, high approaching flow velocities caused significant local scour downstream of the abutment. Sediment deposition patterns were altered, with deposition dunes forming closer to and sometimes accumulated in front of the abutment, providing partial protection. However, the presence of a rough ice cover led to more pronounced local scour at the abutment's upstream corner and frontal side. Overall, the 45º-alignment dike mitigated scour at low velocities by maintaining a stable erosion pattern and forming protective deposition dunes. However, at high flow velocities, increased erosive forces required further considerations to prevent structural impact on the abutment.
- The spur dikes significantly reduced local scour and erosion around the abutments. The presence of a dike created a relatively tranquil zone between the abutment and the dike, reducing kinematic energy downstream and diminishing shear stress levels. This effective disruption of rapid flow resulted in a smaller-scale scour zone compared to an unaffected area by the dike.

3. **Sediment Deposition Patterns**:
    - Deposition dunes formed downstream of the abutments varied with water surface cover conditions and flow characteristics. Under rough-covered flow conditions, deposition dunes extended closer to the abutments, providing additional protection against the erosive eddies and local scour. These patterns underscore the importance of considering water surface cover conditions in sediment management strategies.
    - The highest points of deposition dunes often occurred near the abutment's frontal face, enhancing protection against localized erosion. This finding highlights the role of sediment deposition in mitigating the impact of erosive forces on the abutments.
4. **Ice Cover and Surface Roughness**:
    - The presence of an ice cover on the water surface leads to an increase in the roughness coefficient and notably amplifies the erosive forces of the vortex system, particularly the horseshoe vortex. The rough ice cover shifts the maximum velocity closer to the channel bed, elevating shear stress levels and causing significant enlargement of the scour hole. The result highlights the critical influence of the ice cover roughness on the flow dynamics and sediment transport.
    - A reduction of flow depth under an ice cover intensified the formation of robust horseshoe vortices, generating deeper scour holes. Higher approaching flow velocities further increased the kinematic energy around the abutment, enlarging the scour hole downstream of the abutment and towards the channel bank. These

findings emphasize the need to consider water surface cover conditions and flow characteristics in designing effective scour protection measures.

5. **Influence of Flow Depth and Velocity**:
    - Both flow depth and approaching flow velocity significantly impacted the size and shape of scour holes. Lower flow depths generally led to deeper scour holes, while higher velocities expanded the scour hole dimensions. This relationship underscores the critical role of hydraulic conditions in shaping scour patterns.
    - The interplay between flow depth and velocity influenced the extent of sediment deposition and the development of vortex systems around the abutments. Higher velocities and lower flow depths intensified the erosive forces, leading to more significant scour and sediment displacement.

Overall, the study presented in this section highlights the importance of the flow dynamics and water surface cover conditions in designing effective measures to prevent local scour around the abutment. The findings provide valuable insights for optimizing spur dike configurations to mitigate local scour around the downstream abutment and enhance the structural integrity of hydraulic structures. By understanding the complex interactions between hydraulic factors, sediment transport mechanisms, and structural features, engineers can develop more robust and practical solutions to protect infrastructure from the erosive forces of flowing water and local scour.

5.5 Bibliography

Arneson, L. (2013). *Evaluating scour at bridges*.

Basser, H., Karami, H., Shamshirband, S., Jahangirzadeh, A., Akib, S., & Saboohi, H. (2014). Predicting optimum parameters of a protective spur dike using soft computing methodologies–A comparative study. *Computers & Fluids*, *97*, 168-176.

Beg, M., & Beg, S. (2013). Scour reduction around bridge piers: A review. *International Journal of Engineering Inventions*, *2*(7), 7-15.

Briaud, J.-L., Hurlebaus, S., Chang, K.-A., Yao, C., Sharma, H., Yu, O.-Y., Darby, C., Hunt, B. E., & Price, G. R. (2011). *Realtime monitoring of bridge scour using remote monitoring technology*.

Brice, J., Blodgett, J., Carpenter, P., Cook, M., Craig Jr, G., Eckhardt, D., Hines, M., Lindskov, K., Moore, D., & Parker, R. (1978). *Countermeasures for Hydraulic Problems at Bridges, Volume 1—Analysis and Assessment: Washington, DC*.

Chiew, Y.-M. (1992). Scour protection at bridge piers. *Journal of Hydraulic Engineering*, *118*(9), 1260-1269.

Dargahi, B. (1990). Controlling mechanism of local scouring. *Journal of Hydraulic Engineering*, *116*(10), 1197-1214.

Deng, L., & Cai, C. (2010). Bridge scour: Prediction, modeling, monitoring, and countermeasures. *Practice periodical on structural design and construction*, *15*(2), 125-134.

Dey, S., & Raikar, R. V. (2007). Characteristics of horseshoe vortex in developing scour holes at piers. *Journal of Hydraulic Engineering*, *133*(4), 399-413.

Duan, J. G., & Nanda, S. (2006). Two-dimensional depth-averaged model simulation of suspended sediment concentration distribution in a groyne field. *Journal of Hydrology*, *327*(3-4), 426-437.

Esmaeli, P., Boudaghpour, S., Rostami, M., & Mirzaee, M. (2022). Experimental investigation of permeability and length of a series of spur dikes effects on the control of bank erosion in the meandering channel. *Ain Shams Engineering Journal*, *13*(4), 101701.

Ettema, R., Melville, B. W., & Barkdoll, B. (1998). Scale effect in pier-scour experiments. *Journal of Hydraulic Engineering*, *124*(6), 639-642.

Fang, D., Sui, J., Thring, R. W., & Zhang, H. (2006). Impacts of dimension and slope of submerged spur dikes on local scour processes- an experimental study. *International Journal of Sediment Research*, *21*(2), 89-100.

Fotherby, L. M., & Randle, T. J. (2007). SedVeg-Gen3 Platte River model: a sediment transport and riparian vegetation model. World Environmental and Water Resources Congress 2007: Restoring Our Natural Habitat,

Gupta, A., & Gangadharaiah, T. (1992). Local scour reduction by a delta wing-like passive device. Proceeding of 8th Congress of Asia & Pacific Reg. Div,

Haltigin, T. W., Biron, P. M., & Lapointe, M. F. (2007). Predicting equilibrium scour-hole geometry near angled stream deflectors using a three-dimensional numerical flow model. *Journal of Hydraulic Engineering*, *133*(8), 983-988.

Heibaum, M., & Trentmann, J. (2010). Partial grouted riprap for enhanced scour resistance. In *Scour and Erosion* (pp. 1-10).

Ishigaki, T., Baba, Y., & Muto, Y. (2000). Vortex motion around a plate with footing in open channel flow and its effect on local scouring. *Advances in Hydro Science and-Engineering*, *4*, 169-176.

Jafari, R., & Sui, J. (2021). Velocity Field and Turbulence Structure around Spur Dikes with Different Angles of Orientation under Ice Covered Flow Conditions. *Water*, *13*(13), 1844.

Karami, H., Ardeshir, A., Behzadian, K., & Ghodsian, M. (2011). Protective spur dike for scour mitigation of existing spur dikes. *Journal of Hydraulic Research*, *49*(6), 809-813.

Kehe, S. M. (1984). *Streambank Protection by Use of Spur Dikes*. Oregon State University.

Kuhnle, R. A., Alonso, C. V., & Shields, F. D. (1999). Geometry of scour holes associated with 90 spur dikes. *Journal of Hydraulic Engineering*, *125*(9), 972-978.

Lagasse, P. F. (2007). *Countermeasures to protect bridge piers from scour* (Vol. 593). Transportation Research Board.

Li, H., Kuhnle, R., & Barkdoll, B. D. (2005). Spur dikes as an abutment scour countermeasure. In *Impacts of Global Climate Change* (pp. 1-12).

Manual, S.-I. S. U. s. (2017). SonTek-IQ Series Intelligent Flow Featuring Smart Pulse HD User's Manual [User's Manual]. *Xylem brand*, *SmartPulse HD*

User's Manual(Firmware Version 3.0), 135. https://doi.org/SonTek-IQ Series

Intelligent Flow (Xylem Inc)

Markovic, M. (2012). Multi criteria analysis of hydraulic structures for river training works. *Water Resources Management*, *26*(13), 3893-3906.

Melville, B. W., & Coleman, S. E. (2000). *Bridge scour*. Water Resources Publication.

Namaee, M., & Sui, J. (2019). Local scour around two side-by-side cylindrical bridge piers under ice-covered conditions. *International Journal of Sediment Research*, *34*(4), 355-367.

Nazari, A., Mccorquodale, J., & Solari, L. (2017). Numerical study on the effect of the spur dikes on sedimentation pattern. *Ain Shams Engineering Journal*. https://doi.org/http://creativecommons.org/licenses/by-nc-nd/4.0/. 10.1016/j.asej.2017.02.007.

Pandey, M., Karbasi, M., Jamei, M., Malik, A., & Pu, J. H. (2023). A comprehensive experimental and computational investigation on estimation of scour depth at bridge abutment: emerging ensemble intelligent systems. *Water Resources Management*, *37*(9), 3745-3767.

Pizarro, A., Manfreda, S., & Tubaldi, E. (2020). The science behind scour at bridge foundations: A review. *Water*, *12*(2), 374.

Rajaratnam, N., & Nwachukwu, B. (1983). Erosion near groyne-like structures. *Journal of Hydraulic Research*, *21*(4), 277-287.

Richardson, E. V., & Davis, S. R. (1995). *Evaluating scour at bridges*.

Sadat, S. H. (2015). *MODIFICATION OF SPUR-DIKE WITH FOOTING OR PILE-GROUP TO STABILIZE RIVER MORPHOLOGY AND REDUCE LOCAL SCOUR* [Dissertation, Nagoya Institute of Technology]. http://doi.org/10.20602/00003162

Saneie, M. (2011). Experimental study on effect of minor spur dike to reduce main spur dike scouring. *Watershed Engineering and Management*, *3*(3), 140-148.

Shields Jr, F. D., Bowie, A., & Cooper, C. (1995). CONTROL OF STREAMBANK EROSION DUE TO BED DEGRADATION WITH VEGETATION AND STRUCTURE 1. *JAWRA Journal of the American Water Resources Association*, *31*(3), 475-489.

Sui, J., Hicks, F. E., & Menounos, B. (2006). Observations of riverbed scour under a developing hanging ice dam. *Canadian Journal of Civil Engineering*, *33*(2), 214-218.

Vaghefi, M., Solati, S., & Abdi Chooplou, C. (2021). The effect of upstream T-shaped spur dike on reducing the amount of scouring around downstream bridge pier located at a 180 sharp bend. *International journal of river basin management*, *19*(3), 307-318.

Wang, C., Yu, X., & Liang, F. (2017). A review of bridge scour: mechanism, estimation, monitoring and countermeasures. *Natural Hazards*, *87*, 1881-1906.

Wörman, A. (1989). Riprap protection without filter layers. *Journal of Hydraulic Engineering*, *115*(12), 1615-1630.

Zarrati, A., Nazariha, M., & Mashahir, M. (2006). Reduction of local scour in the vicinity of bridge pier groups using collars and riprap. *Journal of Hydraulic Engineering*, *132*(2), 154-162.

Zdravkovic, S. K., & Tsiampousi, A. (2023). International society for soil mechanics and geotechnical engineering.

6 CHAPTER SIX: General Conclusions

6.1 Conclusions of Chapter 3

This chapter explores the complex interactions between spur dikes, ice cover, and flow dynamics. The research aims to understand how different spur dike orientation angles and varying ice cover conditions influence velocity fields, turbulence structures, and local scour patterns.

6.1.1 Impact of Ice Cover on Flow Dynamics

A significant aspect of this study is the analysis of how ice cover affects the flow characteristics around spur dikes. The presence of ice cover introduces an additional boundary layer, fundamentally altering the velocity profile and increasing the complexity of the flow. Key observations include:

- Turbulence Intensities: The presence of ice cover significantly increases turbulence intensities. For smooth ice cover, turbulence intensities increased by approximately 10%, while rough ice cover increased by up to 30%. This rise in turbulence intensity is attributed to the added roughness and friction from the ice cover, which enhances velocity fluctuations and shear stress near the riverbed.
- Velocity Components: The experiments revealed that the maximum values of the 3D velocity components (streamwise, lateral, and vertical) are significantly influenced by the presence and roughness of the ice cover. The rough ice cover increases the magnitude of these velocity components and shifts their maximum values closer to the riverbed. This shift is critical as it results in higher shear stress at the sand bed, leading to more extensive sediment movement and deeper scour holes.

6.1.2 Orientation Angle of Spur Dikes

The study meticulously examines spur dikes set at different orientation angles (90°, 60°, and 45°) relative to the flow direction. The orientation angle of the spur dike significantly affects flow separation, vortex formation, and subsequent scour patterns:

- At 90° Orientation, the spur dike oriented perpendicular to the flow generates the most pronounced flow separation, forming strong horseshoe vortices at the upstream face of the dike. These vortices play a significant role in sediment entrainment and transport. Moreover, this configuration exhibits the highest turbulence intensity and bed shear stress. The strong downflows and powerful vortices create deep scour holes closely downstream of the dike. The perpendicular orientation results in the deepest scour holes, with a significant increase in scour depth due to the enhanced flow blockage and increased energy dissipation around the dike.
- At 60°, the vortices generated are less intense compared to the 90° orientation. Flow separation occurs, but the reduced angle allows a smoother flow transition around the dike. The turbulence intensity and bed shear stress are moderate, leading to less severe scour than the perpendicular orientation. This angle provides a balance between flow disruption and sediment transport. The scour holes formed are shallower than those at 90°, indicating reduced sediment transport capacity and erosion potential.
- The 45° orientation angle results in the least flow disruption, as the dike aligns more closely with the natural flow direction. This reduces the formation of strong vortices and minimizes turbulence. The turbulence intensity and bed shear stress are significantly lower, creating a more stable flow regime around the dike. The reduced blockage ratio allows for smoother flow and less aggressive sediment transport. The shallowest scour holes are observed at this angle, with a 5% to 10% reduction in scour depth for each 10° decrease from 90°. This

demonstrates the direct correlation between orientation angle and scour depth, highlighting the importance of angle optimization in dike design.

The orientation angle of spur dikes significantly influences the hydraulic and sediment transport characteristics in rivers. By carefully selecting and optimizing the orientation angle, engineers can enhance the effectiveness of spur dikes in river management. Engineers must consider these effects when designing spur dikes to achieve optimal performance. For instance, a 90° orientation might be suitable for applications requiring significant flow diversion and sediment entrainment, whereas a 45° orientation could be preferred for minimizing erosion and maintaining flow stability.

6.1.3 Analysis of Velocity Components

The study presents a comprehensive analysis of the three-dimensional (3D) velocity components, streamwise (Ux), lateral (Uy), and vertical (Uz), around spur dikes with different orientation angles under various flow conditions, including the presence of ice cover. Key findings include:

- Streamwise Velocity (Ux): Ux exhibits the highest magnitude among the three velocity components, highlighting its dominant role in flow dynamics. The streamwise velocity is generally lower inside the scour hole than in regions outside the hole, but it shows significant fluctuation, especially near the dike tip. Furthermore, the presence of an ice cover increases the maximum values of Ux by approximately 10% to 25%, depending on the roughness of the ice. Rough ice cover, in particular, enhances the velocity fluctuations, shifting the location of maximum velocity closer to the riverbed, thereby increasing bed shear stress and sediment transport potential. Under different surface conditions, the streamwise velocity profile inside the scour hole displays a convex shape, with the minimum velocity at the bottom of the scour hole and increasing towards the mid-water depth.

- Lateral Velocity (Uy): Uy demonstrates high variability and irregularities in its vertical distribution, making it less predictable than Ux. The values of Uy are generally smaller than Ux but can be significantly influenced by surface conditions. The presence of ice cover, particularly rough ice, increases the magnitude of Uy. This indicates that ice cover not only affects the primary flow direction but also induces substantial lateral flow variations, which can enhance lateral sediment transport and impact bank stability. Unlike Ux, the vertical distribution of Uy does not follow a consistent trend across different experimental conditions. However, Uy is observed to be mostly positive inside and outside the scour hole, indicating a net lateral movement of water.
- Vertical Velocity (Uz): Uz is typically negative inside and outside the scour holes, signifying strong downflow around the spur dike. This downflow contributes to the formation and deepening of scour holes by enhancing sediment entrainment from the bed. Ice cover significantly modifies the vertical velocity distribution. The presence of an ice cover, especially with higher roughness, increases the magnitude of Uz, bringing the maximum vertical velocity closer to the bed. This results in higher sediment transport rates and deeper scour holes. The vertical velocity profile exhibits a parabolic shape, with the minimum Uz value at the bottom of the scour hole and increasing towards the original sand bed level before reducing again towards the water surface. This pattern reflects the complex interaction between downflow and the horseshoe vortex system around the spur dike.

By analyzing the velocity components, engineers can optimize the orientation angle and structural design of spur dikes to minimize adverse scour effects and enhance stability. Insights into the vertical and lateral velocity components help develop better sediment management strategies, ensure balanced sediment transport, and reduce the risk of excessive erosion or deposition.

6.1.4 Turbulence Intensities and Reynolds Shear Stress

This section delves into the intricate details of turbulence intensities and Reynolds shear stress as observed in the study, providing insights into their implications for river engineering and management.

- Spatial Distribution and Ice Cover: The highest turbulence intensities were observed near the spur dike tip and just above the scour hole, where the interaction between the flow and the structure is most intense. The turbulence intensity profiles exhibited a distinct pattern, with streamwise turbulence (ux') being the largest, followed by lateral (uy') and vertical (uz') turbulence components, indicating a hierarchy of turbulence strength. The presence of ice cover significantly increased turbulence intensities. Smooth ice cover raised turbulence intensities by approximately 15%, while rough ice cover increased by up to 30%. Also, the roughness of the ice cover amplified the velocity fluctuations, enhancing the energy dissipation and mixing within the flow. This increase in turbulence intensities directly impacts sediment transport and scour processes.
- Flow Rate and Dike Orientation: Higher flow rates were associated with increased turbulence intensities. The study found that with a higher approach velocity, the maximum depth of the scour hole was achieved in a shorter time, and the scour hole became larger. The orientation angle of the spur dike also influenced turbulence intensities. A 90° orientation generated the strongest turbulence, while decreasing the angle to 45° resulted in reduced turbulence intensity, corresponding to a decrease in scour depth.

- Reynolds Shear Stress: Inside the scour holes, Reynolds shear stress was found to be negative, indicating upward vertical momentum transport caused by a negative velocity gradient. This phenomenon is critical for sediment entrainment from the bed. The Shear stress reached its maximum slightly above the scour hole, aligning with the initial level of the sand bed, and then decreased towards the flow surface, forming a parabolic distribution. Ice cover, especially rough ice, increased the absolute value of Reynolds shear stress. This enhancement in shear stress is attributed to the increased velocity fluctuations and turbulence intensities induced by the ice cover. The ice cover created higher shear stress at the bed, resulting in more pronounced sediment movement and deeper scour holes. Rough ice cover, in particular, intensified these effects, highlighting the importance of considering ice conditions in hydraulic design. Higher flow rates corresponded to increased Reynolds shear stress, indicating a stronger momentum transfer and greater potential for sediment entrainment. The orientation angle of the spur dike significantly affected the distribution and magnitude of Reynolds shear stress. A perpendicular orientation (90°) resulted in the highest shear stress, while a smaller angle (45°) reduced the shear stress, contributing to a decrease in scour depth and turbulence intensity.
- These findings provide a scientific basis for improving the design and performance of spur dikes, contributing to more sustainable and resilient river management practices. Engineers can optimize spur dike orientation and design parameters to effectively manage turbulence and shear stress, minimizing adverse scour effects and ensuring structural stability. Insights into turbulence and shear stress dynamics facilitate better sediment management practices, enabling the control of sediment transport and deposition in river systems, particularly in regions with seasonal ice cover. By accounting for the increased turbulence and shear stress

under ice-covered conditions, hydraulic structures can be designed to withstand enhanced erosive forces, reducing the risk of structural failure and environmental impact.

6.2 Conclusions of Chapter 4

6.2.1 Scour Hole Geometry and Influence of Ice Cover

The presence of ice cover on the water surface significantly altered the geometry of the scour holes. Under open channel conditions, scour holes around the dike exhibited a more circular shape. However, under ice-covered conditions, especially rough ice, the scour holes expanded laterally and became more elliptical. This indicates that the roughness of the ice cover intensifies the scour process, leading to a wider and deeper scour hole. The rough ice cover, simulating ice jams, led to increased turbulence and stronger vortex formation, exacerbating bed deformation.

The alignment angle of the spur dike greatly influenced the extent of scour holes. When the dike angle was reduced from 90º to 60º, the upstream length of the scour hole decreased by approximately 60%. This reduction in dike angle led to a decrease in the intensity of vortices and, consequently, less scouring in the upstream direction. Conversely, the downstream length of the scour hole increased by 20% with a 50% increase in flow rate, indicating that higher flow rates enhance downstream erosion due to increased flow velocity and turbulence.

6.2.2 Impact of Dike Alignment Angle

The dike alignment angle was found to be a crucial factor in vortex formation and strength. At a 90º alignment angle, the primary vortices were more substantial and lasted longer, causing deeper and more extensive scour holes. As the dike alignment angle decreased, the primary vortices became less intense, resulting in less severe scouring. The study also found that reducing the dike alignment angle from 90º to 45º transformed the shape of the scour hole from semi-circular to elliptical, indicating a significant change in flow patterns and bed erosion dynamics.

The dike alignment angle influenced the dike tip's flow acceleration and the downflow creation. A 90º dike caused a more substantial flow contraction and separation, increasing flow velocity at the dike tip by up to 60% of the approaching flow velocity. This increased velocity led to stronger downflow and more severe scouring at the dike toe. Reducing the dike alignment angle mitigated these effects, leading to less intense scouring and a shift in the location of maximum scour depth downstream.

6.2.3 Effect of Flow Conditions

Higher flow velocities and Froude numbers were associated with deeper and wider scour holes. Under high flow conditions, the kinetic energy and turbulence intensity increased, leading to more severe bed erosion. The study found that an increase in flow Froude number by 15% resulted in a 5% to 10% increase in maximum scour depth. Additionally, the impact of flow depth was significant; shallower flows with higher velocities led to more scouring compared to deeper flows with lower velocities.

The median grain size of the bed material (D_{50}) played a significant role in scour dynamics. Finer bed material led to deeper scour holes due to easier entrainment and transport of sediment particles. The study observed increased bed material fineness resulted in larger maximum scour depths regardless of flow surface cover conditions.

6.2.4 Development and Dynamics of Vortex Systems

The formation of primary vortices at the upstream side of the dike toe was a critical factor in initiating local scour. These vortices were influenced by the dike alignment angle and approaching velocity. The secondary vortices, known as horseshoe vortices, developed within the scour hole and were the primary mechanism for ongoing scouring. The study found that under ice-covered conditions, the intensity of these vortices increased, leading to deeper and wider scour holes.

The horseshoe vortices were observed to last the longest and were the major cause of scour hole expansion. The wake vortices, formed in the low-velocity zone downstream of the dike, also contributed to sediment transport and deposition. The interaction between these vortex systems and the flow dynamics around the dike was critical in determining the final shape and size of the scour holes.

6.2.5 Equations for Maximum Scour Depth

The study derived equations to predict the maximum depth of scour holes around spur dikes under open and ice-covered flow conditions. These equations incorporated key parameters such as flow velocity, depth, sediment characteristics, dike alignment angle, and roughness coefficients of the ice cover and riverbed. The derived equations demonstrated high accuracy in predicting scour depths, with significant implications for the design and assessment of in-stream infrastructures.

The study highlighted differences in the impact of flow conditions on scour depths between open and ice-covered scenarios. Under ice-covered conditions, the influence of the flow Froude number was less evident than in open channel conditions. However, the presence of ice cover, particularly rough ice, led to deeper and more extensive scour holes due to increased flow resistance and turbulence. The findings underscore the importance of considering these factors in the design and implementation of hydraulic structures in cold regions. The derived predictive equations provide valuable tools for engineers to anticipate and mitigate the impacts of scour, ensuring the stability and longevity of in-stream infrastructures.

6.3 Conclusions of Chapter 5

6.3.1 Scour at Abutments

Scour initiation was observed at the upstream corner of the abutment due to intensified flow dynamics and the formation of a robust horseshoe vortex. This initial scour gradually expanded in all directions, forming a semi-circular scour hole. Sediment particles dislodged from the scour hole were carried downstream by the vortex system, settling in a low-velocity zone to form deposition dunes. Higher flow velocities resulted in larger scour holes, while variations in water depth showed minimal impact on the scour hole's dimensions.

The presence of an ice cover significantly influenced the scour hole patterns. The ice cover led to the enlargement and deepening of the scour holes, which expanded upstream and downstream, often reaching the river bank within eight hours. The scour holes at both corners of the abutment converged, forming a large scour hole along the frontal side of the abutment. Flow depth and approach velocity had notable effects on the scour hole characteristics, with reduced flow depth resulting in deeper scour holes and higher velocities increasing the scour hole area.

Increasing the roughness coefficient of the ice cover further expanded the scour hole in all dimensions, particularly along the flow direction. The larger scour holes prompted the deposition dunes to shift closer to the abutment, significantly altering the sediment deposition pattern. Reduced flow depth under rough cover conditions led to deeper scour holes, especially at the frontal side of the abutment. Approaching flow velocity influenced the overall enlargement of the scour hole, particularly in higher velocities, which increased the area and depth of the scour hole.

6.3.2 Application of Spur Dikes

- 90º Spur Dike Positioned 25 cm Upstream: This configuration proved the most effective in preventing scour around the abutments. The perpendicular alignment of the dike effectively redirected the rapid flow, creating a tranquil zone downstream and diminishing the erosive impact of the vortex system. Under varying flow conditions and surface covers, this setup consistently prevented scour holes from forming around the abutment.
- 90º Spur Dike Positioned 50 cm Upstream: This alignment effectively reduced local scour under open, smooth, and rough ice cover conditions. The spur dike minimized the direct impact of the flow on the abutment, leading to very small scour holes. The setup proved effective even under higher flow velocities and lower depths.
- 60º Spur Dike: The scour dynamics varied significantly with the flow velocity. At low velocities, sediment deposition dunes formed close to the upstream side of the abutment, serving as protective barriers and effectively preventing scouring at the upstream side. However, scouring at the downstream corner remained evident, though relatively minor. Significant scouring was observed at the abutment corners at high velocities, with the downstream corner exhibiting greater depth and area. Despite the increased scouring, the dike provided substantial protection against local scour surrounding the abutment.
- 45º Spur Dike: The impact of this configuration varied considerably between low and high approach velocities. At low velocities, the dike effectively minimized scouring at the upstream corner of the abutment. However, scouring consistently occurred at the downstream corner, particularly under rough cover scenarios, where the scour hole extended to the upstream corner of the abutment. Significant scouring was observed downstream of the abutment at

high velocities, with sediment deposition patterns altering to provide partial protection. Rough ice cover led to more scouring at the abutment's upstream and frontal corners.

6.3.3 Sediment Deposition Patterns

Sediment deposition patterns downstream of the abutments exhibited significant variability influenced by surface conditions and flow characteristics. In open surface conditions, the deposition dunes were generally located at a greater distance from the abutments. The absence of surface cover resulted in a more dispersed sediment deposition, primarily driven by the less obstructed flow dynamics. The dunes formed under these conditions were typically smaller and positioned further downstream, offering limited abutment protection.

Under smooth cover, the deposition dunes exhibited a downstream expansion pattern. Although the dunes extended closer to the abutments than open surface conditions, they did not achieve the same level of protection as observed under rough cover conditions. The smooth ice cover facilitated a more streamlined flow, leading to less turbulent interaction and a less extensive sediment deposition pattern. The smooth cover facilitated a more uniform flow, influencing the scour hole patterns by enlarging and deepening the holes. The smoother surface reduced the turbulence intensity, leading to less scouring.

In scenarios with rough cover, the sediment deposition dunes extended closer to the abutments, providing additional protection against erosive eddies and local scour. The highest points of the deposition dunes frequently formed near the frontal face of the abutments, creating a natural barrier that enhanced protection against localized erosion. This phenomenon was particularly evident under rough cover conditions, where the increased roughness of the ice cover facilitated the displacement of sediment closer to the abutments. The pyramid-shaped deposition dunes, characteristic of rough cover conditions, underscored the enhanced sediment trapping efficacy due to the intensified interaction between the wake vortex generated by the dike and the horseshoe vortex at the abutments.

6.3.4 Influence of Flow Depth and Velocity

The interplay between flow depth and velocity was a crucial determinant of the scour hole dimensions and sediment deposition patterns around the abutments. Lower flow depths generally result in deeper scour holes due to the concentration of erosive forces in a reduced vertical space. Conversely, higher flow depths tended to disperse the erosive forces over a larger vertical range, resulting in shallower scour holes but larger in the area of the hole. This dispersion reduced the intensity of the shear stress exerted on the bed material, leading to less scouring.

Approach velocity also played a significant role in shaping the scour morphology. Higher velocities increased the flow's kinetic energy, thereby enhancing the erosive potential of the vortex systems around the abutments. This increase in velocity led to larger and deeper scour holes, particularly at the downstream corners of the abutments. The higher velocities also influenced the sediment deposition patterns, promoting the formation of more extensive deposition dunes downstream. In contrast, lower velocities resulted in less scouring and smaller scour holes. The reduced kinetic energy of the flow led to a more controlled sediment transport and deposition process, with smaller and less extensive deposition dunes forming downstream.

6.4 Limitations of this experimental study

The experimental investigations undertaken in this research were subject to certain constraints. Despite implementing various strategies to mitigate these limitations, some were inevitable.

One of the constraints was associated with the Acoustic Doppler Velocimeter (ADV) used in the study. The ADV was unable to capture data from a depth of 10 cm below its transmitter, resulting in the absence of data for the top 10 cm below the water surface. Additionally, the power of the water pump limited the maximum flow rate capacity. The pump could provide a maximum flow rate of 120 litres per second. Moreover, the study employed specific sediment sizes (0.48 mm, 0.60 mm, and 0.90 mm) to simulate riverbed conditions. However, natural riverbeds typically exhibit a wider range of sediment sizes and compositions, potentially affecting scour processes in ways not fully replicated in the experimental conditions.

6.5 Future Directions

Based on the results and conclusions of this experimental study, here are several recommendations for future directions and further study:

1) Extended Field Studies: Conduct field studies in various river environments to validate the experimental findings. Different river conditions, sediment types, and ice cover variations should be considered to ensure the applicability and robustness of the results across diverse natural settings.
2) Long-term Monitoring: Implement long-term monitoring of scour and sediment dynamics around bridge abutments with spur dikes. This will provide insights into the temporal evolution of scour and the long-term effectiveness of different spur dike configurations.

3) Hydrodynamic Modeling: Use advanced hydrodynamic models to simulate the flow conditions and scour patterns observed in experiments. These models can help understand the complex interactions between flow, sediment transport, and spur dike configurations, providing a predictive tool for future designs.
4) Impact of Climate Change: Study the potential impacts of climate change on local scour dynamics. Changes in river flow patterns, ice cover duration, and frequency due to climate change could affect the performance of scour mitigation measures.
5) Integration with Other Mitigation Measures: Explore the integration of spur dikes with other scour mitigation measures, such as riprap, collars, and bed sills. Combining different strategies might provide enhanced protection against scour.
6) Ecological Impact Assessment: Assess the ecological impacts of installing spur dikes in rivers. Studies should focus on how these structures affect local habitats, aquatic life, and overall river health.

By addressing these future directions, researchers can further advance the understanding and effectiveness of scour mitigation techniques, ensuring the stability and safety of bridge abutments in various hydraulic environments.

APPENDIX

Table I. 1:Experimental data and the results of Chapter 4

Sand Size (mm)	Dike Angle	Surface Condition	Water Depth (cm)	Approach velocity (cm/s)	Fr	Le/B	D_{50}/H	n_i/n_b	Sin θ	Scour Max (cm)
0.9	90°	Open	11	29.08633	0.28	0.25	0.009	-	1	11.6
			21	30.1414	0.21	0.25	0.0045	-	1	12.0
			29	21.92688	0.13	0.25	0.003	-	1	8.2
		Smooth	12	28.2097	0.26	0.25	0.009	1.068	1	14.0
			23	27.03777	0.18	0.25	0.0045	1.068	1	14.8
			32	24.8049	0.14	0.25	0.003	1.068	1	10.0
		Rough	10	29.71363	0.3	0.25	0.009	2.46	1	16.3
			22	29.38163	0.2	0.25	0.0045	2.46	1	16.0
			32	26.57668	0.15	0.25	0.003	2.46	1	12.2
	60°	Open	11	25.96993	0.25	0.22	0.009	-	0.86	9.6
			23	33.04617	0.22	0.22	0.0045	-	0.86	13.5
			34	29.22092	0.16	0.22	0.003	-	0.86	8.8
		Smooth	9	21.61143	0.23	0.22	0.009	1.068	0.86	11.5
			21	24.40018	0.17	0.22	0.0045	1.068	0.86	14.5
			32	21.26135	0.12	0.22	0.003	1.068	0.86	10.6
		Rough	11	28.04753	0.27	0.22	0.009	2.46	0.86	14.5
			22	27.91255	0.19	0.22	0.0045	2.46	0.86	15.8
			33	19.79175	0.11	0.22	0.003	2.46	0.86	12.8
	45°	Open	13	27.103	0.24	0.18	0.009	-	0.7	8.3
			24	30.68811	0.2	0.18	0.0045	-	0.7	8.9
			33	23.39025	0.13	0.18	0.003	-	0.7	6.3
		Smooth	11	25.96993	0.25	0.18	0.009	1.068	0.7	10.2
			24	30.68811	0.2	0.18	0.0045	1.068	0.7	11.1
			34	21.91569	0.12	0.18	0.003	1.068	0.7	8.0
		Rough	9	26.30957	0.28	0.18	0.009	2.46	0.7	12.4
			18	29.23435	0.22	0.18	0.0045	2.46	0.7	12.7
			33	23.39025	0.13	0.18	0.003	2.46	0.7	10.2
0.6	90°	Open	12	20.61478	0.19	0.25	0.006	-	1	9.5
			26	23.9559	0.15	0.25	0.003	-	1	12.0
			32	17.71779	0.1	0.25	0.002	-	1	7.2
		Smooth	8	15.06012	0.17	0.25	0.006	1.142	1	11.3
			21	18.65896	0.13	0.25	0.003	1.142	1	14.2
			33	16.19325	0.09	0.25	0.002	1.142	1	9.4

		Rough	12	22.78476	0.21	0.25	0.006	2.636	1	13.5
			24	21.48168	0.14	0.25	0.003	2.636	1	16.7
			36	20.67181	0.11	0.25	0.002	2.636	1	11.7
	60°	**Open**	11	20.77595	0.2	0.22	0.006	-	0.86	8.0
			22	23.5053	0.16	0.22	0.003	-	0.86	9.3
			32	17.71779	0.1	0.22	0.002	-	0.86	6.2
		Smooth	12	16.27483	0.15	0.22	0.006	1.142	0.86	9.8
			23	21.02938	0.14	0.22	0.003	1.142	0.86	11.4
			35	16.67674	0.09	0.22	0.002	1.142	0.86	8.3
		Rough	10	16.83773	0.17	0.22	0.006	2.636	0.86	11.5
			21	21.52957	0.15	0.22	0.003	2.636	0.86	13.8
			34	12.78415	0.07	0.22	0.002	2.636	0.86	10.7
	45°	**Open**	9	16.9133	0.18	0.18	0.006	-	0.7	7.2
			23	24.03358	0.16	0.18	0.003	-	0.7	10.8
			29	16.86683	0.1	0.18	0.002	-	0.7	5.4
		Smooth	11	17.65956	0.17	0.18	0.006	1.142	0.7	8.9
			20	19.61	0.14	0.18	0.003	1.142	0.7	12.6
			32	14.17423	0.08	0.18	0.002	1.142	0.7	7.2
		Rough	11	18.69835	0.18	0.18	0.006	2.636	0.7	10.6
			21	18.65896	0.13	0.18	0.003	2.636	0.7	14.4
			32	14.17423	0.08	0.18	0.002	2.636	0.7	9.6
0.9	**90°**	**Open**	11	28.04753	0.27	0.25	0.009	-	1	12.7
			22	27.91255	0.19	0.25	0.0045	-	1	11.5
			36	26.30957	0.14	0.25	0.003	-	1	8.2
		Smooth	12	27.12471	0.25	0.25	0.009	1.068	1	14.8
			22	29.38163	0.2	0.25	0.0045	1.068	1	13.3
			34	21.91569	0.12	0.25	0.003	1.068	1	10.3
		Rough	7	19.88817	0.24	0.25	0.009	2.46	1	16.5
			17	23.2451	0.18	0.25	0.0045	2.46	1	15.6
			28	18.23082	0.11	0.25	0.003	2.46	1	12.0
0.6	**90°**	**Open**	10	16.83773	0.17	0.25	0.006	-	1	7.5
			20	21.01071	0.15	0.25	0.003	-	1	11.0
			30	17.15517	0.1	0.25	0.002	-	1	7.2
		Smooth	12	16.27483	0.15	0.25	0.006	1.142	1	9.6
			21	20.09427	0.14	0.25	0.003	1.142	1	13.2
			32	15.94601	0.09	0.25	0.002	1.142	1	9.0
		Rough	11	18.69835	0.18	0.25	0.006	2.636	1	11.8
			22	24.97438	0.17	0.25	0.003	2.636	1	15.7
			31	13.951	0.08	0.25	0.002	2.636	1	11.3

0.48	**90°**	**Open**	12	20.61478	0.19	0.25	0.0048	-	1	13.5
			21	20.09427	0.14	0.25	0.0024	-	1	13.8
			30	18.87069	0.11	0.25	0.0016	-	1	14.0
		Smooth	13	22.58584	0.2	0.25	0.0048	1.186	1	14.8
			22	23.5053	0.16	0.25	0.0024	1.186	1	15.4
			34	23.742	0.13	0.25	0.0016	1.186	1	15.7
		Rough	9	19.73218	0.21	0.25	0.0048	2.737	1	16.7
			22	22.03622	0.15	0.25	0.0024	2.737	1	17.5
			31	19.18262	0.11	0.25	0.0016	2.737	1	17.2
	90°	**Open**	8	15.94601	0.18	0.25	0.0048	-	1	11.2
			18	15.94601	0.12	0.25	0.0024	-	1	8.2
			29	16.86683	0.1	0.25	0.0016	-	1	9.1
		Smooth	12	18.4448	0.17	0.25	0.0048	1.186	1	13.1
			22	19.09806	0.13	0.25	0.0024	1.186	1	10.8
			31	15.69487	0.09	0.25	0.0016	1.186	1	10.9
		Rough	25	32.88697	0.21	0.25	0.0048	2.737	1	15.2
			24	23.01608	0.15	0.25	0.0024	2.737	1	12.5
			33	14.394	0.08	0.25	0.0016	2.737	1	12.7
	60°	**Open**	13	25.97371	0.23	0.22	0.0048	-	0.86	14.8
			24	24.55049	0.16	0.22	0.0024	-	0.86	14.2
			36	18.79255	0.1	0.22	0.0016	-	0.86	12.1
		Smooth	11	20.77595	0.2	0.22	0.0048	1.186	0.86	16.4
			22	20.56714	0.14	0.22	0.0024	1.186	0.86	16.2
			32	21.26135	0.12	0.22	0.0016	1.186	0.86	14.5
		Rough	11	24.93114	0.24	0.22	0.0048	2.737	0.86	18.5
			21	24.40018	0.17	0.22	0.0024	2.737	0.86	18.0
			33	25.1895	0.14	0.22	0.0016	2.737	0.86	15.8
	45°	**Open**	12	17.35982	0.16	0.18	0.0048	-	0.7	9.0
			19	17.74821	0.13	0.18	0.0024	-	0.7	7.7
			27	16.27483	0.1	0.18	0.0016	-	0.7	6.0
		Smooth	11	18.69835	0.18	0.18	0.0048	1.186	0.7	11.1
			21	15.78835	0.11	0.18	0.0024	1.186	0.7	9.2
			33	12.59475	0.07	0.18	0.0016	1.186	0.7	8.3
		Rough	11	20.77595	0.2	0.18	0.0048	2.737	0.7	13.4
			21	21.52957	0.15	0.18	0.0024	2.737	0.7	11.0
			32	14.17423	0.08	0.18	0.0016	2.737	0.7	10.5

Table I. 2:Experimental data and the results of Chapter 5

Sand Size D50 (mm)	Dike Angle	Distance from Dik (cm)	Flow Depth (cm)	Velocity (cm/s)	Maximum Scour Depth (cm)								
					Open Flow			Smooth-covered			Rough-covered		
					with Dike	without Dike	Scour Reduction (%)	with Dike	without Dike	Scour Reduction (%)	with Dike	without Dike	Scour Reduction (%)
0.6	90	50	11	28	0.2	7	97%	1.54	8.2	81%	2.9	9.3	69%
	90	50	11	56	0.23	7.6	97%	1.61	9	82%	3.25	10.4	69%
	90	50	22	14	0.2	6.3	97%	0.71	7.1	90%	1.47	8	82%
	90	50	22	28	0.21	7	97%	1.1	7.5	85%	1.84	8.5	78%
0.9	90	50	13.5	22.5	0.17	6	97%	1.27	7.3	83%	2.3	8.4	73%
	90	50	13.5	44.3	0.2	6.8	97%	1.55	8.5	82%	2.84	9.7	71%
	90	50	26	11.7	0.15	5	97%	0.43	5.8	93%	1	6.2	84%
	90	50	26	23	0.15	5.9	97%	0.79	6.6	88%	1.565	7.5	79%
0.6	60	50	11	28	0.8	7	89%	1.72	8.2	79%	2.5	9.3	73%
	60	50	11	56	0.94	7.6	88%	2.46	9	73%	3.34	10.4	68%
	60	50	22	14	0.52	6.3	92%	1	7.1	86%	1.15	8	86%
	60	50	22	28	0.79	7	89%	1.65	7.5	78%	1.95	8.5	77%
0.9	60	50	13.5	22.5	0.55	6	91%	1.52	7.3	79%	2	8.4	76%
	60	50	13.5	44.3	0.72	6.8	89%	2.4	8.5	72%	2.86	9.7	71%
	60	50	26	11.7	0.2	5	96%	0.734	5.8	87%	0.82	6.2	87%
	60	50	26	23	0.51	5.9	91%	1.4	6.6	79%	1.67	7.5	78%
0.6	45	50	11	28	0.58	7	92%	2.73	8.2	67%	6.1	9.3	34%
	45	50	11	56	0.2	7.6	97%	3.81	9	58%	7.8	10.4	25%
	45	50	22	14	1.03	6.3	84%	1.13	7.1	84%	3	8	63%
	45	50	22	28	0.32	7	95%	1.85	7.5	75%	5.2	8.5	39%
0.9	45	50	13.5	22.5	0.5	6	92%	2.455	7.3	66%	5.7	8.4	32%
	45	50	13.5	44.3	0.12	6.8	98%	3.5	8.5	59%	7.5	9.7	23%
	45	50	26	11.7	0.92	5	82%	0.9	5.8	84%	2.67	6.2	57%
	45	50	26	23	0.2	5.9	97%	1.6	6.6	76%	4.74	7.5	37%
0.6	90	25	11	28	0	7	100%	0	8.2	100%	0	9.3	100%
	90	25	11	56	0	7.6	100%	0	9	100%	0	10.4	100%
	90	25	22	14	0	6.3	100%	0	7.1	100%	0	8	100%
	90	25	22	28	0	7	100%	0	7.5	100%	0	8.5	100%
0.9	90	25	13.5	22.5	0	6	100%	0	7.3	100%	0	8.4	100%
	90	25	13.5	44.3	0	6.8	100%	0	8.5	100%	0	9.7	100%
	90	25	26	11.7	0	5	100%	0	5.8	100%	0	6.2	100%
	90	25	26	23	0	5.9	100%	0	6.6	100%	0	7.5	100%